

Volume I
of
Final Report Under Contract NAS 8-11523

Zero Leakage Design For Ducts And Tube Connections
For Deep Space Travel

FUNDAMENTAL INVESTIGATIONS

by

J.A. Bain
J.P. Laniewski

GPO PRICE \$ _____

CFSTI PRICE(S) \$ _____

Hard copy (HC) 3.00

Microfiche (MF) 1.65

ff 653 July 65

FACILITY FORM 602

N 68-20974

(ACCESSION NUMBER)

(THRU)

180
(PAGES)

1
(CODE)

CR-93925
(NASA CR OR TMX OR AD NUMBER)

15
(CATEGORY)

15 March 1967

GENERAL ELECTRIC

RESEARCH
AND
DEVELOPMENT
CENTER

SCHENECTADY, NEW YORK

S-67-1157
Volume I

ZERO LEAKAGE DESIGN FOR DUCTS AND TUBE CONNECTIONS
FOR DEEP SPACE TRAVEL

FUNDAMENTAL INVESTIGATIONS

Volume I
of
Final Report Prepared under Contract No. NAS 8-11523

15 March 1967

Prepared for
PROPULSION AND VEHICLE ENGINEERING DIVISION
GEORGE C. MARSHALL SPACE FLIGHT CENTER
NATIONAL AERONAUTICS AND SPACE ADMINISTRATION
HUNTSVILLE, ALABAMA

Prepared by
J. A. Bain
J. P. Laniewski
Mechanical Equipment Branch
Mechanical Technology Laboratory
Research and Development Center
General Electric Company
Schenectady, New York

Sponsored by
Missile and Space Division
General Electric Company
Philadelphia, Pennsylvania

General Electric Company Project Engineer: J.A. Bain
NASA Technical Manager: H. Fuhrmann, (R-P&VE-PM)

FOREWORD

This is volume I of a six volume final report covering work accomplished by the Research and Development Center of the General Electric Company, Schenectady, New York from 5 July 1963 to 30 June 1967. This program was sponsored by the Missile and Space Division of the General Electric Company, Philadelphia, Pennsylvania, under National Aeronautics and Space Administration Contract NAS 8-11523, "Zero Leakage Design for Ducts and Tube Connectors for Deep Space Travel."

The six volumes contained in this final report are:

- Volume I -- "Fundamental Investigations"
- Volume II -- "Connector Concept Studies"
- Volume III -- "Guide in Selecting Duct, Tubing
and Gasketing Materials for
Space Vehicles and Missiles"
- Volume IV -- "New Connector Designs and
Testing"
- Volume V -- "Tube Connector Design Principles
and Evaluation"
- Volume VI -- "X-Connector Feasibility Studies"

TABLE OF CONTENTS

<u>Section</u>		<u>Page</u>
1	INTRODUCTION	1
	Scope of Work	1
2	CONCLUSIONS	3
	Biaxial Stress Relaxation Study	3
	Optical Studies of Seal Interface Contact	3
	Leak Detection and Evaluation of Seal Para- meters which Affect Leakage	3
	Creep Study	4
3	RECOMMENDATIONS	5
4	BIAXIAL STRESS RELAXATION STUDIES	7
	Introduction	7
	Test Procedure	7
	Results	12
5	OPTICAL STUDIES OF INTERFACE CONTACT	17
	Introduction	17
	Experimental Equipment	17
	Interpretation of Observations	23
	Observations of Surfaces in Contact	27
6	LEAK DETECTION AND EVALUATION OF SEAL PARAMETERS WHICH AFFECT LEAKAGE	43
	Introduction	43
	Hydrogen Sulfide Individual Leak Path Inves- tigation	43
	Repeatability of Data Investigation	52
	Seal Width Studies	60
	Nuclei Leak Detection Study	63
7	CREEP STUDY	67
	Introduction	67
	Relaxation Design of Separable Tube Connectors	67
8	REFERENCES	69

TABLE OF CONTENTS (continued)

APPENDICES

- I The Condensation Nuclei Detector Potential Applications to Propellants and Oxidizers.
- II Condensation Nuclei, A New Technique for Gas Analysis
- III A New Instrument for the Continuous Measurement of Condensation Nuclei
- IV Leakage Units Conversion Tables
- V Creep Study Report

Section 1

INTRODUCTION

This is Volume I of a six volume report covering work accomplished during the period from July 5, 1963 to June 30, 1967, under NASA Contract No. 8-11523, "Zero Leakage Design for Ducts and Tube Connections for Deep-space Travel."

SCOPE OF WORK

The work reported in this volume involved fundamental leakage and structural investigations of fluid connectors and seals. Specific subjects of study included:

- Biaxial stress relaxation
- Optical studies of seal interface contact
- Leak detection and evaluation of seal parameters which affect leakage
- Creep investigation for high temperature connector design

Biaxial stress relaxation occurs when normal stresses are imposed on a seal and environmental conditions superpose stresses in a plane perpendicular to the normal direction. Such relaxation in the seal element of connectors can result in severe leakage around the seal. Section 4 of this volume is a detailed discussion of bi-axial stress relaxation as studied during the reporting period.

Optical methods were used to observe a seal interface as various load criteria were imposed upon it. Various seal materials and configurations were forced against a glass surface; observation of the interface was made with a microscope/camera combination to record the surface patterns. Section 5 of this volume is an elaboration of work accomplished and the techniques involved.

In Section 6 of this volume, contract efforts in leak detection and seal evaluation are discussed at length. Briefly, the major points are summarized as follows:

- The feasibility of using hydrogen sulfide gas as an aid in the determination of leak paths in an experimental system was established. Gas reaction with the seal formed a colored oxide which could be easily detected by optical methods, thereby providing a "map" of the leak paths.

- A test series was designed to determine the degree of repeatability that can be obtained in a typical, experimental leak test. Test samples were made as nearly identical as possible and test procedures were kept constant. Several seal systems were tested to factor in one variable at a time to determine its effect.
- Another test series was conducted to ascertain the effect on sealing of various widths of an annular gasket seal. It was learned that a narrow gasket requires a lower total load for sealing than a wider gasket. While the test data definitely established this trend, it is recognized that there must be a lower limit of gasket width. This limit was not determined by this test series.
- A nuclei leak detection technique was evaluated for possible application. The Research and Development Center has been active in the development of nuclei detection techniques for some time. One study report and two published papers on this subject are included as Appendices I, II and III to provide the reader with a more detailed reference on the topic. The study conducted under this contract indicates considerable promise for this technique as a portable leak detector for equipment in the field.

Section 7 presents results of a study on relaxation or time to leakage for separable tube connectors, based upon the steady-state creep law. Creep is the tendency of a material to exhibit time-dependent strains at a constant stress level, typical of metals at elevated temperatures. The study was conducted by Battelle Memorial Institute, subcontractor for the General Electric Company, under Subcontract No. 63-30, Contract No. NAS 8-11523. A copy of the final report submitted by Battelle is included as Appendix V.

Briefly, the study resulted in the recommendation that René 41 be used as the material for a high temperature connector to be built by General Electric and reported in Volume IV of this series. A design procedure that utilizes the steady-state creep law also evolved from this study. The Battelle Memorial Institute made sample calculations for bolted-flanged and threaded connectors. These calculations proved very useful in development of the high temperature connector. In addition, the study yielded a number of useful property tables for various materials at high temperature.

Section 2

CONCLUSIONS

Specific conclusions derived from the fundamental investigations are divided by the subject of study and listed below.

BIAXIAL STRESS RELAXATION STUDY

1. Seal material exhibits definite relaxation with combined high normal loads and relative lateral displacement between seal faces.
2. Greatest seal relaxation occurs in the first few cycles of relative movement.
3. Copper gaskets (and probably most ductile gasket materials) will loosen because of gasket relaxation if clamping forces are high and if there is relative lateral displacement between tube flanges.

OPTICAL STUDIES OF SEAL INTERFACE CONTACT

1. With optical test equipment, strong reflections are received from areas on the seal which are within less than 1 microinch of the contact. Weaker, but recordable reflections are obtained from areas up to 2 microinches from true contact. No recordable reflections are obtained from areas over 2 microinches from true contact.
2. It is possible to achieve resolution as fine as 0.0001 inch in the plane of contact if proper care is exercised. Consequently, leak passages on the order of 10^{-4} inches wide by 2×10^{-6} inches deep should be discernible.
3. All seal areas in contact with the rigid connector surface reflect light. This conclusion was deduced from experiments using materials (i.e., copper, silver, aluminum) which flow plastically and make full contact.
4. Extreme load pressures (e.g. for this study, above 5000 pounds) will flatten seal until continuous contact between connector surfaces occurs. Continuous contact occurs first along the inner edge of the seal width.

LEAK DETECTION AND EVALUATION OF SEAL PARAMETERS WHICH AFFECT LEAKAGE

Hydrogen Sulfide Individual Leak Path Investigation

1. A test using a silver gasket with hydrogen sulfide showed that the reaction time and concentration of hydrogen sulfide was too excessive to be practical.

2. A copper gasket test showed that hydrogen sulfide can be effectively used as a tracer gas to determine leak paths. In most cases, these paths can be observed optically.

Repeatability of Data Investigation

1. The results of six aluminum gasket tests and six teflon gasket tests indicated a high degree of repeatability.

2. The aluminum gasket tests showed that reliable repeatable data can be obtained using a single representative test for a particular seal system.

3. The six teflon FEP gasket tests showed that data from any one test are adequate in the prediction of leakage both during increases in stress and pressure.

Seal Width Studies

1. Seal widths can be made as narrow as possible to utilize lower total loads (for a given mean seal diameter). This promotes the design of lighter weight connectors.

2. Flat gasketed seals in widths from 1/16 to 1/4 inch were tested and found to be fully acceptable.

Nuclei Leak Detection Study

1. The portable nuclei detector cannot detect all gases, but many gases which could be used to detect a leak, can be combined with other gases or with water vapor to form nuclei.

2. This nuclei detection system is capable of detecting smaller amounts of tracer gases than most other systems.

CREEP STUDY

Conclusions on the Creep Study are given on Pages 2 and 3 of Appendix V, "Relaxation Design of Separable Tube Connectors."

Section 3

RECOMMENDATIONS

Based on the results of this study program, the following recommendations are made:

1. Additional research should be conducted to specifically determine the degree of movement to be expected between seal faces and adjacent structural material. Once clearly defined, allowances can be incorporated into the design of any connector system. For example, expected gasket thickness changes can be compensated for by tightening and/or retightening procedure specifications.
2. The magnitude and origin of forces causing relative seal face movement should be further investigated. Outcome of these studies would allow design concepts and procedures to be established for minimizing such forces.
3. Further preliminary connector and seal investigations for new or proposed designs should be accomplished using the Optical Technique described in this report for studying surface contact. The use of this technique is also recommended because it reduces the need for expensive test fixtures.
4. More experimental work is needed to refine the use of the hydrogen sulfide technique for leak path investigation. Proper gas mixtures and exposure times need to be established to result in obtaining observable oxides and moreover to eliminate leak paths. The possibility of using other gases and materials should be investigated to expand on the knowledge gained in this study.
5. The repeatability gasket tests indicated that, for the gaskets investigated, one test is representative. Different gasket and seal surface finishes should be studied and then effect on leakage repeatability ascertained.
6. On the basis of the present study, it is recommended that further investigations be carried out to establish relationships between seal widths and sealability. The minimum seal narrowness has not been determined along with consideration of parameters such as materials, surface finishes and the direction of surface asperities.
7. Further studies should be conducted experimenting with the nuclei leak detector to determine what gases it is sensitive to and how combinations can be created to allow for detection.
8. Recommendations resulting from the Creep Study are summarized on page 3 of Appendix V, "Relaxation Design of Separable Tube Connectors."

Section 4

BIAXIAL STRESS RELAXATION STUDIES

INTRODUCTION

Biaxial stress relaxation occurs when unusual motion, (i.e., rotation, vibration, relative displacement etc.), of two sealing surfaces in a transverse direction causes forces on the seal other than those deliberately imposed in the longitudinal direction. When this transverse motion occurs, the seal tends to relax. This is known as biaxial stress relaxation.

In a system using gasket sealing, normal stresses applied to the gaskets must be at least twice the yield strength for a good seal (Ref. 1). Several experiments have shown that some metals subjected to longitudinal stress levels well above yield strength become extremely ductile in the transverse direction. In standard tensile specimen cycle fatigue tests, the small spring load of a displacement gage has been sufficient to cause deep gouges in the specimens. Some gasket sealing systems loosen up catastrophically under vibration and thermal cycles present during static tests on missiles. Both lateral vibration of the connector and thermal cycling would cause relative displacements between the sealing surfaces which apply normal stresses to the gasket.

Experiments were conducted to see if repeated lateral displacement would cause a decrease in the thickness of copper; this copper being subjected to constant normal loads inducing a compressive stress of twice its yield.

TEST PROCEDURE

A series of tests were conducted using the test apparatus shown in Figures 1 and 2. These tests were made to establish whether lateral translation of a gasket, subjected to high normal forces, will cause gasket relaxation.

Four copper strips $1/16$ by $1/8$ by $1\ 1/2$ inches in length were loaded normally between three rigid anvils. A hydraulic press was affixed to the center anvil which allows it to move 0.0005 inch. Figure 1 shows the assembled test apparatus, the three anvils, and the hydraulic jack, in the compression testing machine. Four 0.0001 in/div. dial indicators are used to measure the translation of the center anvil and the change in gap between the outer anvils. Figure 2 shows the test apparatus with the top anvil removed. The dark portion on the anvil is toolmaker's bluing used to detect slippage of the copper strips.

PRECEDING PAGE BLANK NOT FILMED.

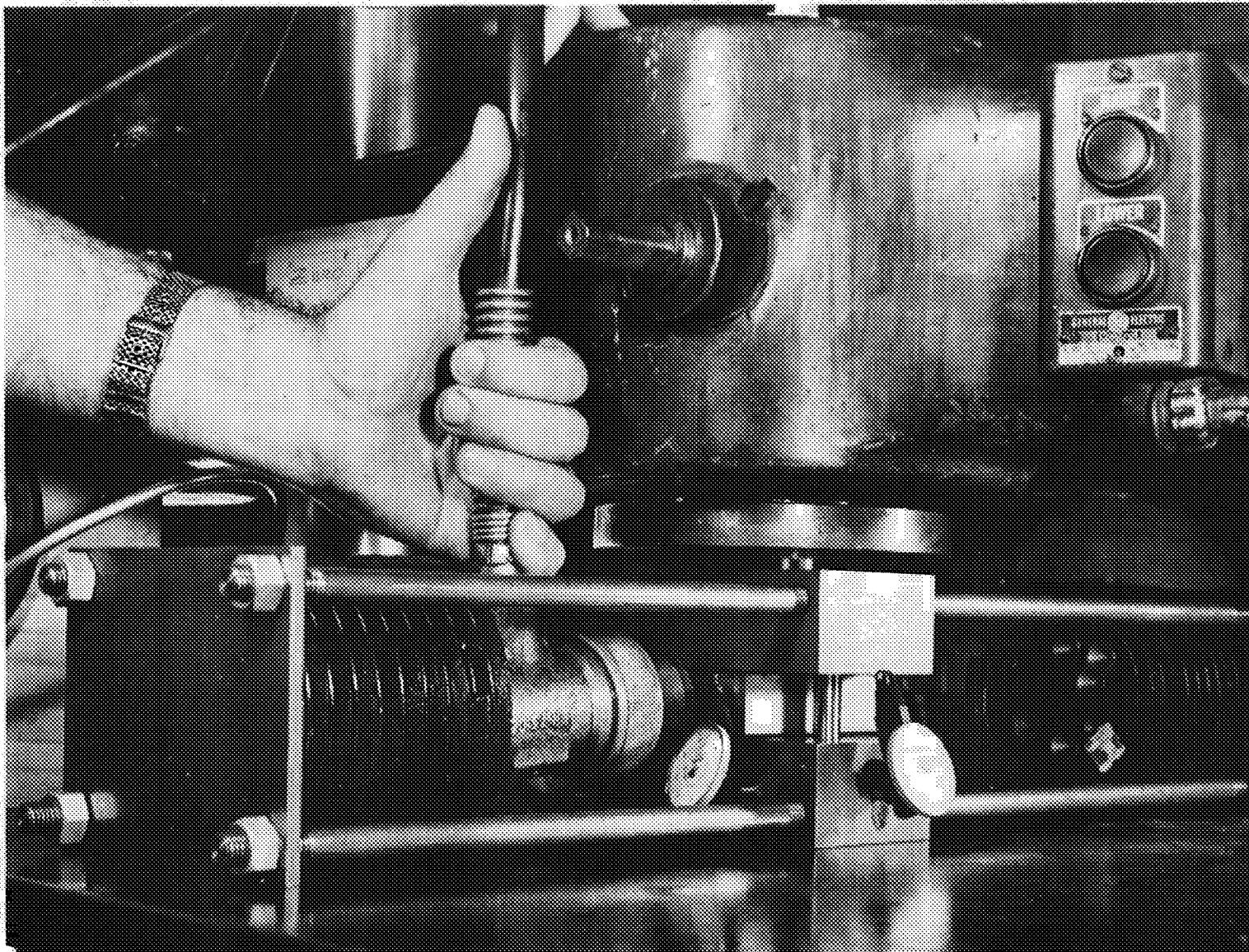


Figure 1. Gasket Compression - Translation Test Apparatus Showing Three Anvils, Compression Testing Machine and Lateral Displacement Press

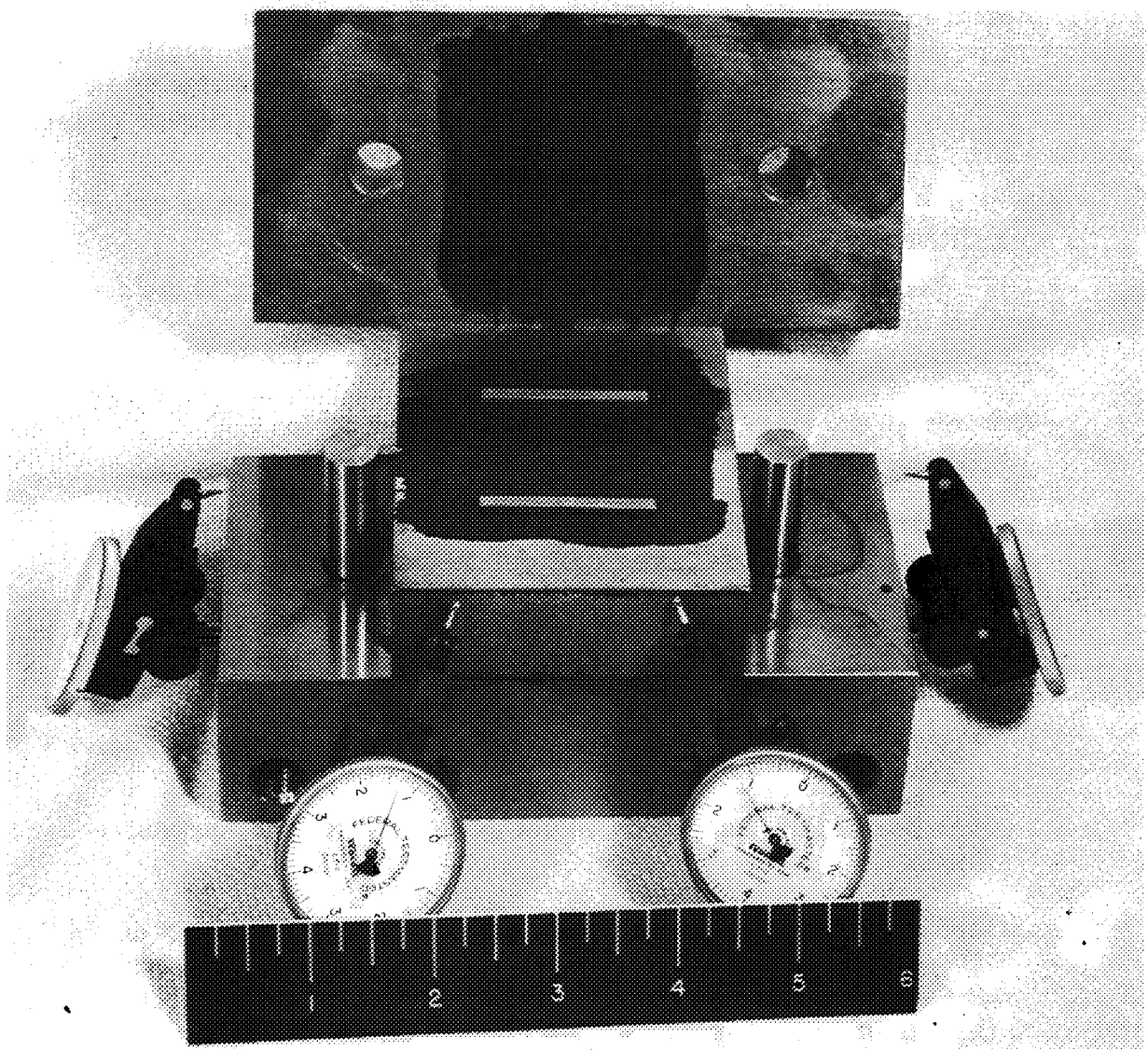


Figure 2. Components of Gasket Compression - Translation Test Apparatus:
Three Anvils, Dial Gages, Copper Strips

Five tests were conducted with compressive loads producing 12250, 15650, 20000, 25600, and 40000 psi stresses in four copper strips. A new set of four copper strips 1/16 by 1/8 by 1 1/2 inches in length, with the load applied normal to the 1/8-by 1 1/2-inch face, were used for each test. A lateral movement of 0.0005 inch from each side of the central equilibrium position was imparted to the center anvil by the hydraulic jack. The testing fixture was designed primarily to determine trends in change of the copper strip thickness, and when changes and thickness ceased to exist. The parameters measured in each test were:

- A change of gap between the top and bottom anvil which is twice the change in thickness of a copper strip
- The lateral movement of the center anvil with respect to the top and bottom anvil
- The magnitude of the compressive load
- The initial and final thickness of each copper strip

Measurement of the change in thickness of the copper strip is influenced by inaccurate gage installation and gage reading error. The Federal Testmaster dial gages used are critical to positioning in the test fixture.

Correction factors must be applied to all readings when the following two conditions exist:

1. The axis of the sensing arm is not normal to the compressive load
2. The axis of the gage body is not parallel to the compressive force.

The estimated installation error of the gages is about 1 percent corresponding to a 5 degree deviation from a normal or parallel position once the dial gages were installed they were not changed during a test. Therefore, no installation is present when comparing the reading in any one test. There is however, a possibility of a 1 percent error when comparing readings from various tests due to the original installation error. Each gage was checked using Johansson blocks to establish a correlation between true deflection recorded by the dial gage. A maximum error of 3.3 percent was observed over the entire 10 mil travel of the gage arm. Figure 3 shows the influence of recording error on percent change of thickness.

A measurement of the center anvil's lateral movement was taken. Two dial gages were used to detect rotation of the center anvil and two gages were used to record thickness changes and monitor the tilt of the top anvil. The average of the two values were taken to determine the change of thickness. The lateral force applied to the center anvil was measured with the pressure gauge in the hydraulic line of the jack. A deviation of 100 pounds

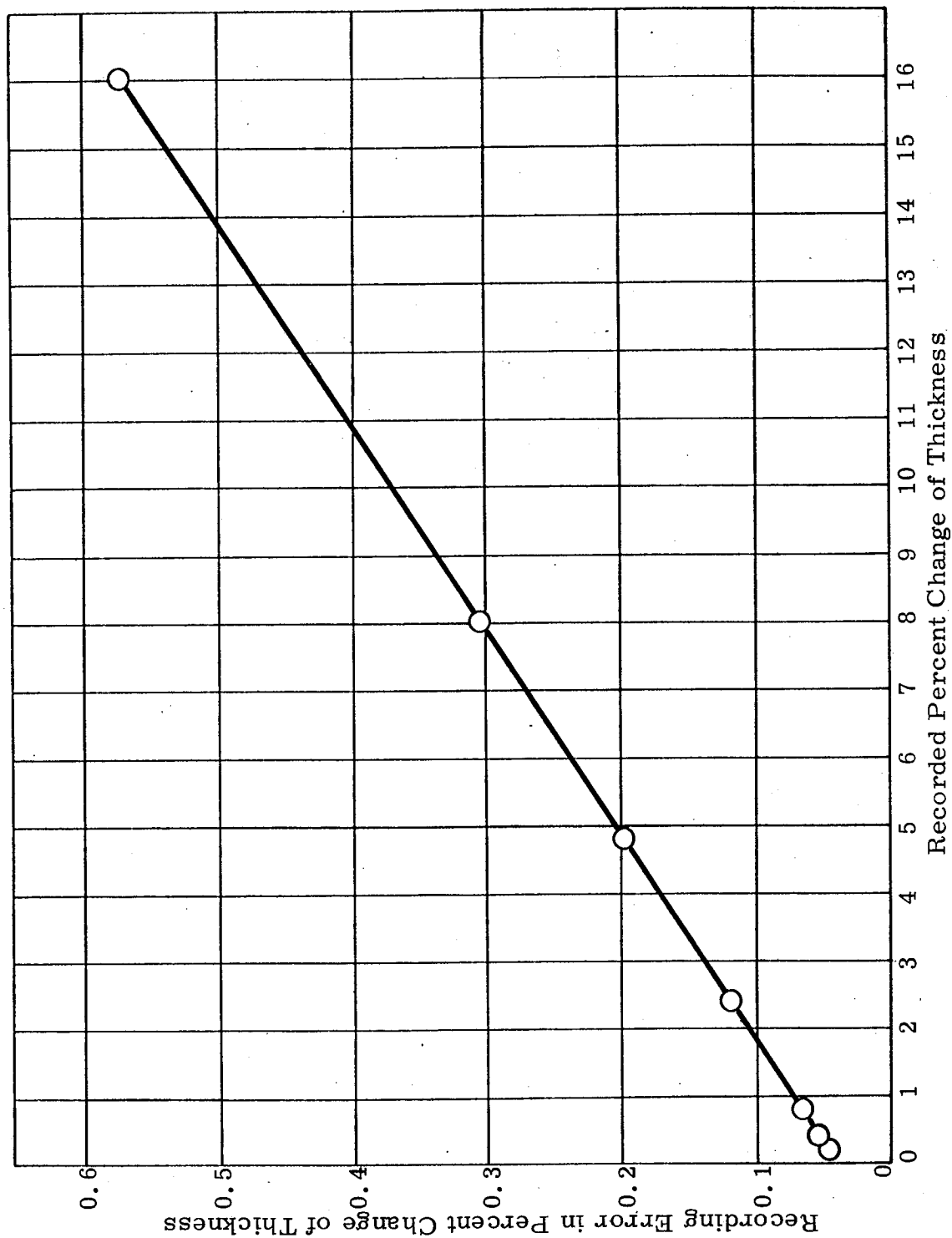


Figure 3. Influence of Recording Error on Percent Change of Thickness

was observed when 3500 pounds is applied. This corresponds to a 2.85 percent error. The reading error, which is one-half the deviation or in this case 50 pounds, must also be applied. At applied loads of 1500 pounds, the reading error corresponds to an error of 3.33 percent. The 1/16 inch dimension of the copper strips were measured at the center and both ends before and after the test to determine if any high spots were present.

RESULTS

Figure 4 shows the percent change in thickness of a rectangular copper strip as a function of lateral displacement cycles. Results show that there are three distinct regions with different rates of deformation. These are called:

- The initial deformation region
- The transient strain region
- The steady-state region

The largest change in thickness occurs during the first cycle of lateral displacement. In the second region, the rate of thickness change has decreased and in the third region, the change of thickness ceases to occur. G. J. Moyer and G. M. Sinclair (Reference 2) also observed three distinct regions when they subjected a hollow copper tube under axial stress to a cyclic torsional stress.

A steady-state region between 20 and 30 cycles was observed for copper strips subjected to compressive stresses of 12250, 15650, and 20000 psi. After 60 cycles, no steady-state region was obtained for copper strips having 26600 and 40400 psi compressive stress.

The test results are time-dependent since copper is strain hardenable. Creep and thickness change was noticed only when the normal stress was 40,000 psi. Two minutes were required before the creeping stopped. The amount of creep is shown by the first data point in Figure 4.

The lateral forces required in each of the tests are given in Table I.

Table I

Normal Stress (psi)	Minimum - Maximum Load (pounds)	
12,250	1,100	1,650
15,650	1,300	1,800
20,000	1,725	2,400
26,000	2,100	3,150
40,000	2,700	5,100

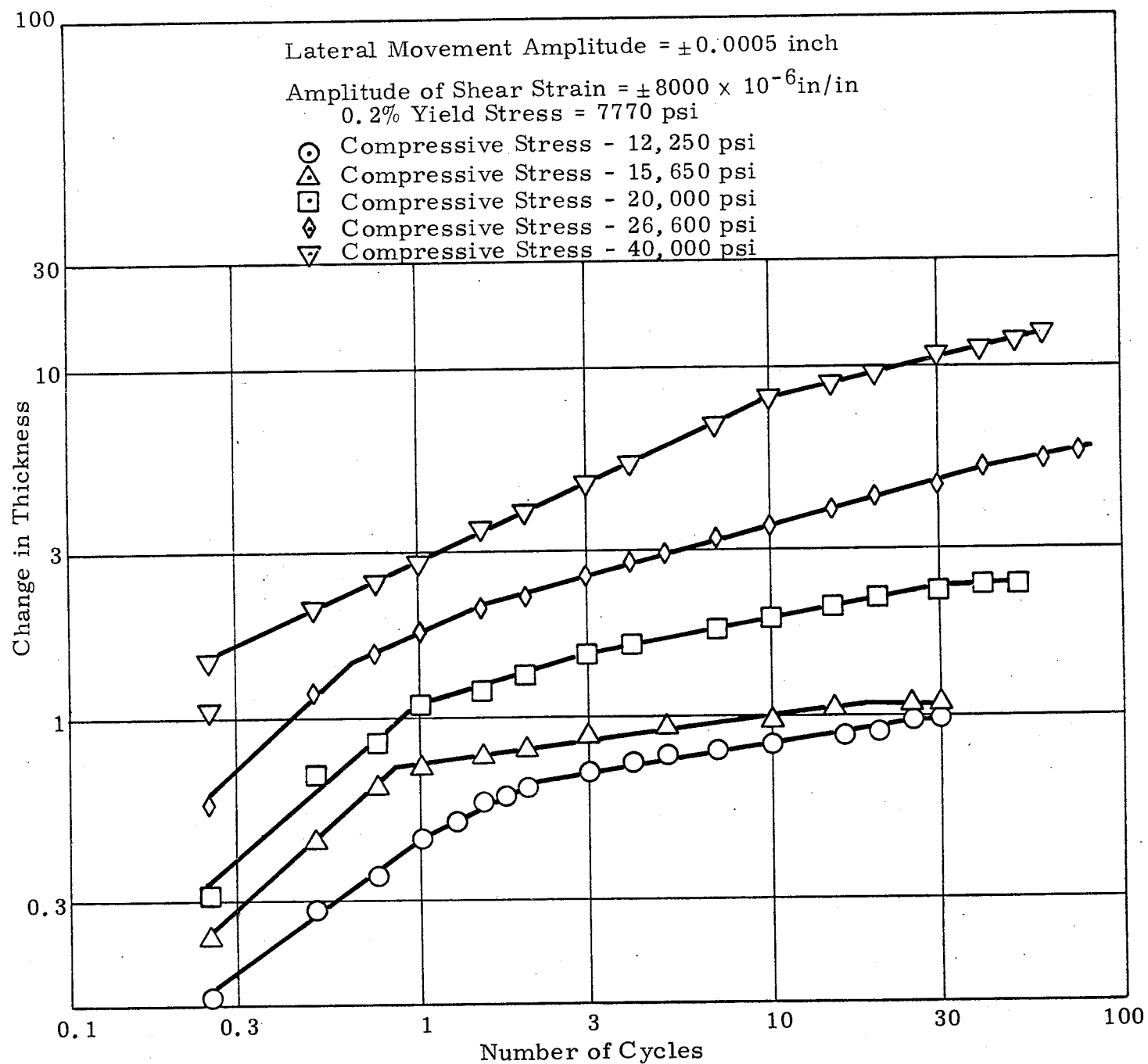


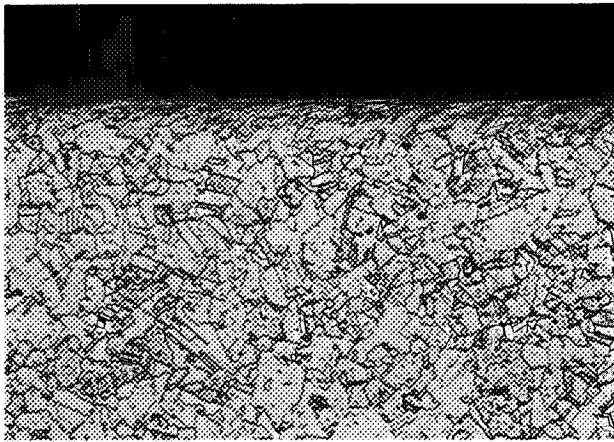
Figure 4. Combined Stress on 99.9 Percent Copper

The values shown are the maximum and minimum loads required to displace the center anvil 0.0005 inch. Two trends were evident during the tests:

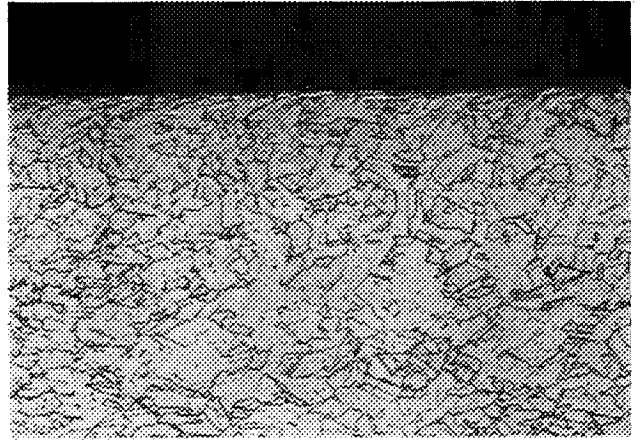
- The forces required to move the center anvil increased as the number of cycles increased. This leveled off in the steady-state region as measured within the accuracy of the test fixture
- A larger force was required to move the center anvil away from the center equilibrium position than to move the block toward the center equilibrium position. The difference was as much as 200 to 300 pounds

The minimum detectable movement of the center anvil, with sufficient accuracy, is about 100 microinches. This is lower than the 0.2 percent yield strain of about 250 microinches for copper. No noticeable elastic motion was seen.

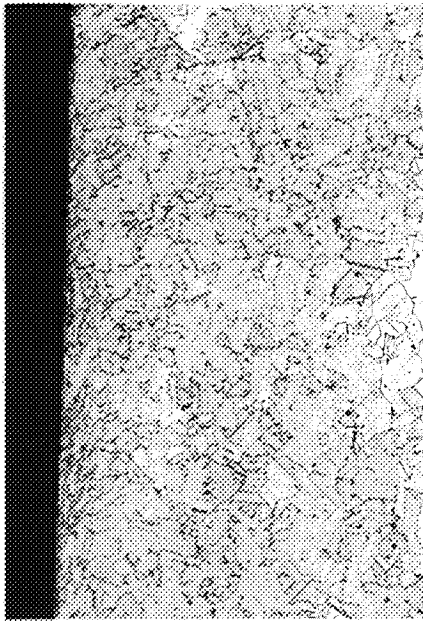
One copper strip from each test and one strip not subjected to a load were cut along three mutually perpendicular planes. These three strips were mounted and etched in order to view the grain structure. The influence of the combined stresses had no noticeable effect on the grain structure. Figure 5 shows the grain structure of two specimens when viewing the 1/8-by 1/16-inch face at the center of the strip.



a) NO LOAD
1/8" TOP EDGE
100X



b) SUBJECTED TO 40,000 PSI STRESS
1/8" TOP EDGE
100X



c) NO LOAD
1/16" SIDE EDGE
100X



d) 40,000 PSI STRESS
1/16" SIDE EDGE
100X

Figure 5. Grain Structure of the Central Cross Section

Section 5

OPTICAL STUDIES OF INTERFACE CONTACT

INTRODUCTION

The weight of a fluid connector is related to the contact force needed to reliably effect a leak-tight seal. The force needed to make a seal by bringing two flat surfaces in contact is a function of seal width. It is desirable to make the seal width as narrow as possible without reducing reliability. An overly narrow seal may contain irregularities, such as tool marks, extending across its width and require excessive force to effect a good seal.

It is necessary to know what force will be required to insure a reliable seal for given materials, various surfaces, and seal geometries.

An optical technique was used to study surfaces on a microscopic scale. This was necessary to establish whether surfaces are in true contact or whether voids are present between them. It is virtually impossible to separate, examine, and replace two surfaces in the identical position; this technique allows seal analysis without separation of the contact surfaces.

These experimental results can be applied to new situations and mathematical models can be established for predicting the probability of leakage.

EXPERIMENTAL EQUIPMENT

If light passes through an optically smooth surface from a medium of higher index of refraction to a medium of lower index of refraction, it is bent in accordance with Snell's Law. Furthermore, if the incident angle exceeds a critical angle, the light is totally reflected. If the medium of higher index of refraction is a piece of glass, the lower index medium is air, and the incident angle exceeds the critical angle, the light will be totally reflected in the glass and not emerge into the air. If a second piece of glass is brought into true contact with the first, effectively replacing the air, the light will no longer experience a change of index at the interface and will be transmitted rather than reflected. The shift from total internal reflection to transmission occurs smoothly as the distance between the two pieces of glass decreases from one wavelength of light to zero. The degree of transmission versus reflection can be used to measure gaps in this range. The exact curve of gap versus percent reflection depends on the index of the glass.

If an opaque object is used instead of a second piece of glass, a very similar effect takes place. When the gap between the surface is over one wavelength, the glass may be examined (through another optically smooth

PRECEDING PAGE BLANK NOT FILMED.

surface) to see what light is being internally reflected. As the gap is reduced below one wavelength, an opaque object is seen instead of the total reflection.

If a piece of glass, an opaque object in contact with it and light are suitably arranged, those areas in true contact and those areas separated by more than some very small distance can be seen (Figure 6). Light rays, such as A in Figure 6, are reflected because no object can be seen in contact with the glass. Light rays, such as B in Figure 6 which see an opaque object in true contact with the glass, are partly absorbed. The reflected light is distributed in a non-specular reflection with relatively little of it reaching the observer's eye.

A simple demonstration of the above phenomenon is described by Harrick (Reference 3), where the technique was used for photographing fingerprints without the need for messy black ink.

There are two major difficulties inherent in the system described. First, within the field to be studied, the effective path length to all points must be the same in order to focus an image under a microscope. Rays (Figure 6) from the opaque surface to the eye travel partly in glass (or plastic) and partly in the air. The length of the paths from different points on the opaque surface are different. The system is acceptable for observations with an unaided eye or at low magnifications. Use of a prism instead of a glass block does not avoid this problem. A second deficiency is that the system shown in Figure 6 provides a "light field" type picture (i. e., one where the background is brightly illuminated and the useful information is a reduced brilliant pattern). For greater sensitivity it is desirable to have a "dark field" picture (i. e., where everything is black except the useful information which appears as varying shades of gray).

An improved system, which simultaneously takes care of both difficulties, is simply to observe rays B' rather than A' as illustrated in Figure 6. A dark field picture is obtained and the problems of optical distortions, aberrations, and focusing are essentially those inherent in a normal use of a microscope.

A test fixture, using the improved optical systems, was built for observing seals as shown in Figures 7 through 10. Shown in Figure 8 is the central loading screw which comes up from the bottom, the pipe to the leak detector, and the leads for the wire strain gages which measure the load applied to the seal. Figure 9 shows an O-ring seal in test position; the view is through the side wall of the glass giving a "light field" illuminated picture with the contacting O-ring appearing dark. Figure 10 shows the complete setup with the microscope head just above the test fixtures. A black paper has been placed around the glass block portion for three purposes:

- Keep out stray light

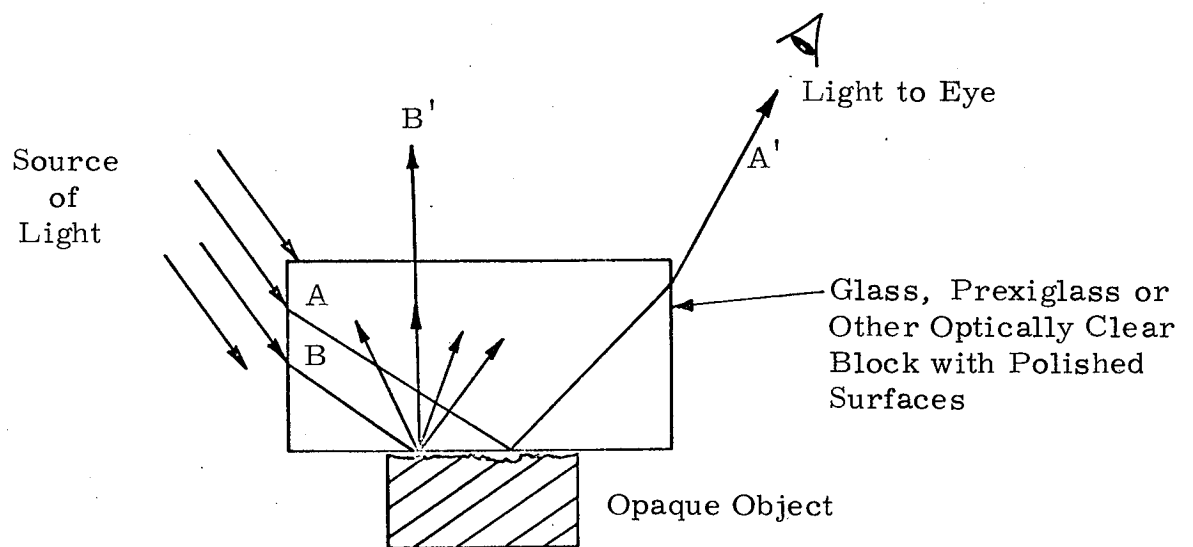


Figure 6. Reflection Demonstration

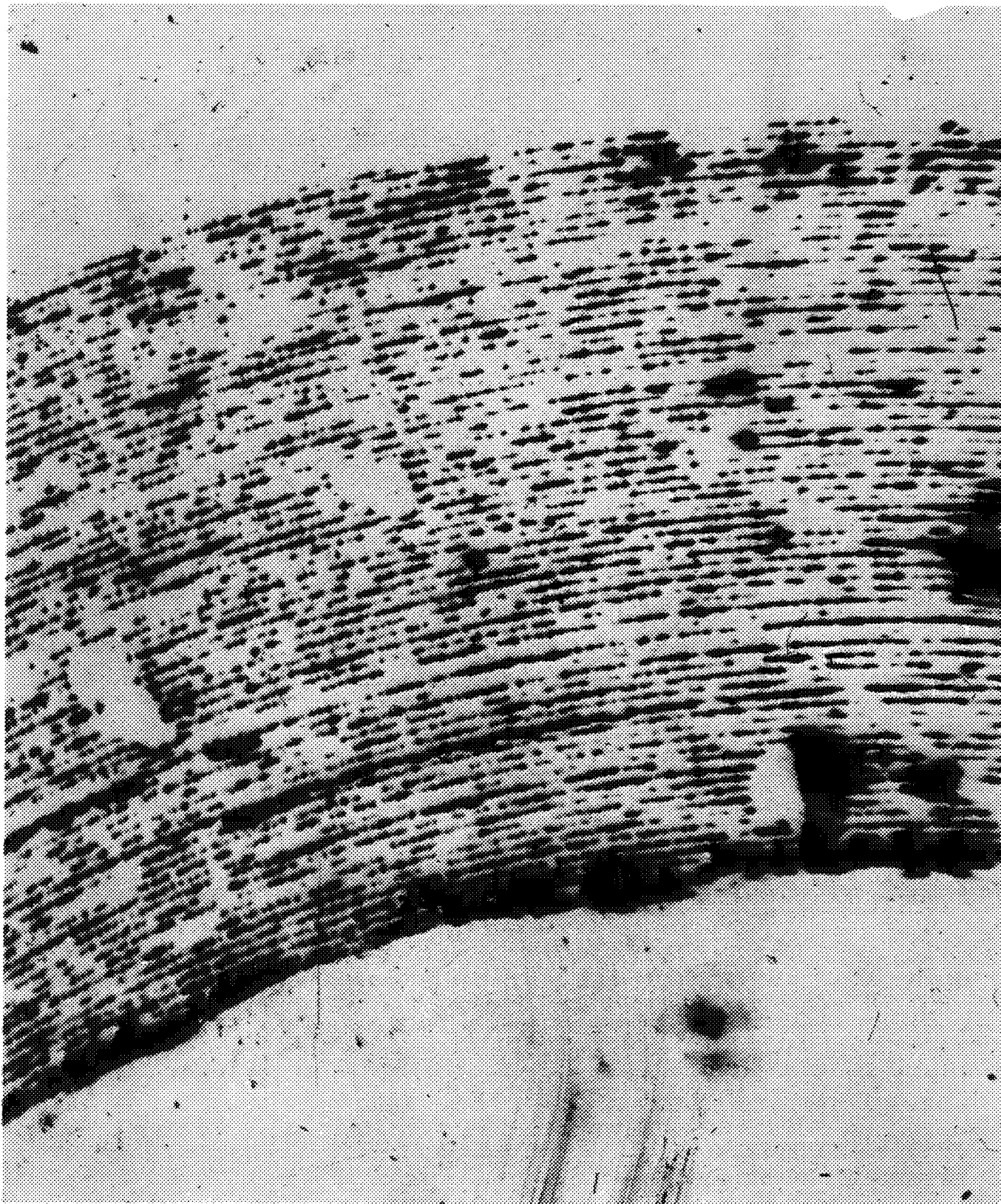


Figure 7. Contact Pattern for Aluminum Seal at 6450 psi Sealing Stress

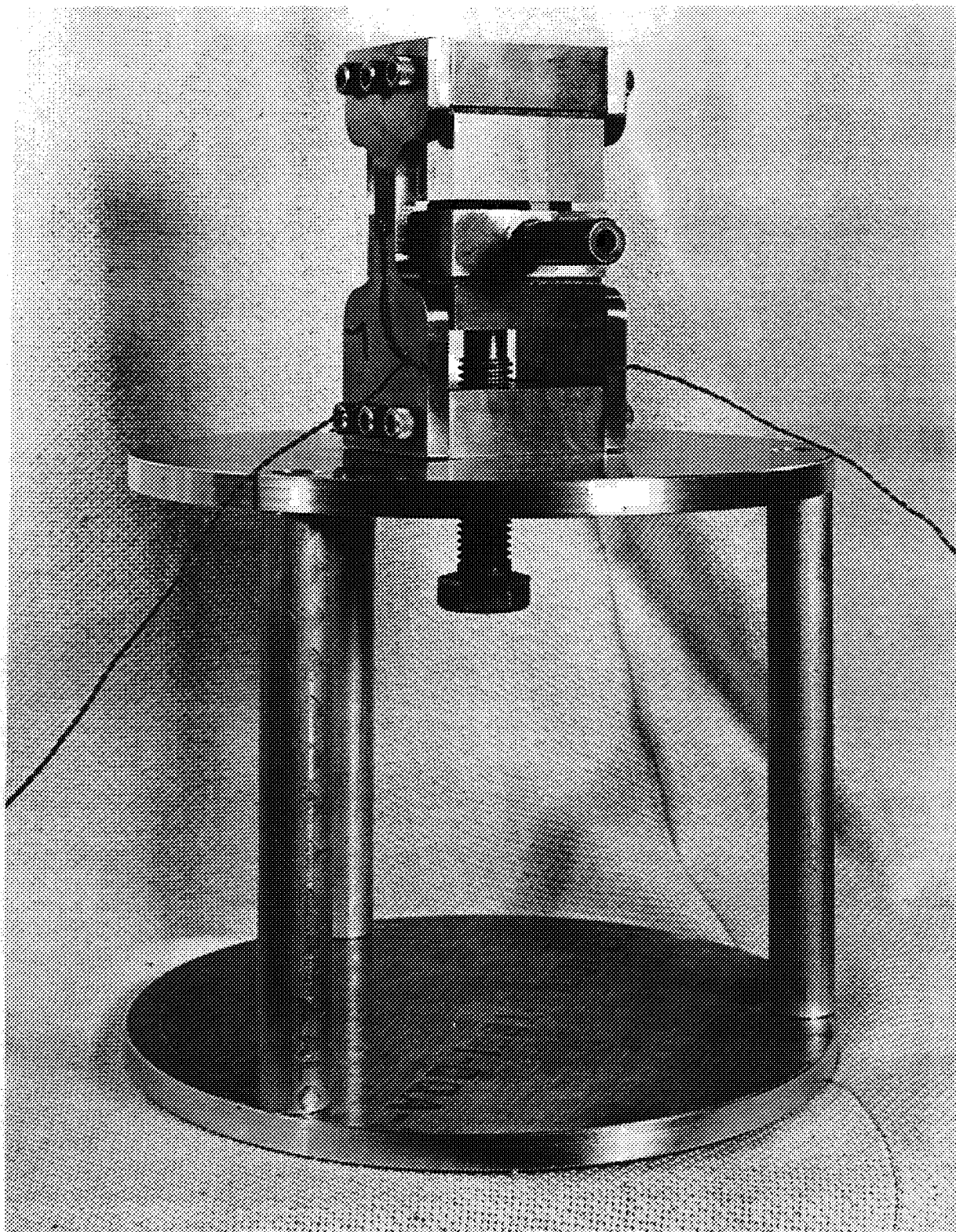


Figure 8. Optical Load-Area of Contact Experimental Apparatus. Load is Applied by Increasing Torque on Bolt

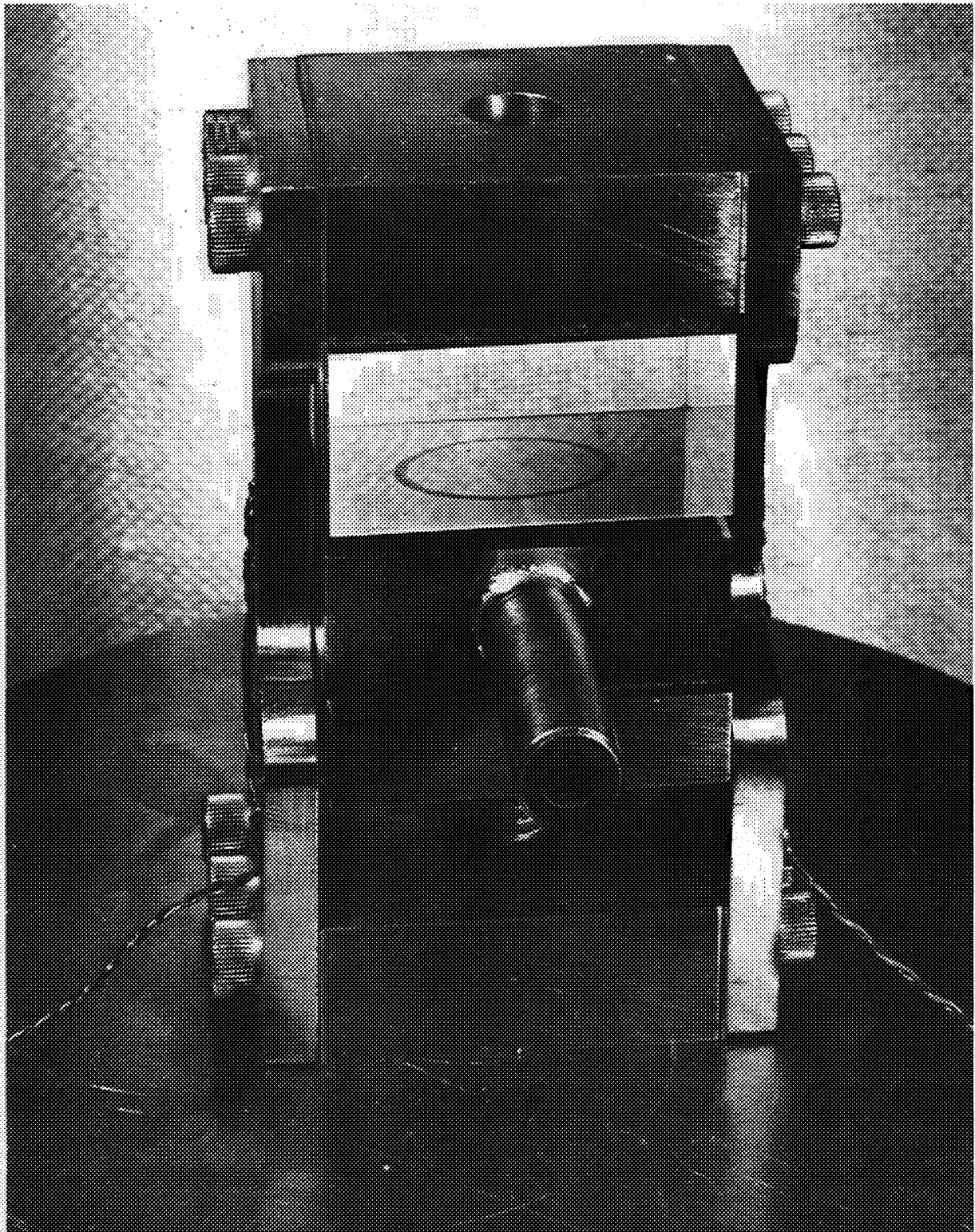


Figure 9. Close-up of Optical Load-Area of Contact Experimental Apparatus. O-Ring Can Be Seen in Contact With Glass Block. Tube Shown is for Evacuating Volume Inside O-Ring. Load Measuring Strain Gages Can Be Seen on the Sides of the Attachment

- Absorb light which is not intended to reach the microscope, but if reflected might eventually do so
- Act as a container so the volume just outside the seal may be flooded with helium

A helium tube enters this "container" from the left as shown in Figure 10. The light source and tube to the leak detector are on the right side. This system is capable of simultaneously permitting optical observation of the area of the seal in true contact. This includes high resolution photomicrography, measurement of the load applied to the seal, measurement of the leakage rate across the seal for one atmosphere pressure, and the ability to increase or decrease the load while continuing all observations. A variation of the equipment permits operating with high pressure helium inside the seal parameter. It also allows connection of the mass spectrometer leak-detector to a volume just outside the seal permitting measurement of leakage for other than one atmosphere pressure differential.

INTERPRETATION OF OBSERVATIONS

A shift from total internal reflection to an illumination of the opaque object was noted at points where the gap between glass and object become a fraction of a wavelength. Using a transparent instead of an opaque object, the transition function between internal reflection and transmission depends on the following:

- Index of refraction of the glass
- Angle of incidence of the light
- Gap measured in wavelengths of light

The 50 percent point is usually reached at a gap of about 0.3λ . Thus, for light with a wavelength of 5,000A, $0.3 \lambda = 6$ microinches. There are additional factors to consider in determining the intensity of light received versus gap for a system using an opaque object and light reflected normal to the glass surface. An experiment was devised where a ball was brought into contact with the glass reflecting surface under varying loads. Specifically, the Carboloy ball used was 0.5000 inch \pm 0.0001 inch in diameter having an exceptionally high polish. Contact loads between the ball and the glass range from one-half gram to 127 grams. Pictures were taken through a microscope with a Polaroid film pack using film with an ASA rating of 3,000 and an exposure time of up to 10 minutes. The microscope and camera were arranged to give an approximately one-half millimeter, 1 millimeter, or 2 millimeter film distance for a 0.001 inch real distance. Figure 11 shows the contact area as it appeared when three of the loads were observed. A plot of the mean contact diameters for various loads versus load is given in Figure 12. The mean diameter was about 0.0019 inch larger than the theoretical contact diameter. Theoretical diameter was calculated from the Hertzian stress consideration and the formula on the following page.

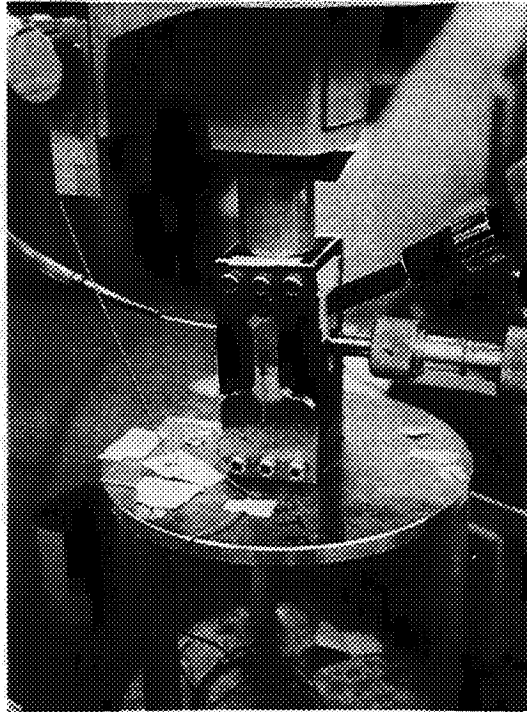
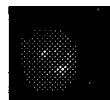


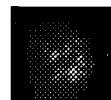
Figure 10. Close-up of Optical Test Apparatus



1 gram



8 grams



27 grams

Figure 11. Contact Between One-half Inch Diameter Carboloy Ball and Glass at Various Loads. Scale: 1 mm = 0.0005 Inche

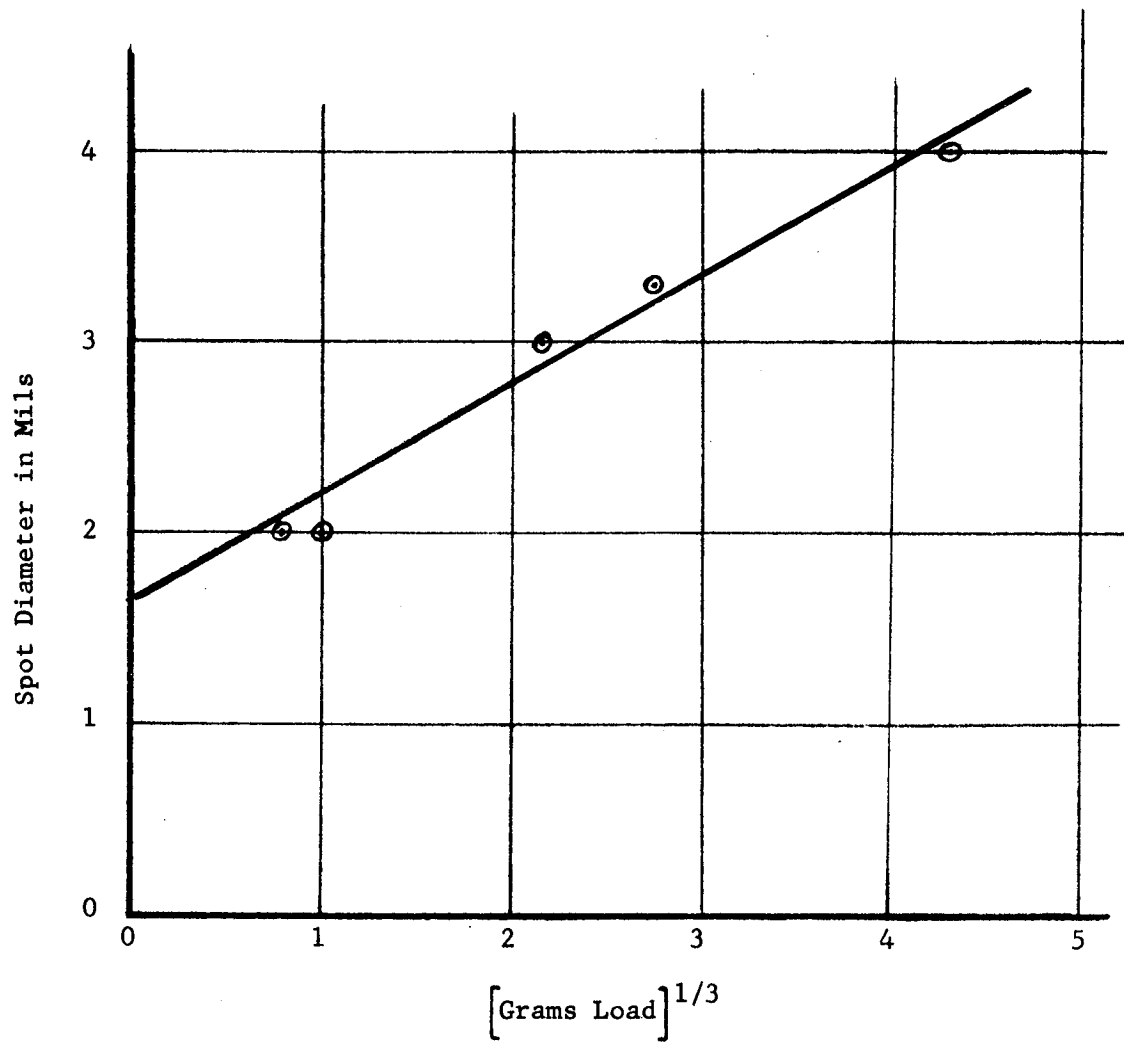


Figure 12. Determination of Spot Diameter for Zero Load

$$d = 1.442 \left[PD \left(\frac{1-v_1^2}{E_1} + \frac{1-v_2^2}{E_2} \right) \right]^{1/3}$$

which reduces to

$$d = 0.493 \times P^{1/3} \quad (d = \text{mils, } P = \text{grams})$$

when the values of Poisson's ratio and Young's modulus for glass and Carboly are inserted.

The spot on the photograph appears dimmer as well as smaller for loads under 10 grams. At loads of one-half and 1 gram it is extremely difficult to observe the spot and measure its diameter; at highest magnification it appears on the film as a four millimeter diameter area. It is probable that the observed diameters of these two points are inaccurate and too small.

Based on the 0.0019 inch overage in diameter of the contact area, observable light is reflected from surfaces which are within approximately 1.8 microinches or less of the glass surface. It is not reflected from points at distances greater than 1.8 microinches.

Observation of the contact area shows that it is not of uniform intensity. Bright spots with typical dimensions around 0.0005 inch exists separated by duller areas of the same magnitude. Moving the point of contact on the glass did not alter the pattern, indicating that the pattern is characteristic of the surface of the ball. There were also specks of light which stayed with the glass and indicate scratches, dirt or other defects on it. The ball contact area could be placed to avoid these. Considering the observed contacts, it appears that under loading of one or two grams, contact is made on a few peaks, each individually discernable, and each a few ten-thousandths of an inch in diameter. For higher loads, these areas reach dimensions typically around one-half mil in diameter (for the ball used), and are distributed over a larger diameter contact circle. Within the contact circle, dimmer areas appear, and it is concluded that these must be of the order of 1 to 2 microinches from contact. This indicated surface roughness is not unreasonable. A Talysurf measurement on the ball showed an average peak to valley distance of about two microinches.

It is concluded that for the system and technique used:

- Strong reflections are received from areas which are probably within less than one microinch of true contact
- Weaker but recordable reflections are obtained for areas up to two microinches from true contact
- No recordable reflections are obtained from areas beyond two microinches gap

If care is taken, resolution in the plane of contact as fine as 0.0001 inch is possible. Also, passages of the order of 10^{-4} inches wide by 2×10^{-6} inches deep should be discernable.

This experiment does not prove that all areas of contact reflect light. Figures 13 through 15 show a copper seal at various loadings. As the load increased, the initial contact areas on the crest lines of the tool marks grew in area and eventually (particularly near the inner radius) merged into a continuous "contact". It was not possible to increase load beyond an estimated 5,000 pounds; an attempt to reach 5,130 pounds broke the glass. The copper seal dimensions were 0.450 inch outer diameter, 0.300 inch inner diameter, and 0.032 inch thick.

OBSERVATION OF SURFACES IN CONTACT

Figure 13 shows (in addition to contacts which obviously are crest lines of the tool marks) several oval shaped areas of contact. These are impurities on the surface of the copper. They are of value as index points to accurately locate areas of interest in pictures taken with progressively greater loads. Many of the crest lines do not appear and those that do are discontinuous. Figure 14 shows that only a few crest lines, primarily near the inner diameter, have yet failed to contact and there are fewer breaks in crest lines. Close examination shows occasional blockage of the spiral path, representing the valley cut by the tool. In Figure 15, the load is sufficiently high and the tool marks near the inner radius are beginning to be obliterated. Almost 100 percent true contact is being made. By counting ridges outward from a convenient index point, it may be observed that the broad contact band at the outer diameter represents the outer two ridges and valley between them (Figure 14). It also indicates that true contact over essentially the full area is developing at the outer diameter.

Observations with similar results have been made on lathe turned aluminum surfaces using rings of the same dimensions (i. e., 0.450 inch outer diameter, 0.300 inch inner diameter, and 0.032 inch thick). A series shown in Figures 16 through 20 include the effect of removal and reapplication of load. Figure 20 shows that with an initial application of a light load, a quite heavy contact exists at the inner and outer diameters, and the inner diameter is irregular. This is attributed to attempts in the shop to break the sharp corners, causing a very slight upset of material. It is also attributed to the fact that when a flat ring is pressed lightly against a flat block the elastic deformations will peak at the inner and outer radii. Also evident in Figure 16 is a piece of lint, about 1/16" long and a few mils in diameter. The contact pattern for final initial application of load is shown in Figure 17. Some areas can be noted where ridge line contact still has numerous breaks, which represent potential leak paths if they match up properly.

Figure 18 shows the pattern after the load has been removed and a light load (too small to measure) has been reapplied. It is apparent that the

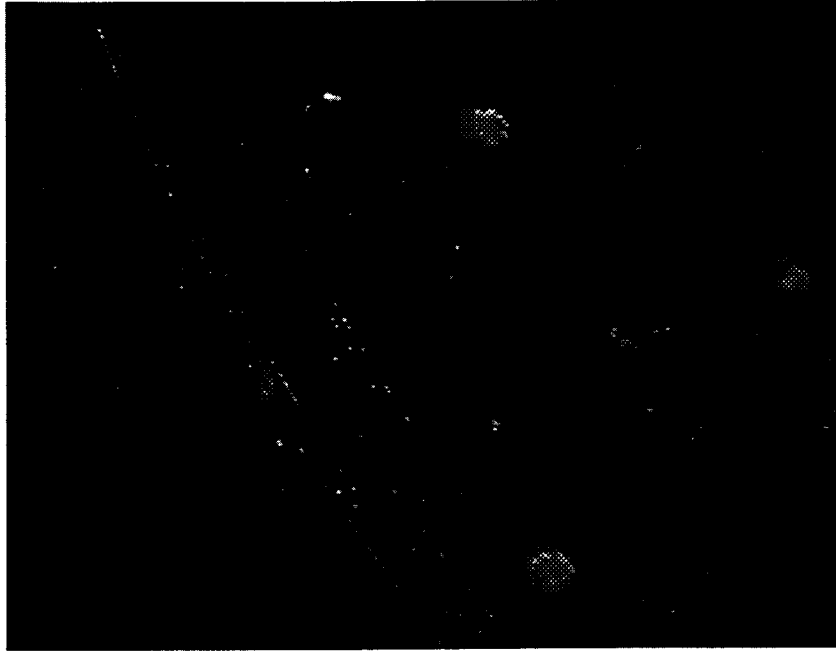


Figure 13. Copper Seal at Essentially Zero Load

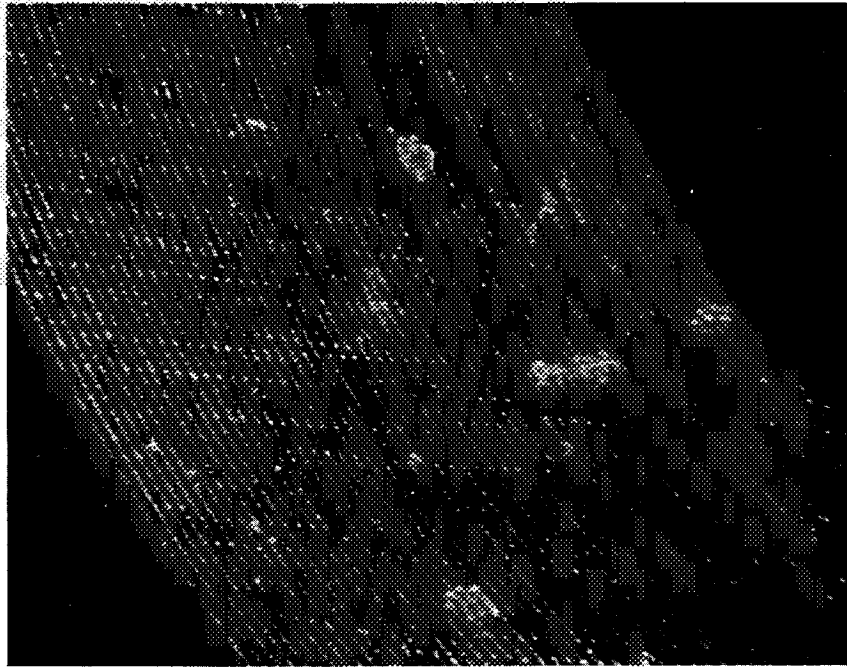


Figure 14. Copper Seal at 1140 Pounds Load (Nominal Stress - 13,000 psi)

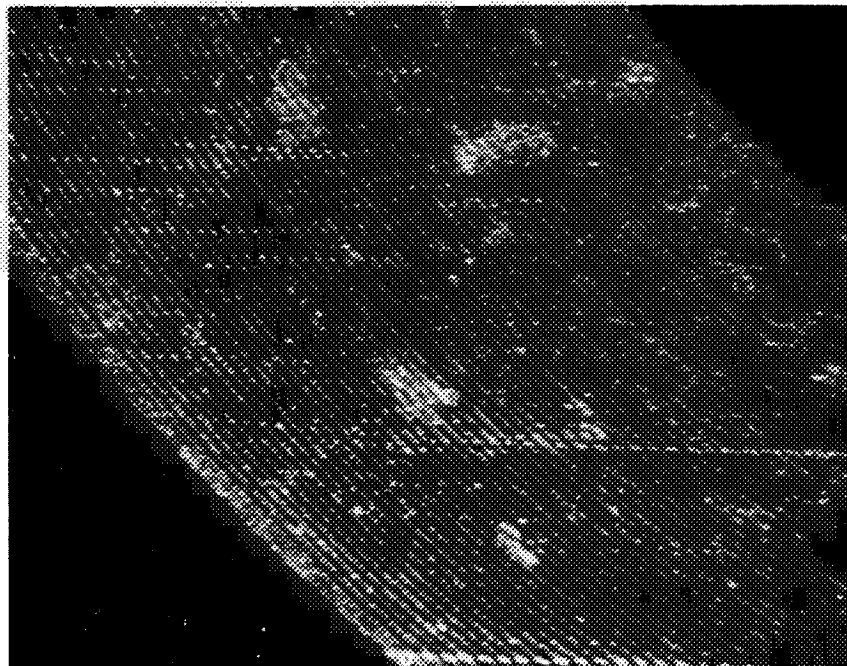


Figure 15. Copper Seal at 4560 Pounds Load (Nominal Stress - 52,000 psi)



Figure 16. Initial Application of Seal Load = 570 Pounds, Nominal Stress $\approx 0.55 S_y$



Figure 17. Initial Application of Seal Load = 1710 Pounds, Nominal Stress $\approx 1.65 S_y$

initial application of load has plastically deformed the ring. It is no longer of uniform thickness and is thinner at its inner and outer radius. Thus, contact is first made near the middle of the seal width. The fine pattern of that area which is in contact, Figure 18, is essentially identical to that shown in Figure 17, and to that which resulted in Figures 19 and 20 as reloading progressed. The technique to check for variations in fine pattern detail was the use of a transparent negative film of one figure. This was superimposed over a transparent positive film of the second figure. If the films are carefully aligned, light areas on one film coincide with darker areas on the second film. A large area of "uniform grey" is observed in the areas where both figures have identical fine detail. A mismatch in fine detail produces either a lighter or darker small area which is easily picked out. A slight mismatch in alignment produces interesting patterns with a three-dimensional effect. Thus, for example, it was first learned that the fine detail was essentially identical, but the piece of lint had shifted several mils between the load removal and reapplication. In Figures 19 and 20 a dark area is shown toward the lower left end of the lint indicating no contact. This is a mold or cavity embossed into the aluminum surface by the lint on the first application of load. This is significant in demonstrating the sensitivity of surfaces being damaged by contamination, including contaminants not usually considered particularly hard or abrasive.

Figure 21 shows the pattern for a lathe turned silver ring at light loading. Contact is heaviest at the edges as expected for elastic deformation. However, for reasons not yet understood, the patterns in Figures 22 through 24 show plastic deformation and obliteration of the tool marks starting near the center of the contact area and extending gradually to the edges. It is hypothesized that friction characteristics of the metal against the glass may enter into the explanation.

Surfaces other than lathe turned have also been examined. Figure 25 shows a surface lapped to about 1/2 microinch CLA roughness and under a very low nominal stress. A slight motley effect is observed, indicating all the areas within about 1 microinch of contact, but not all at the same distance. One tool mark which was deeper and not lapped out is visible at the inner edge. The light specks in the upper right are due to dust in the optics and should be disregarded. Figure 26 shows a coarser lapped surface. The almost complete lack of oriented patterns is apparent. A few "scratch lines" exist in random directions.

A directional pattern would be expected when observing ground surfaces. Figures 27 through 30 show the progress of making contact with a surface ground aluminum seal. Even at a nominal stress of 19,500 psi, potential leak paths which extend across a major fraction of the seal width can be picked out.

The technique of observing true area of contact is also applicable to opaque nonmetals. Figure 31 shows the contact made by a rubber O-ring

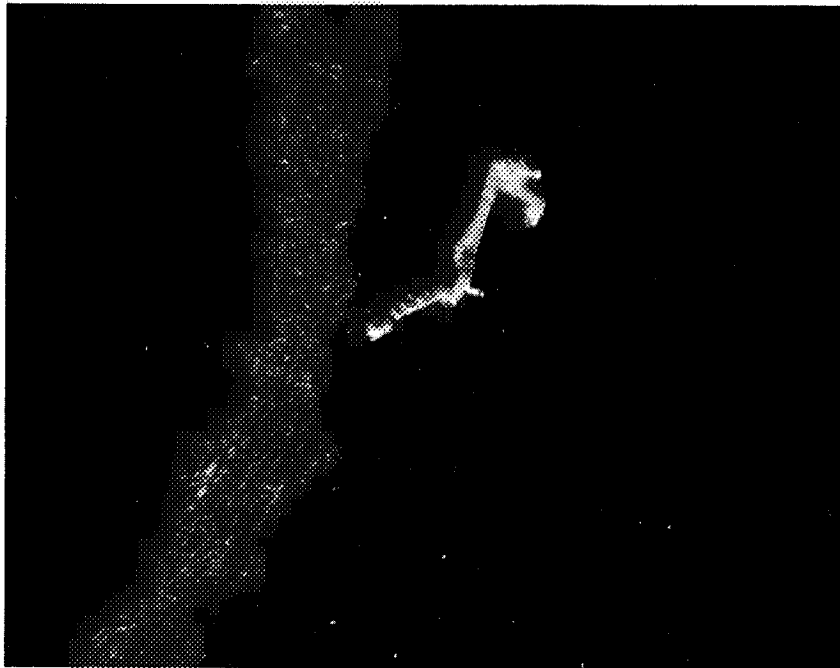


Figure 18. Reapplication of Seal Load = Nil



Figure 19. Reapplication of Seal Load = 570 Pounds, Nominal Stress $\approx 0.55 S_y$

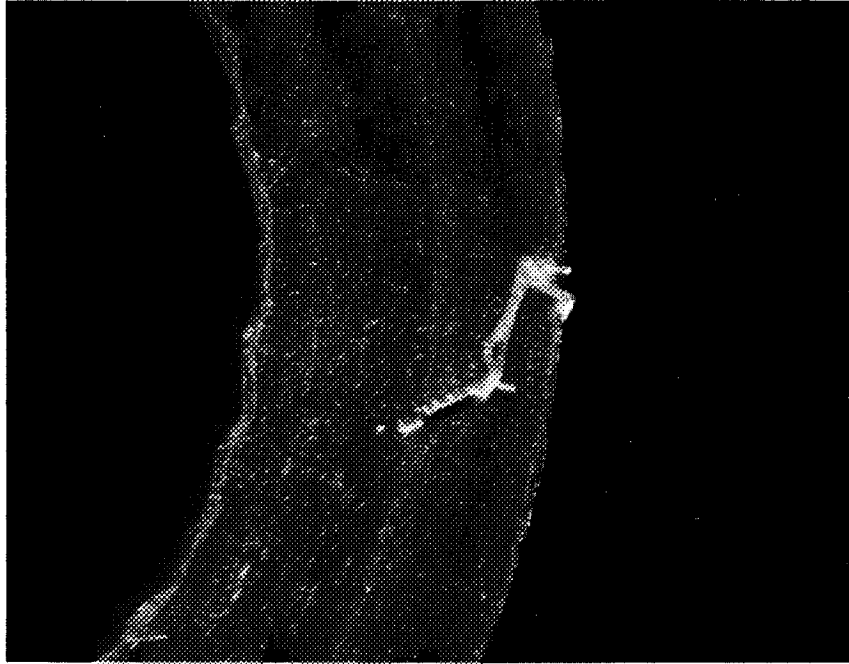


Figure 20. Reapplication of Seal Load = 1710 Pounds, Nominal Stress $\approx 1.65 S_y$

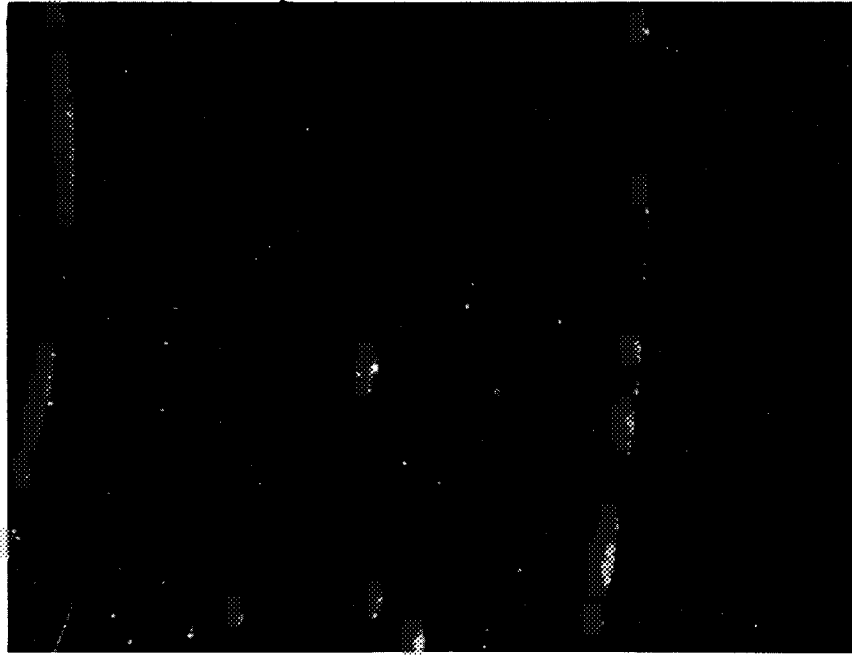


Figure 21. Contact Pattern of Fine-Turned Silver Seal, Estimated Load One Pound, Initial Roughness Approximately 9 Microinches CL

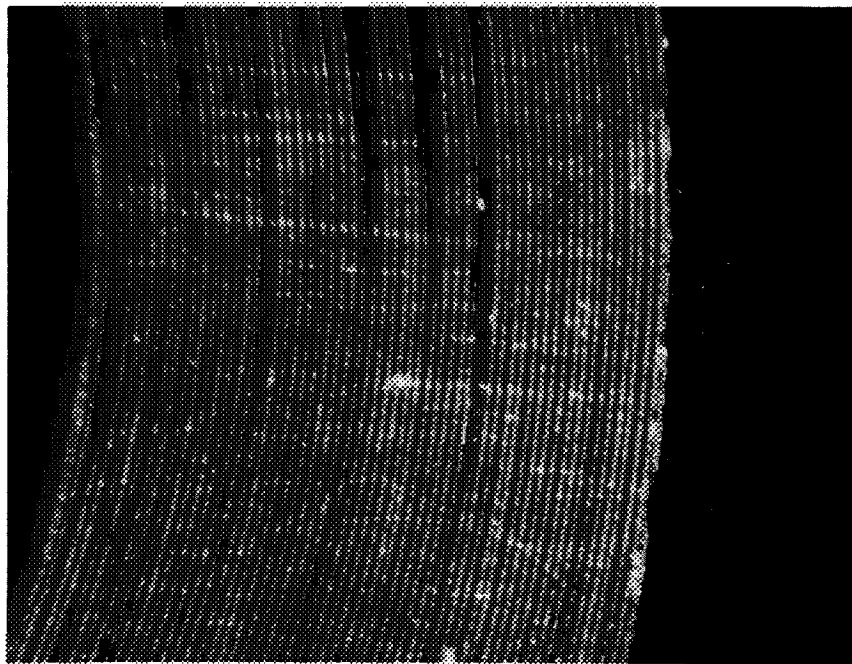


Figure 22. Contact Pattern of Fine-Turned Silver Seal at Nominal Stress of 2160 psi

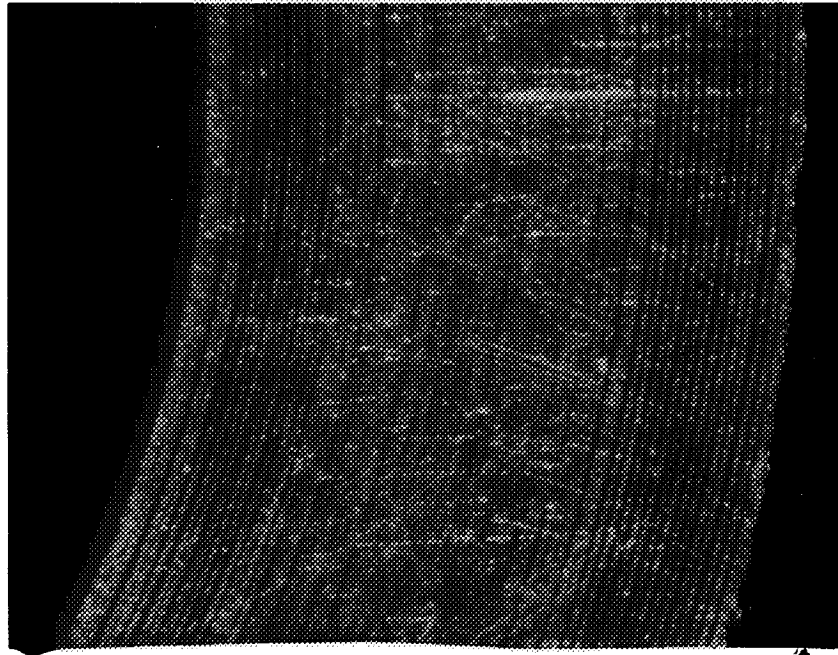


Figure 23. Contact Pattern for Fine-Turned Silver Seal at Nominal Stress of 19,500 psi

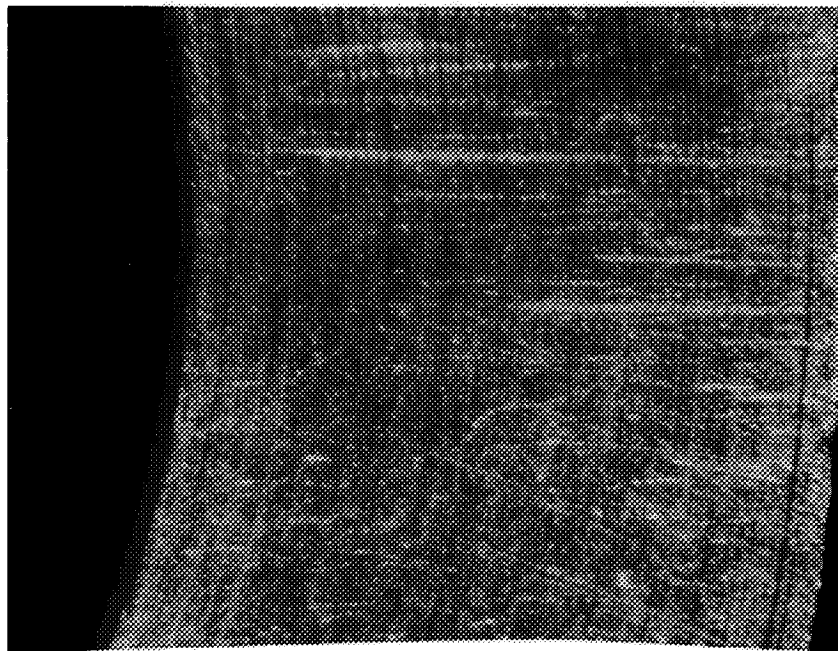


Figure 24. Contact Pattern for Fine-Turned Silver Seal at Nominal Stress of 30,199 psi

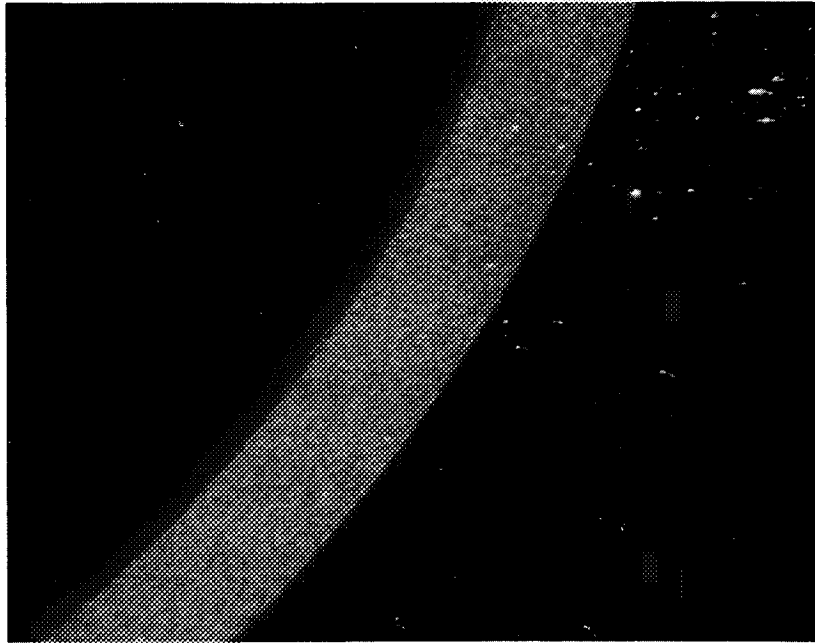


Figure 25. Pattern for A286 Seal at Estimated One Pound Load. Nominal Stress = 58 psi

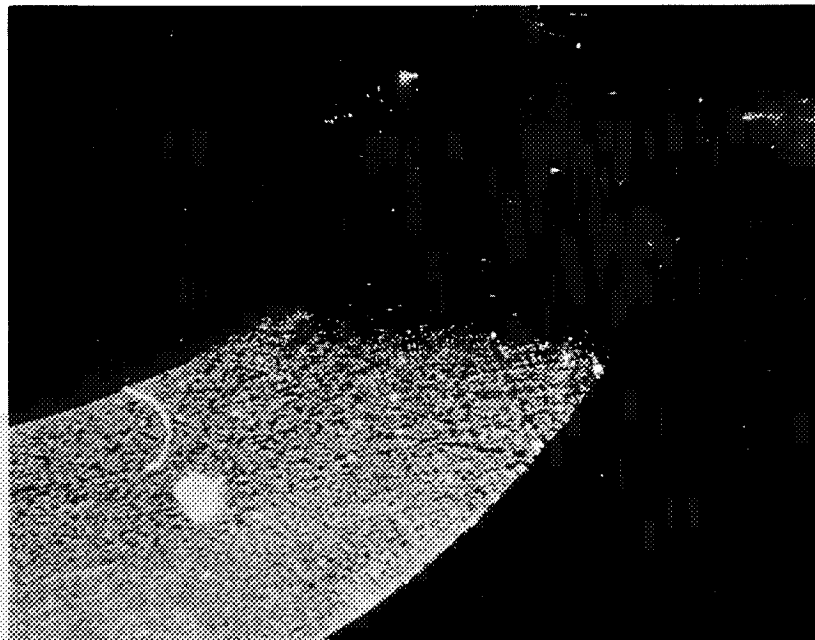


Figure 26. Contact Pattern of Lapped Aluminum Seal

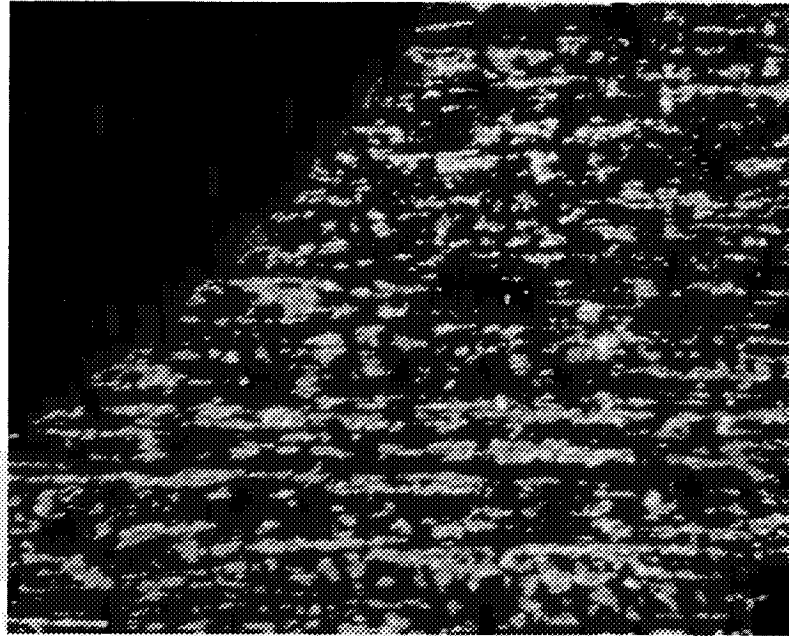


Figure 27. Contact Pattern for Surface Ground Aluminum Seal at 570 Pounds Load. Nominal Stress = 6500 psi. Initial Roughness = 50 Microinches CLA

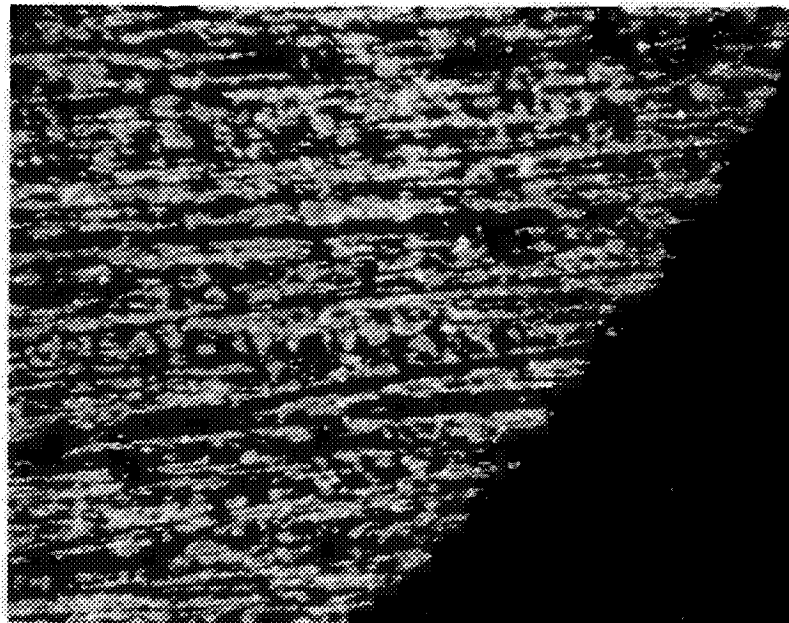


Figure 28. Contact Pattern for Surface Ground Aluminum Seal at 1140 Pounds Load. Nominal Stress = 13,000 psi

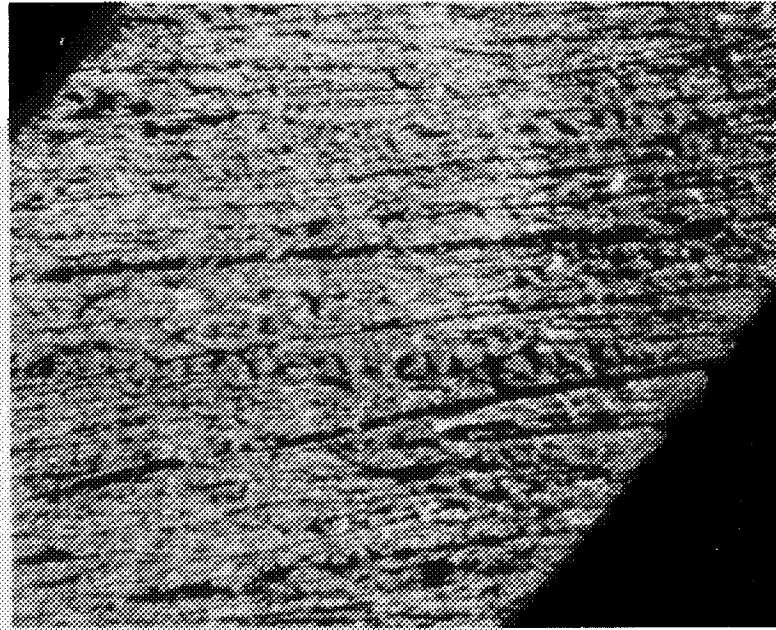


Figure 29. Contact Pattern for Surface Ground Aluminum Seal for 1710 Pounds Load. Nominal Stress = 19,500 psi

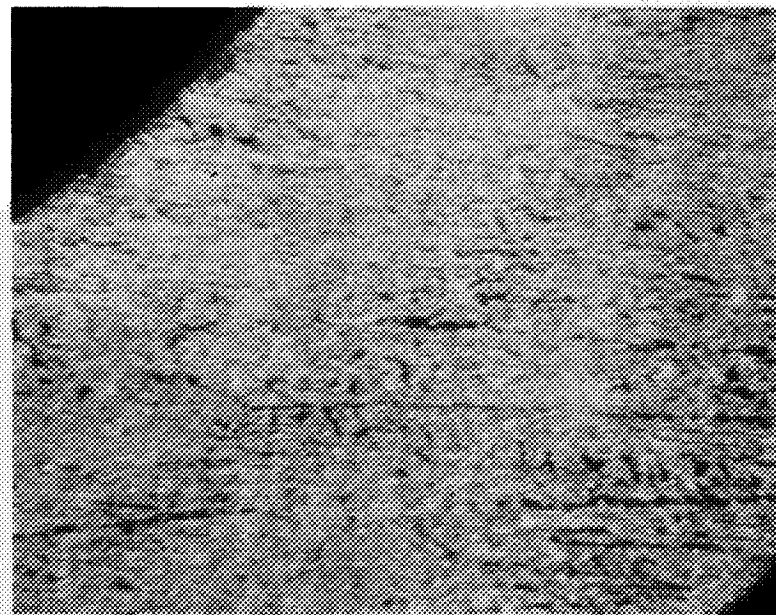


Figure 30. Contact Pattern for Surface Ground Aluminum Seal for 2280 Pounds Load. Nominal Stress = 26,000 psi

under very light load. It is unusual because tool marks apparently have been transferred from the mold to the rubber and appear in the picture. These are usually not observable. The horizontal scale of dimensions is visualized by noting that the pitch of the tool mark is about 0.002 inch. The ring had a 9/16 inch inner diameter and a 1/16 inch cross-section diameter. Under a modest load, the contact area spreads to about 0.013 inch wide. Contact is almost complete as shown in Figure 32. A trace of the valley between ridge lines is still present, and a few "pits" in the order of 0.001 inch in diameter are visible. Figure 32 illustrates why a rubber O-ring has the capability of sealing fluids so readily when properly applied. It conforms easily and in minute detail to the mating surface.

O-rings are sometimes coated with Teflon to give them improved sliding characteristics. However, Figure 33 shows that such a surface may not be capable of conforming in minute detail to effect a leak-tight seal even under appreciable load. The O-ring illustrated had a 5/8 inch outer diameter and a 3/32 inch cross-section diameter and as shown, is compressed to a point where the apparent area is 0.044" wide, or about half the cross-section diameter. The explanation is found in the rubber, which deforms and does not exert sufficient force to cause the stiffer plastic coating to conform in fine detail. The prime effect of increasing pressure is simply to further deform the rubber and increase nominal seal area, but makes very little change in the fine details of true contacting. The opposite of this effect has been utilized for some time; soft metals are plated over harder less yielding metals to improve sealing. Silver and gold plate have long been used as sealing surfaces.



Figure 31. Rubber O-Ring. Light Load

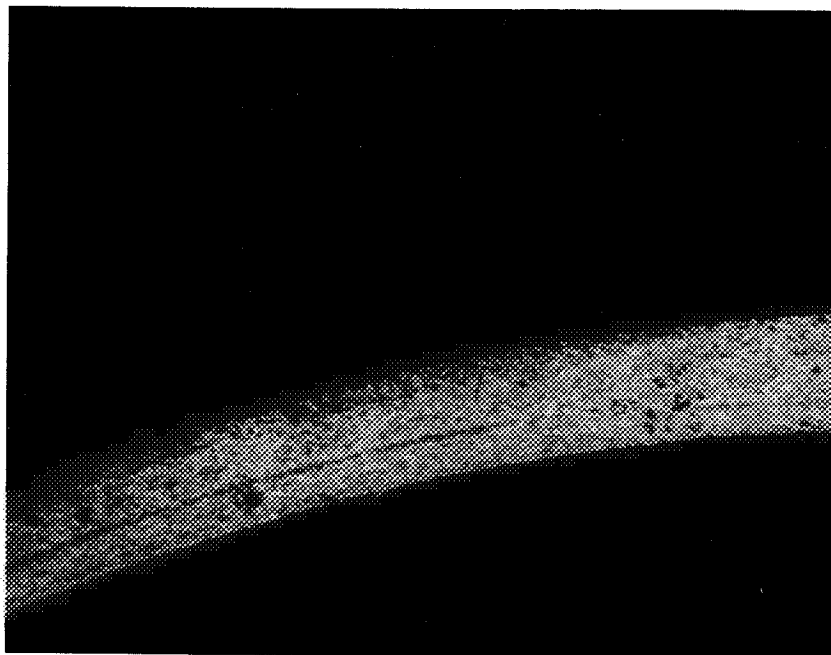


Figure 32. Rubber O-Ring. Higher Load



Figure 33. Teflon Coated O-Ring. Heavier Load

Section 6

LEAK DETECTION AND EVALUATION OF SEAL PARAMETERS WHICH AFFECT LEAKAGE

INTRODUCTION

Leak detection and seal evaluation are discussed at length in this section.

Briefly, a summary of the four major areas of investigation are as follows:

- Hydrogen Sulfide Individual Leak Path Investigation -- the feasibility of using hydrogen sulfide gas to determine leak paths by reacting with the seal. This would form a colored oxide and provide optical detection of leak paths.
- Repeatability of Data Investigation -- the degree of repeatability that can be obtained in a typical, experimental leak test.
- Seal Width Studies -- tests conducted to observe the effect on sealing of various widths of annular gasket seals.
- Nuclei Leak Detection Studies -- evaluation of a nuclei leak detection technique.

HYDROGEN SULFIDE INDIVIDUAL LEAK PATH INVESTIGATION

Efforts to locate individual leak paths using a reactive gas mixture were undertaken in this study. The actual leak path or paths exist locally and are extremely small in a sealing surface-gasket system. Much of the gasket is in firm contact with the sealing surface. The introduction of hydrogen sulfide gas into a helium leak study apparatus made paths or areas of leakage noticeable because of their discoloration. The gas penetrated the voids and reacted with the metals forming the seal system to form easily seen sulfides.

This method allows the following to be determined:

- The size and number of leak paths
- A minimum width of a gasket
- The true area of contact necessary to obtain a seal
- An appraisal of the actual mechanisms of flow existing in a seal

Procedure and Tests

Preliminary tests had shown that a hydrogen sulfide-air mixture discolored silver to the extent of easy observation. The leak test facilities were modified to allow a mixture to be injected into the high pressure helium.

A conventional leak test was conducted using a silver gasket and allowing hydrogen sulfide to pass through the existing leak. The test procedure was as follows:

1. A leak rate of approximately 10^{-4} atm cc/sec was established at an internal pressure of 100 psi and the required normal stress. At this time, only helium existed in the system.
2. The helium was shut off and the pressure allowed to drop to atmospheric.
3. Hydrogen sulfide and air were injected into the system at slightly higher than atmospheric pressure.
4. The system was then re-pressurized with helium to 1100 psi. A helium-air-hydrogen-sulfide mixture existed in the sealed cavity.
5. This mixture was allowed to pass through the existing leak for approximately two hours.
6. The internal cavity was purged with helium several times to eliminate any remaining trace of hydrogen sulfide.
7. The system was leak checked again to determine whether the hydrogen sulfide reduced the leak to any extent.
8. The gasket was then removed from the apparatus and inspected visually under high magnification.

An initial test was made using this procedure. A flat pure silver gasket with a 0.9375-inch inside diameter, a 1.1875-inch outside diameter, and a 0.03-inch thickness, was compressed between two aluminum sealing surfaces. The sealing surfaces were circumferentially machined and the silver gasket was radially ground. The visual results of this test are shown in Figures 34 and 35. Figure 34 shows a low magnification photomicrograph of the silver gasket. The gasket curvature can be seen, along with the original radial grind marks. The circumferential indentations formed in the surface from its contact with the sealing surface is also visible. Figure 35 shows a higher magnification photomicrograph of the inner edge. The discolored surface is the dark area near the edge of the photograph.

If the gasket is viewed across one or two circumferential traces, it will be noticed that the discoloration has ceased. Two possible reasons for this are:

- The hydrogen sulfide-silver reaction caused a diminution of the leakage rate
- No hydrogen sulfide remained in the cavity upon completion of the test

It was not known for what time period the hydrogen sulfide-silver reaction took place.

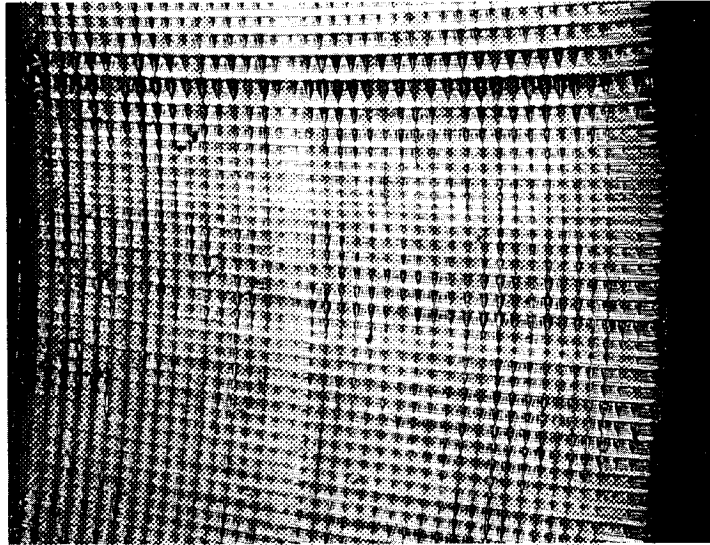


Figure 34. 30X Photomicrograph of Silver Gasket. Gasket Originally Radially Ground, then Mated with Circumferentially Machined Sealing Surface

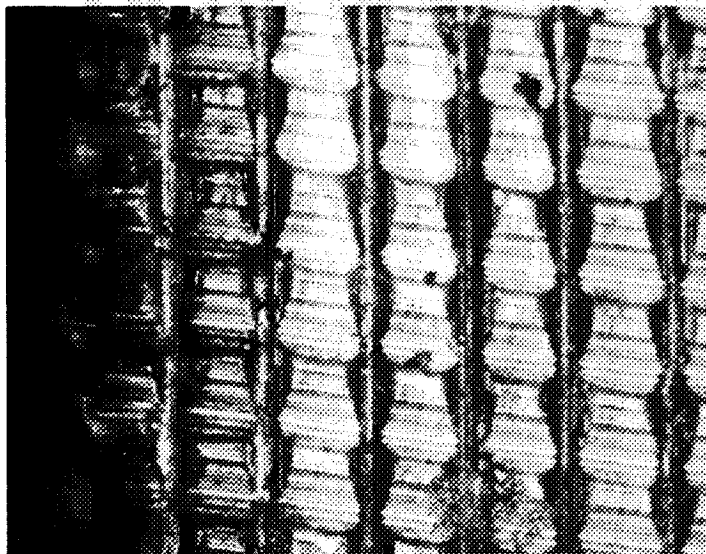


Figure 35. 150X Photomicrograph of Same Silver Gasket as Above. Note Inner Edge, Caused by Reaction with H_2S

Tests were made where a predetermined air-hydrogen sulfide mixture was introduced into the test cavity in a known quantity for a specified period of time. The first test utilized a pure silver gasket between 2024 aluminum sealing surfaces. A hydrogen-sulfide-oxygen mixture (equal parts of each) was injected into the system at one atmospheric pressure. The cavity was then pressurized to 200 psi with helium to insure that the hydrogen sulfide was exhausted prematurely. During the 6 hour test, the cavity was re-charged with hydrogen sulfide every one and one-half hours. The results with the silver gasket were disappointing. A 10^{-4} atm cc/sec leak had been established prior to the injection of the hydrogen sulfide. At the end of the test the leak rate was greatly diminished; however, no discoloration due to the hydrogen sulfide could be seen. This test was therefore impractical as the concentration of hydrogen sulfide or the time needed for such a desirable reaction to take place was excessive. The second experiment, incorporating a QQC-576 copper gasket was made. An oxygen-hydrogen-sulfide mixture was used combined with helium at an internal pressure of 200 psi. The gasket dimensions were:

0.9375-inch inside diameter

1.1875-inch outside diameter

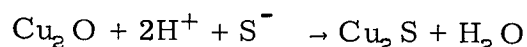
0.03-inch thickness

Both the gasket and the sealing surface were circumferentially machined with a wedge shaped tool. The results of this experiment are shown in Figures 36 through 42, by low magnification photographs of the copper gasket. The hydrogen sulfide affected areas appear black or various shades of gray. The metal which was not affected is shown as a light color. The seven photographs were taken at various locations around the periphery of the gasket. In general about two-thirds of the way from the inside diameter edge toward the outside edge has been affected by the hydrogen sulfide. The hydrogen sulfide has come in contact with the outside edge over a certain sector of the gasket.

Literature Search Investigation

A literature search was conducted to more fully understand the reaction of hydrogen sulfide with copper. The results of this search together with the special knowledge of the laboratory are combined in the following discussion of the reaction.

Evans (Ref. 4) established that the presence of air or water is needed to cause detectable reaction between hydrogen sulfide and copper. Dyers (Ref. 5) postulated that the reaction, in the presence of moisture, proceeds to form sulfide ions via ionization of the H_2S . These sulfide ions replace oxide ions in a cuprous oxide film at the metal surface.



In the absence of precise observations, the nature of the reaction under the conditions of the leak test, i. e., using oxygen in place of water, can only

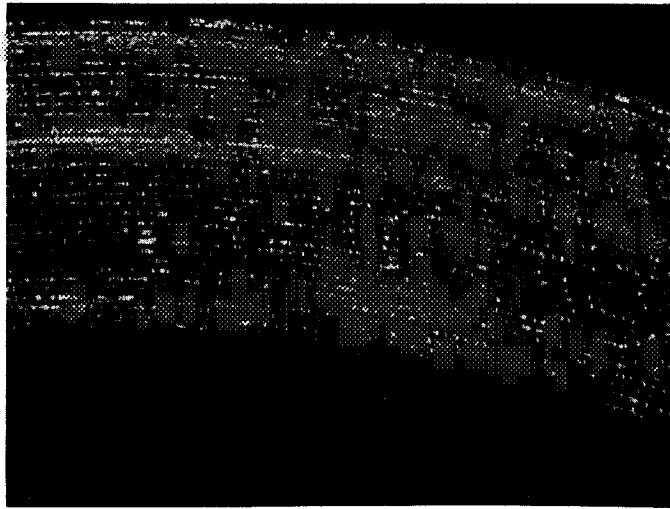


Figure 36. Copper Gasket After Leak Test Experiment in Which H_2S was Injected into High Pressure Cavity (Leak Penetrated Completely Across Seal)

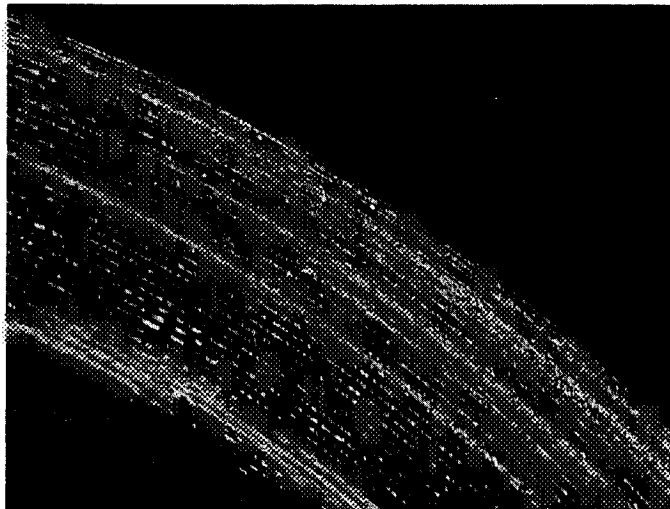


Figure 37. Copper Gasket After Leak Test Experiment in Which H_2S was Injected into High Pressure Cavity (Some Local Areas Where Leak Was Blocked)

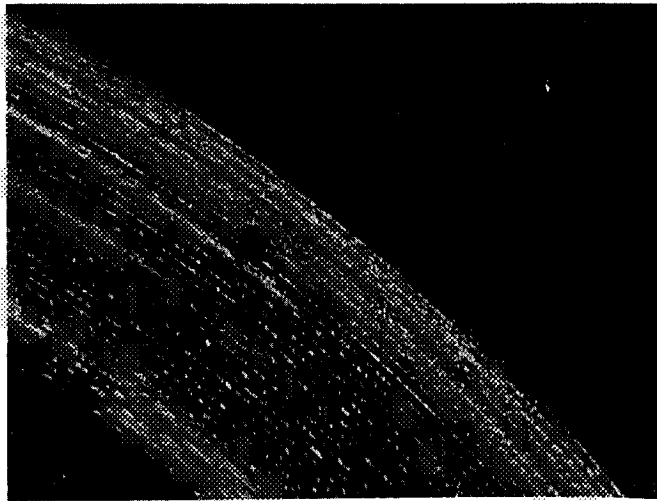


Figure 39. Copper Gasket After Leak Test Experiment in Which H_2S Was Injected Into High Pressure Cavity (Leak Penetrated Approximately 2/3 Across Seal)

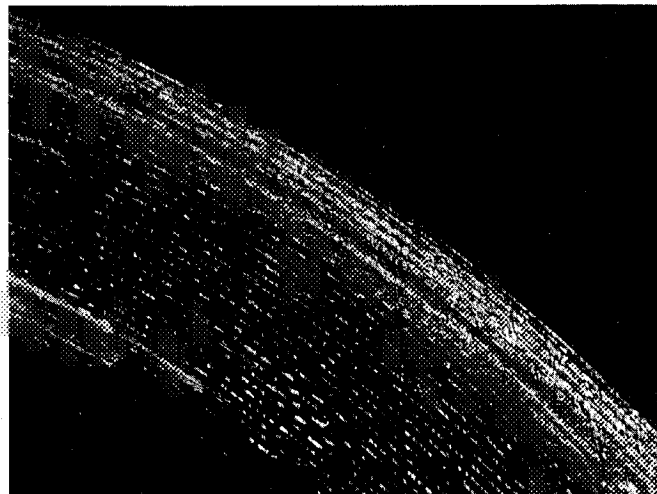


Figure 38. Copper Gasket After Leak Test Experiment in Which H_2S was Injected Into High Pressure Cavity (Outside Edge Was High Area of Contact)

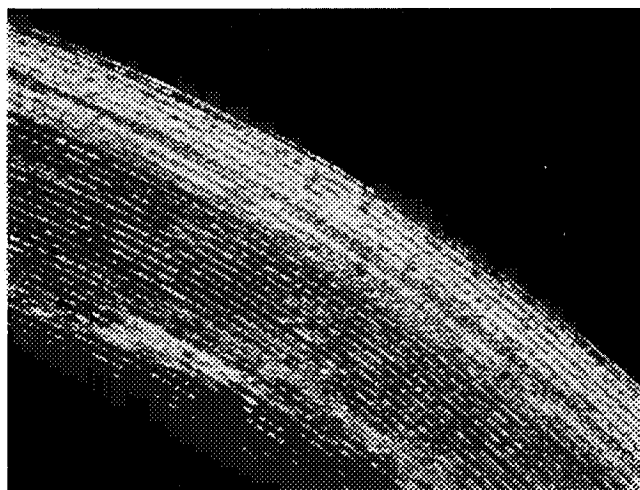


Figure 40. Copper Gasket After Leak Test Experiment in Which H_2S Was Injected Into High Pressure Cavity (Approximately $1/3$ of Gasket Area not Affected by H_2S)

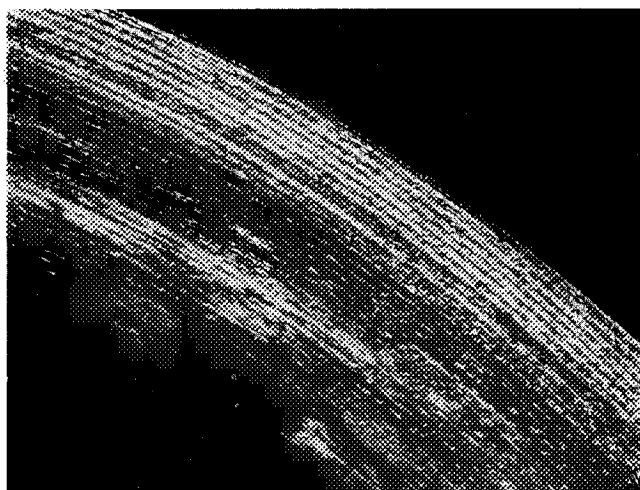


Figure 41. Copper Gasket After Leak Test Experiment in Which H_2S Was Injected into High Pressure Cavity (Local Area Plus Outside each Seated Well)

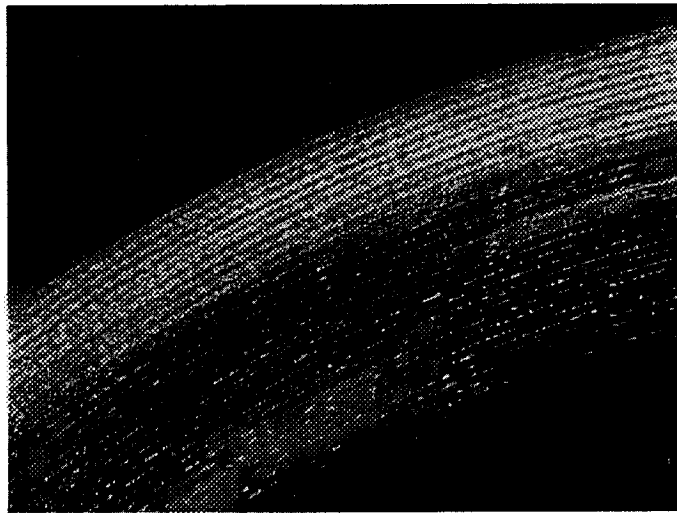


Figure 42. Copper Gasket After Leak Test Experiment in Which H_2S Was Injected Into High Pressure Cavity (No Leakage Reached Outside in This Sector)

be speculated. The above reaction may proceed through the medium of a moisture layer covering the oxide film on the metal, or moisture is absent and the reaction occurs among oxygen, H_2S , and the metal. The solid product of the reaction has been identified as Cu_2S by Kubaschewski (Ref. 6).

Cuprous sulfide exists in two crystal modifications:

The room temperature form is orthorhombic

The high temperature form is hexagonal

The transformation temperature is $100^\circ C$. The specific gravity is about 5.7, and the melting point is $1130^\circ C$ (Ref. 7). Common solvents for cuprous sulfide are nitric acid and ammonium hydroxide solutions. It is stable in air for very long periods (Ref. 5).

The mechanism of film growth and the visible effects produced are of more immediate interest. The following is an explanation of the course of the film formation. When clean copper is exposed to H_2S (in the presence of oxygen or moisture) at a given temperature, a layer of oxide and sulfide forms which thickens with time in a parabolic relationship.

$$\frac{dy}{dt} = \frac{k}{y} \quad \text{where } y \text{ is the instantaneous thickness}$$

The thickness after a given exposure time is proportional to the square root of the time. The rate-controlling step is the diffusion of one of the reactants to the reaction interface. The density of the film, however, is substantially less than that of the metal. The film occupies about 250 percent of the volume of the original metal. When the film becomes sufficiently thick, the resulting stress exceeds the strength of the film and the film cracks. Now fresh metal is again exposed adjacent to the cracks and the rate of reaction in these areas is once again rapid. This process will continue until one of the reactants has been consumed. This sulfide film was observed to be very porous, brittle, non-adherent and voluminous.

The films initially formed are adherent and tough. When the thickness is in the range to produce interference colors, the sulfide coated part is readily distinguishable against the metal surface. The sulfide films progress through the same sequence of colors which is seen when copper is heated in air or oxygen, (Ref. 4). It appears that thin films would be as readily detectable as the thicker ones.

Dyess and Miley (Ref. 5) have measured the thicknesses of sulfide films on copper as a function of color. Their observations are tabulated in Table II.

The test parameters can be easily adjusted to produce the most suitable colors for visual and photographic recording. The most important parameter is the exposure time. Temperature can have a large effect -- the rate constant varies exponentially with absolute temperature -- but normally tests are run at room temperature. The concentration of H_2S in the helium is

probably less important. A leak ten microns wide by 0.5 centimeters long requires only 8×10^{-5} cm³ of H₂S to convert a one micron (10^4 Angstroms) thick layer of copper to cuprous sulfide. Concentration will not normally be rate-controlling.

Table II

<u>Color</u>	<u>Thickness of Sulfide Film (Angstroms)</u>
First Order:	
Dark Brown	340
Red Brown	390
Purple	440
Violet	470
Blue	510
Silvery Green	815
Second Order:	
Yellow	970
Orange	1,100
Red	1,230
Purple Violet	1,450
Blue	1,540

REPEATABILITY OF DATA INVESTIGATION

The empirical leakage rate-stress-internal pressure relationships gained during the work on both NAS 8-4012 and NAS 8-11523 have been mostly results of single experiments. The reproducibility of data for a given system should be shown for empirical data to be worthy of use in predicting the response of various fluid connector systems. Many different combinations of parameters have been tried. The number of tests absolutely necessary to verify the reliability of the data is extremely high. The time-money framework of the contracts makes adequate reliability testing impossible for all combinations tested. To partially justify the use of data from a single experiment, two typical sealing systems were chosen to be subjected to a series of tests rather than single tests. The results of two series of tests do not absolutely prove the reliability of the data from all the tests. These results do give a certain amount of confidence in all of the empirical data gained, if evidencing the reproducibility of leakage responses for the two systems.

Repeatability measurements are also useful in future seal systems technology for a separable connector design. The sensitivity of the seal and its leakage to normally applied stresses is of primary importance. A connector insensitive to load removal is ideal. The third phase of the test procedure was designed to check this characteristic.

The two sealing systems chosen involved the use of flat gaskets as opposed to direct mating of two metallic sealing surfaces. One series of tests utilized a metallic gasket; the other series utilized a plastic gasket. Six tests were accomplished on each system. Each test utilized different pieces of hardware, i.e., different sealing surfaces and different gaskets. The gaskets were of the same material and were machined to the same specifications in each series of tests. The sealing surfaces were of the same material and also machined to the same specifications.

Test Procedure

The test procedure was basically the same for each series of 6 tests for the aluminum gaskets and the teflon FEP gaskets. The test was run in separate phases, using the same test apparatus designed and built on Contract NAS 8-4012 (see "Design Criteria for Zero Leakage Connectors for Launch Vehicles, Vol. 3, Sealing Action at the Interface"). The first phase was to allow a one atmosphere differential of helium pressure to exist across the gasket seal and to increase the normal stress on the gasket until a specified stress resulted. This stress was 4250 psi for the teflon gaskets; it was about 27,000 psi for the aluminum. Small variations existed in the gasket geometries because machining tolerances of these figures are approximate. The leakage levels of the gaskets was very low ($<10^{-6}$ atm cc/sec), with the attainment of this stress level. It was almost to the point of being non-detectable with the mass spectrometer leak detector whose maximum capability is the measurement of a leak down to 10^{-7} atm cc/sec. Leakage for this phase was recorded for each incremental change in applied stress.

The first phase of the test procedure was completed with the attainment of the high gasket stress level. Phase two was the introduction of incremental pressure changes. The normal load applied was kept constant. It was used to produce the stress levels previously indicated with the one atmosphere pressure differential across the gasket. The internal pressure was then increased and the leakage recorded at each pressure level until an 1100 psi pressure differential existed across the gasket seal. The normal stress on the gasket was now reduced because of the high pressure forces existing to oppose the downward load. For the teflon gasket, the net load downward was the original load with one atmosphere pressure differential (1500 pounds), minus the 1100 psi pressure acting over the internal gasket area. This resulted in a net gasket normal stress of approximately 2550 psi. The same reasoning follows for the aluminum gasket configuration.

Phase 3 of the test procedure was designed to check the sensitivity of the seal system to load removal. With the internal pressure at 1100 psi, the normal stress producing load was decreased with leakage being recorded at each level.

Aluminum Gasket Test Results

Each test was made using a flat annular EC aluminum gasket (1060-0). The gaskets nominal dimensions were: 0.9375 inch inside diameter, 1.1875 inches outside diameter, and 0.060 inch thickness. The yield stress of the material was 12,800 psi. This was determined in the test setup using linear variable differential transformer transducers simultaneously with the running of the leak test. The gaskets were compressed between type 347 stainless steel seal pieces whose surfaces were specially machined. The surfaces were machined with a wedge-shaped tool; the diametral lead was 0.002 inches per turn with a resultant finish of about 650 microinches rms. The original surface finish on the gaskets was approximately 40 microinches rms.

The results of the tests are given in two separate presentations and in the order in which the tests were made. The first set of data is shown as a series of three tests. The results of these three tests are shown in Figure 43. These data are given in terms of mass spectrometer amperage versus testing machine load. For clarity, only phase 1 data are shown. These data tell little of the absolute value of leakage rate and normal stress, but do show the degree of agreement of test results. About a five percent change exists between the smallest load, to cause a particular leakage rate (amperage), and the largest value of load for that leakage rate. These results are not conclusive, but they do tend to show that a certain amount of reliability can be accredited to a leakage test. They also show that the response of a given system will not deviate too far from the planned response.

This system is almost completely insensitive to the removal of load. The rough sealing surface finish and the soft gasket material apparently form a tight mechanical joint. A great deal of shear deformation exists in the aluminum gasket. These results are in agreement with the earlier results given in Contract NAS 8-4012. They are consistently insensitive to load removal.

A second group of three tests was made and results, along with the results of the first three tests are plotted in Figure 44. The plot is of mass spectrometer current versus testing machine load. They are directly related to leakage and gasket normal stress. Two sets of data were so close that one line suffices for both. Three lines fall very close together on the graph; these three lines represent four separate tests. One set of test data falls on each side. A generally symmetric spread of data with the most probable values near the center of the range exists. The actual scatter of stress data for a given leak ranges from 27 percent at a current of 10^{-8} amperes (approximately 4×10^{-3} atm. cc/sec.) to 10 percent at a current of 10^{-12} amperes (approximately 4×10^{-7} atm. cc/sec.). Figure 45 supplements the previous results obtained for phase 1. It is plotted as the more realistic parameters of leakage versus normal gasket stress.

The aluminum gasket tests show that reliable data can be achieved using a single representative test for a particular seal system.

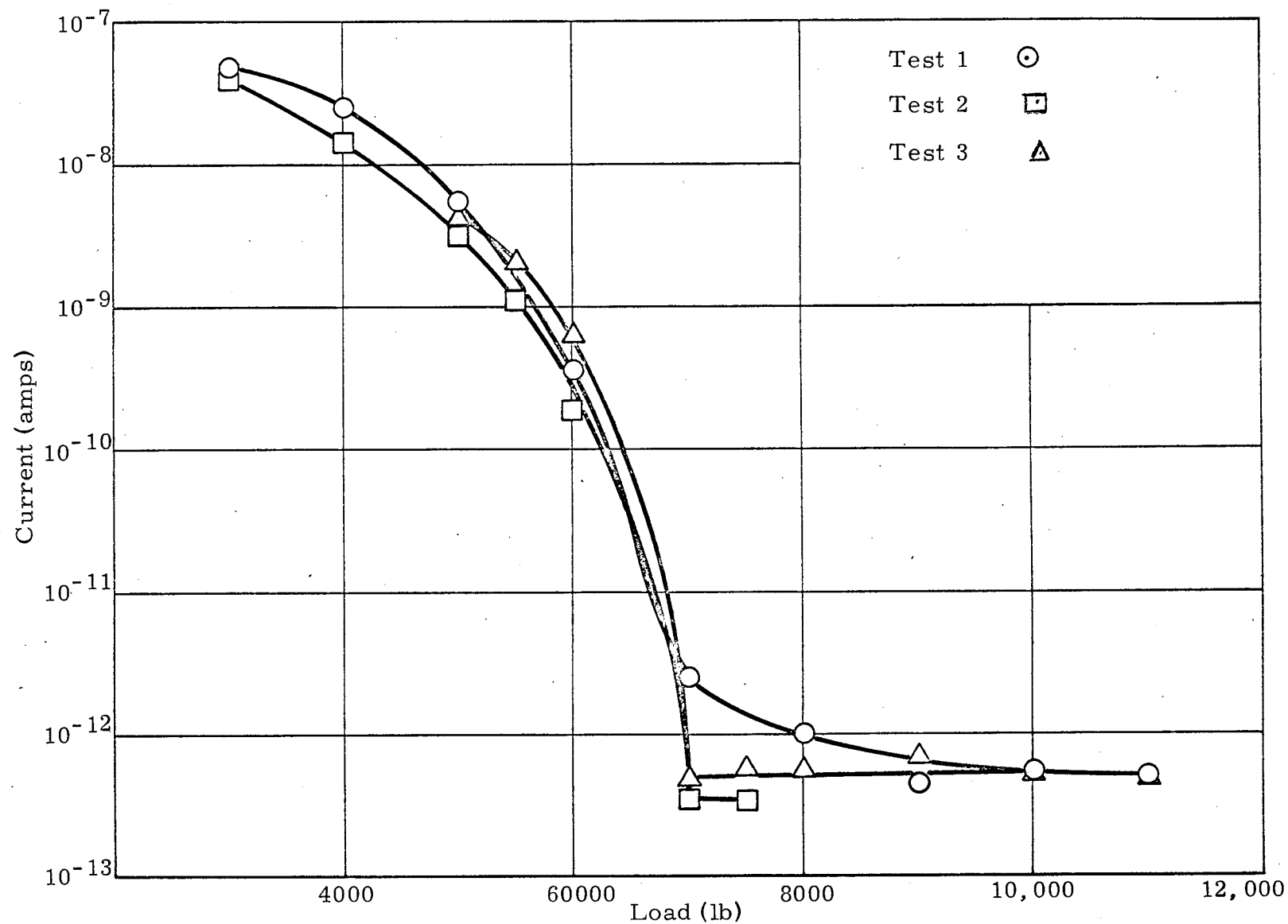


Figure 43. Leak Rate (Current) Versus Normal Stress (Load) for Three Tests With Similar Surface Finishes

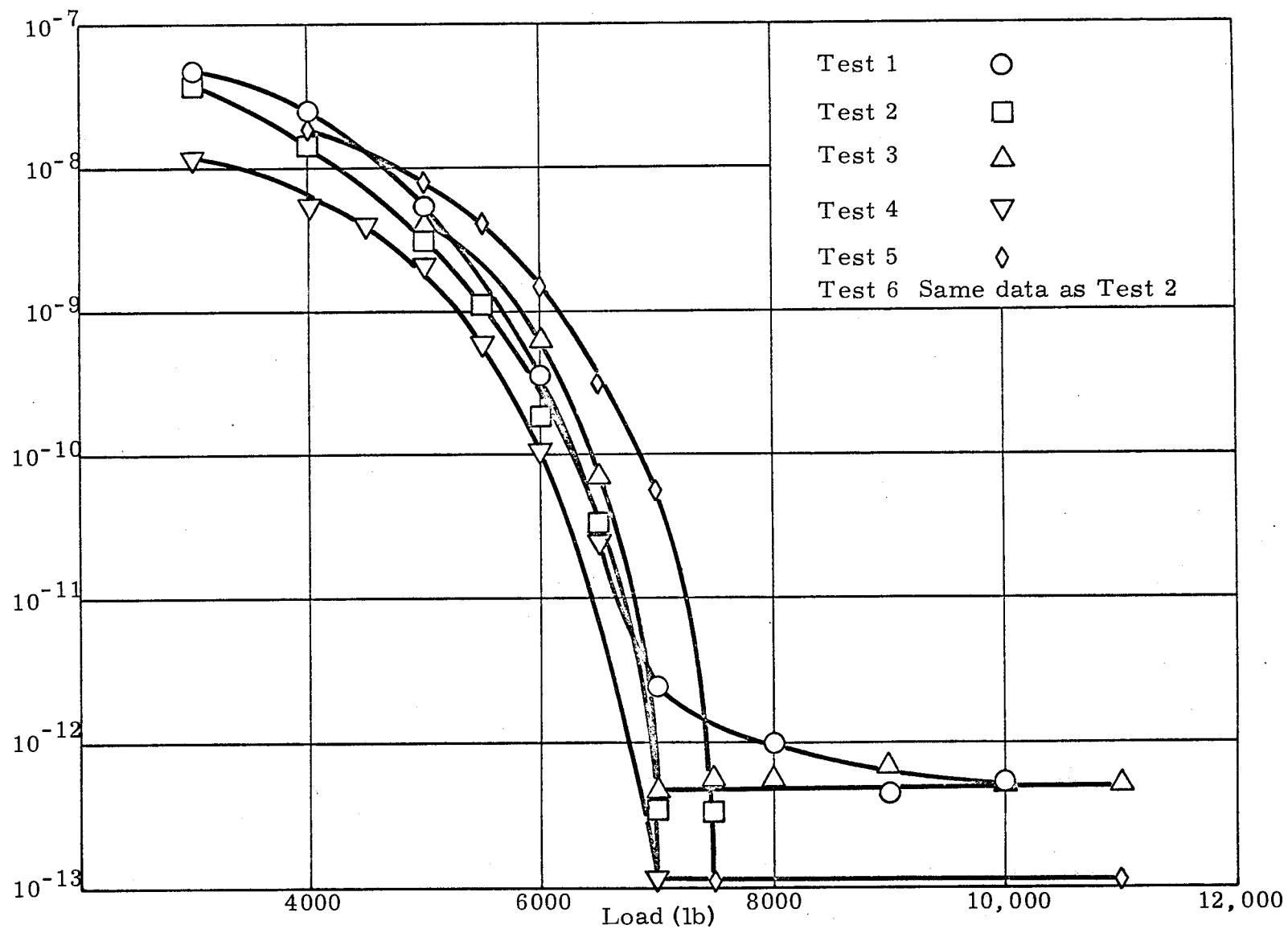


Figure 44. Leak Rate (Current) Versus Normal Stress (Load) for Three Tests With Similar Surface Finishes

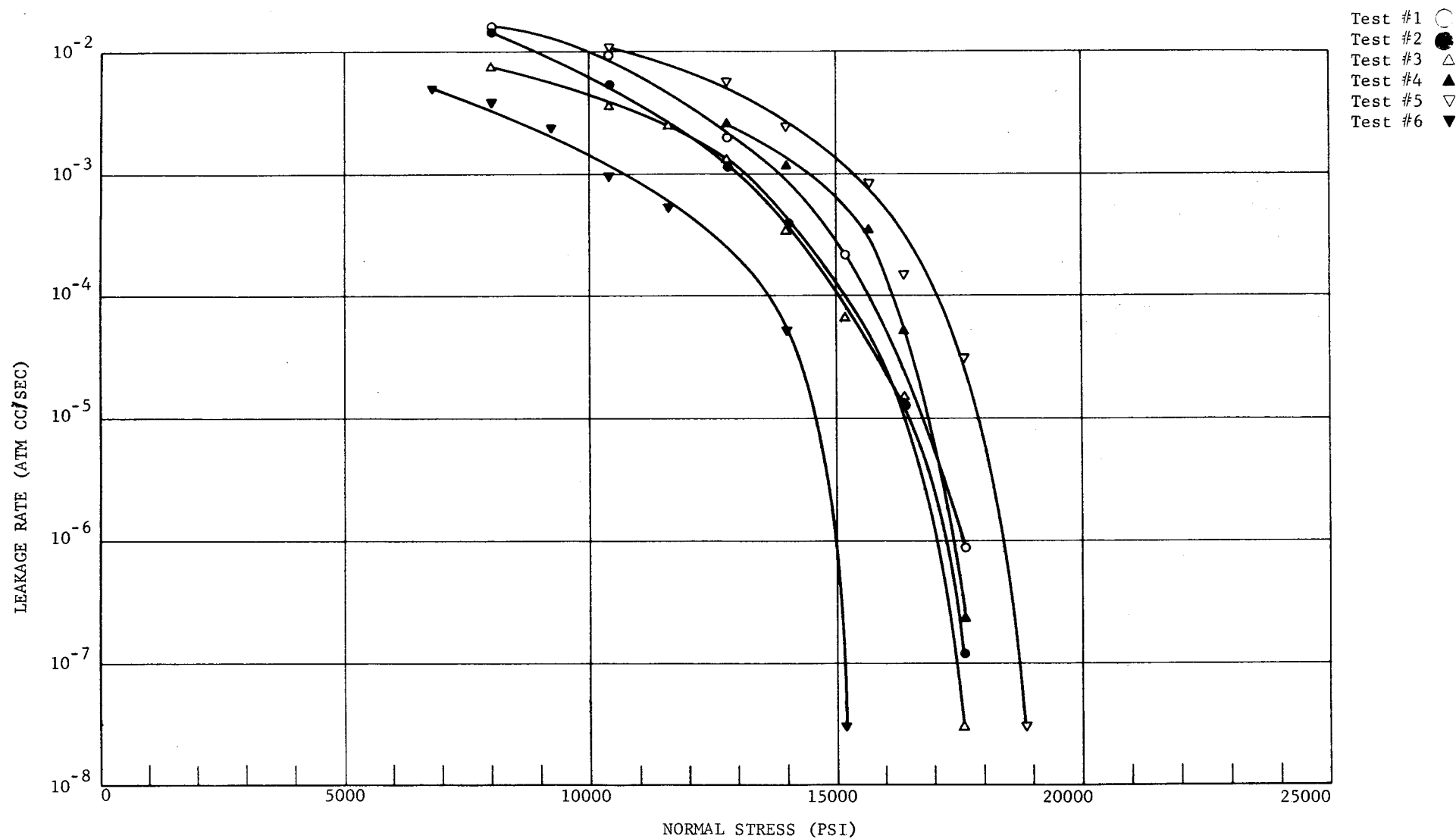


Figure 45. Leakage Versus Normally Applied Stress for Six Identically Manufactured Metal Gasket Systems (One Atmosphere Pressure Differential Across Seal)

Teflon FEP Gasket Test Results

Six teflon FEP gaskets were tested for comparative purposes under controlled conditions to maintain uniformity and obtain similar results. Each gasket was machined to about the same dimensions of 0.03 inch in thickness, 1.1875 inches outside diameter, and 0.9375 inch inside diameter. The surface finish machined onto the gaskets was not prescribed or recorded. It has been shown in previous tests that the surface finish on plastics, when the plastic is compressed between two metallic surfaces, is not an important factor in the leakage response of the system. The plastic gaskets were compressed between sealing surfaces by 2024 aluminum. The surfaces were circumferentially machined with a diametral lead of 0.002 inch. The tool used was a 120° wedge-shaped included angle. Each of the twelve sealing surfaces produced for the six tests were measured and recorded. Talysurf traces were taken on each surface. While some variation due to tool wear was evident, all of the surfaces had the wedge-shaped asperities. Each asperity was not smoothly shaped due to the inherent roughness of the tool and the vibration inherent in the machining process. The peak to valley height of the asperities on the sealing surfaces ranged from approximately 50 to 80 microinches with the average being approximately 55. For a wedge shape or saw tooth asperities distribution, the above peak to valley height is equivalent to approximately a 14-microinch CLA or a 17 to 18 rms distribution.

The results of the tests are shown in Figure 46. The spread in leakage for a given applied stress is approximately 1.2 decades for extremely low stresses. The spread is reduced to approximately one-fifth of a decade as the stress is increased to its ultimate value. This represents extremely good duplication. The leakage rate dropped to below 5×10^{-7} atm cc/sec in all cases when the maximum stress of 4250 psi was applied (for a pressure differential of one atmosphere). The spread in the leakage rate data for low stresses is not unexpected. Four of the six tests grouped very closely. They were within one-tenth of a decade for most of the first experimental phase. Two tests yielded much larger leakage rates. However, the data are not of great interest for the early stress increments since the stress at which the leakage can be curtailed is most important. During the second phase, the leakage response was somewhat unexpected. The data grouped together closely showing good reproduction. During the initial increase in pressure, up to approximately 600 psi, the leakage rate increased rapidly for all tests. Further increase in pressure shows a more gradual increase in leakage rate. At 1100 psi the highest leak recorded was 4×10^{-5} atm cc/sec, while the lowest was approximately 1.3×10^{-5} . During this phase, four sets of data showed the transition from rapid increase in leakage rate to smaller increases in leakage rate at approximately the same stress (the stress dropping off with increasing pressure).

Overall appraisal of the six tests showed that the data from any one of the tests would be quite adequate to use in prediction of the leakage response both during increases in stress and increases in pressure. This would be particularly true if a stress level at which a given leak were attained was to be

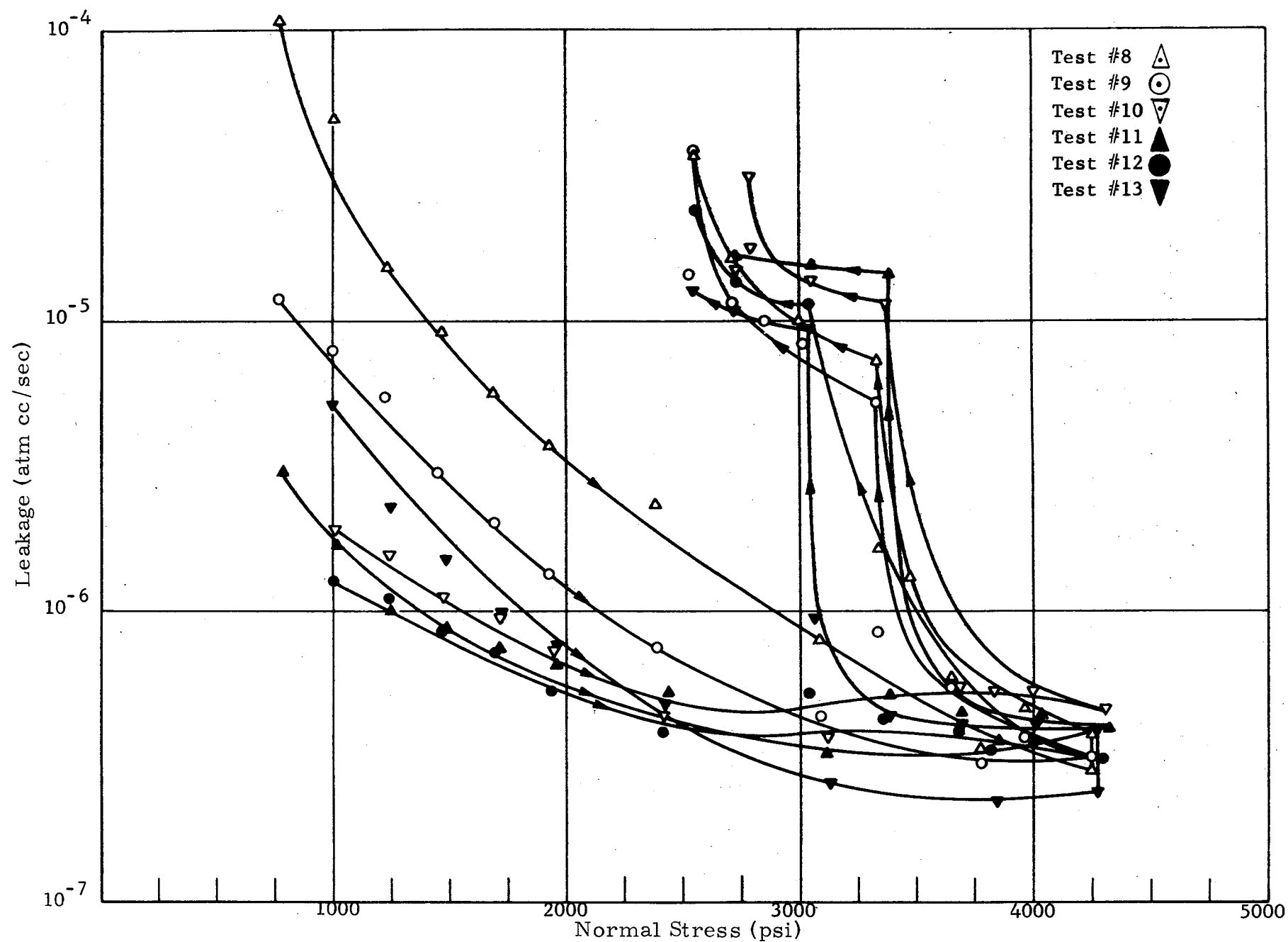


Figure 46. Repeatability of Experimental Data, Plastic Gaskets

prescribed. Similarly, the data would be adequate if a pressure (for a given stress) at which a given leakage rate was desired were to be prescribed.

SEAL WIDTH STUDIES

All of the gasketed and metal-to-metal sealing tests were accomplished with the same sealing geometries in order to allow comparisons to be made among the results gained from flat gasket tests conducted under NAS 8-4012. Where gaskets were used, their inside and outside diameters were 0.9375 and 1.1875 inches respectively. With direct metal-to-metal contact systems, high relief annuli of the same diameters were used. A great deal of data has become available on a system of a given size. This has allowed a great number of comparisons to be made between the various gasket materials, sealing surface materials, gasket finishes, and sealing surface finishes. The assumption has been made that data from such tests can be extrapolated to larger mean diameter systems. This is done by ratioing the perimeter of a newly considered system to the mean perimeter of the system previously tested.

Results from the above test, using a 1/8-inch wide seal, should not be extrapolated to cases where the gasket or seal is of a different width.

The width must have an effect on the system response since it has been shown that response of a given seal is very sensitive to the sealing surface of the stronger material in contact. The sealing area is in general made up of asperities of different sizes. Twelve asperities would exist across the seal width should a sealing surface circumferentially machined with a radial lead of 0.01 inch exist. Should the lead be 0.001 inch, one hundred twenty-five asperities would be present in the same width. Random scratches occur on even extremely well controlled surfaces and the question of length of the scratch versus gasket or sealing surface width frequently arises.

The effects of gasket or sealing surface width and their effect on the sensitivity of system response along with the establishment of a minimum seal width for a given surface finish was being studied analytically under NAS 8-4012 via a statistical analysis approach. Under NAS 8-11523, a limited number of tests have been accomplished where the width of a gasket has been altered in an otherwise identical sealing system. A narrow gasket generally requires a lower total load for sealing than a wider gasket, if a required sealing stress is necessary. It is important to know what is the lower limit of gasket width. It is of interest to know whether a gasket can be reduced to as small a width as the designer desires, or if it is limited by the probability of a continuous leakage path across the circumferential asperities. An important consideration is whether the leakage dependence on stress is the same for all of these gaskets or is an optimum value of width for a given surface finish can be attained. The parameter of the ratio of width to thickness which governs the mode of plastic flow of the gasket, is also important.

Test Procedure and Results

Seven tests were conducted in all with identical sealing surfaces of 2024-T4 aluminum used in each test. Each sealing surface had been circumferentially machined with a radial lead of 0.001 inch. The resultant surface finish had asperities of approximately 60 microinches peak to peak with a wedge-shaped appearance. The sealing surface finish was approximately a fifteen microinch rms finish or an eighteen microinch CLA finish. All tests were conducted with 1060-0 temper aluminum gaskets. Each gasket was 0.060 inch thick and had an outside diameter of 1.1875 inches. Each of the seven gaskets had different inside diameters, allowing each system to have a different gasket width. The inside diameters ranged from 0.6862 inch to 1.061 inches. This made the range of gasket widths approximately one-quarter to one-sixteenth inch. The geometry of each gasket is listed in Table III.

Table III
VARIATION OF GASKET GEOMETRIES

Test No.	Outside Diameter (inch)	Inside Diameter (inch)	Pressure Area (inch ²)	Gasket Width (inch)	Gasket Area (inch ²)	Width To Thickness Ratio
1	1.1879	1.0610	0.884	0.0634	0.222	1.04
2	1.1875	0.9997	0.785	0.0939	0.322	1.56
3	1.1888	0.9369	0.689	0.1259	0.419	2.08
4	1.1873	0.8746	0.601	0.1536	0.505	2.60
5	1.1879	0.8098	0.515	0.1891	0.592	3.12
6	1.1891	0.7496	0.441	0.2198	0.667	3.65
7	1.1890	0.6862	0.370	0.2514	0.732	4.17

The same procedure was used in all seven tests. The normal stress across a pressure differential of one atmosphere was increased until the leakage rate was reduced to below the resolution of the leakage measuring apparatus ($<10^{-7}$ atm cc/sec.). At that time, the internal pressure was increased to approximately 1,100 psi. At the high pressure differential, the stress was increased until the leakage rate was again reduced to the near zero reading. With the internal pressure still at approximately 1,100 psi, the stress was reduced incrementally, allowing the leakage rate to increase gradually with the decreasing stress.

The most noteworthy comparison between the seven systems is the effect of the gasket width on the normal stress needed to effect the seal. The only phase of the total experiment plotted was the first phase of decreasing leakage rate as a function of increasing normal stress (where a one atmospheric pressure differential is applied.) Figure 47 shows all seven tests results. No true monotonic relationship exists between required sealing stress and gasket width. At low stress levels (those which effect a seal leaking at a 10^{-3} atm cc/sec rate), the widest gasket requires the lowest stress.

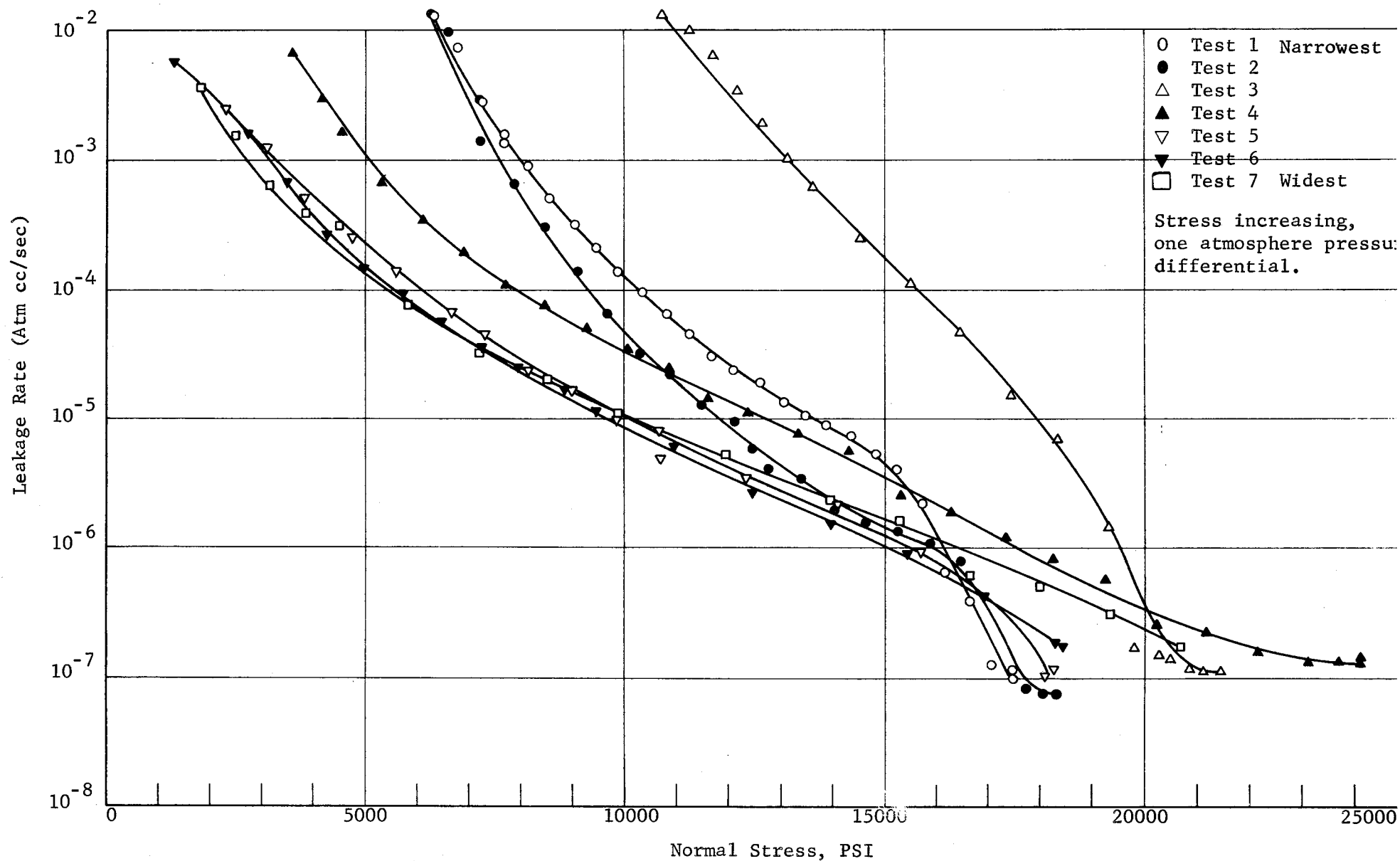


Figure 47. Leakage Rate as a Function of Normally Applied Stress for Seven Aluminum Gasketed Sealing Systems, Gasket Widths Varied

If the narrowest gasket is labeled number 1 and the widest gasket labeled number 7, the stress to seal, from lowest to highest, is in the order 1, 2, 5, 6, 7, 3 and 4. The same general trend appears for leakage rates down to below 10^{-4} atm cc/sec. Below 10^{-5} atm cc/sec, six of the leakage-normal stress curves are grouped together quite closely with only the third narrowest gasket requiring a great deal more stress than the rest. When sealing has been effected down to approximately 10^{-7} atm cc/sec, no trends can be noted between the stress-to-seal and the width of the gasket.

Leakage versus normal stress does not tell the entire story with regard to comparisons between the seven systems. One other plot of the results of the first phase of the experiment are shown. This was leakage rate versus the load per inch periphery for each gasket. The load per linear inch applied to the gasket becomes a meaningful parameter because the pressure area changed in each case, and the mean diameter of the gasket changed in each case. The results plotted in this manner are shown in Figure 48.

While the general trend of lower stress being required for greater width is apparent the trend reverses when leakage is plotted as a function of peripheral load. Four of the curves grouped together for high leakage rates (or low load levels). However, at a leakage rate of 10^{-4} atm cc/sec, the narrowest gasket requires the least load. The next narrower requires the next lower load followed by a group of four curves grouped tightly with the seventh or widest requiring still more force. The third narrowest gasket requires the most load. By the time the leakage reduced to 10^{-5} atm cc/sec, the third narrowest gasket began to move more in line with the trend and the order of increasing load is 1, 2, 5, 4, 6, 3, and 7.

At 10^{-6} atm cc/sec, considered to be an adequate seal, the trend of greater required load per linear inch for wider gaskets becomes complete and the order is 1, 2, 4, 5, 6, and 7. The data points are spread more evenly with the load ranging from approximately 1000 to 4000 pounds per linear inch. It can be seen that for this combination of sealing surfaces and gasket widths, decreasing seal widths require decreasing loads in order to effect a satisfactory seal.

The limit to which the design of narrow seals can be taken has not been found. The relationship between load per inch of periphery and seal width in the cases shown is monotonic.

NUCLEI LEAK DETECTION STUDY

There is a desire for a portable, sensitive and easy to use piece of equipment for leak detection on equipment in the field. The helium mass spectrometer leak detector is a good laboratory tool but does not satisfy the field test requirement. The portable nuclei detector cannot detect gases but many gases which could be used to detect a leak, can be combined with other gases or with water vapor to form nuclei, which can be detected. This nuclei detection system, under ideal conditions, is capable of detecting smaller amounts of tracer gases than most other systems.

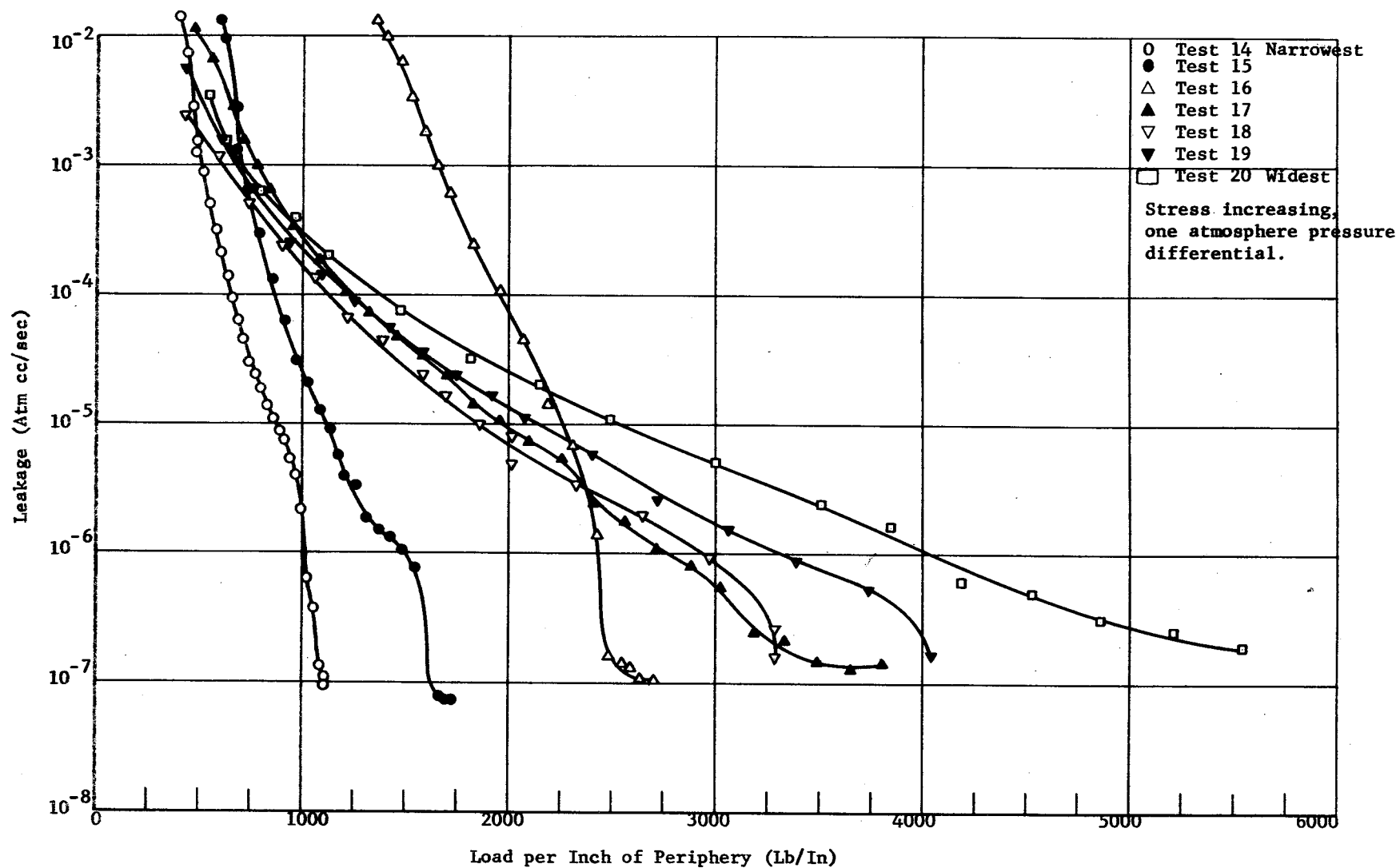


Figure 48. Leakage Rate as a Function of Load per Linear Inch of Periphery for Seven Aluminum Gasketed Sealing Systems, Gasket Widths Varied

A study of the applicability of the nuclei detection technique was carried out within our overall laboratory organization. The report of the details of this work are presented in Appendix I along with an explanation of the operation of the nuclei detector. Included are two published papers, Appendices II and III written by General Electric Research and Development Center personnel active in the development of nuclei detection techniques.

Appendix IV is in the form of three tables to convert leakage from any set of units to those of other units.

Section 7

CREEP STUDY

INTRODUCTION

The effect of creep on sealability is of special interest in high temperature fluid connectors. A creep study was made by Battelle Memorial Institute under subcontract to the General Electric Company. Peak temperature to be considered was 1700°F (although the same type of material and analysis was applicable for up to 1800°F). The temperature of 1440°F was chosen as the design temperature for a materials application study portion. A tentative maximum internal pressure of 4000 psi was established. The size range of connectors considered was from one-eighth to two and one-half inches in diameter. Flanges were considered for one to two and one-half inch sizes with threaded connectors from one inch diameter and smaller. A total life of seventy-five minutes representing twenty-five cycles of three minutes each was agreed on.

RELAXATION DESIGN OF SEPARABLE TUBE CONNECTORS

The Battelle Memorial Institute report is submitted as Appendix V of this report.

It is an investigation of creep as it applies to high temperature tube connectors. It is representative of the technology as of this date and should be modified as technology advances.

PRECEDING PAGE BLANK NOT FILMED.

Section 8

REFERENCES

1. George, R.L., Rathbun, F.O. and Coffin, L.F., "Cyclic Strain Induced Creep - A Separable Connector Design Problem," Proceedings of the Conference on the Design of Leak-tight Fluid Connectors, August 1965.
2. Moyer, G.J. and Sinclair, G.M., "Cyclic Strain Accumulation Under Complex Multiaxial Loading," Proceedings of the International Conference on Creep, Institute of Mechanical Engineers, 1963, pp. 2-47.
3. Harrick, N.J., "Fingerprinting Via Total Internal Reflection," Phillips Technical Review, Vol. 24, No. 9, 1962-1963, pp. 271-274.
4. Evans, V.R., The Corrosion and Oxidation of Metals, Edward Arnold, Ltd., London, 1960, p. 75.
5. Dyess, J.B. and Miley, H.A., Transactions of the American Institute of Mining, Metallurgical, and Petroleum Engineers, Vol. 133, 1939, p. 246.
6. Kubaschewski, O. and Hopkins, B.E., Oxidation of Metals and Alloys, 1st Edition, Butterworth, London, 1953, p. 213.
7. Hansen, M. and Anderko, K., Constitution of Binary Alloys, 2nd Edition, McGraw-Hill Book Company, Inc., New York, 1958, p. 620.

PRECEDING PAGE BLANK NOT FILMED.

APPENDIX I

APPENDIX I

THE CONDENSATION NUCLEI DETECTOR
POTENTIAL APPLICATION TO PROPELLANTS AND OXIDIZERS

by

C.B. Murphy

November 1, 1963

THE CONDENSATION NUCLEI DETECTOR POTENTIAL APPLICATION TO PROPELLANTS AND OXIDIZERS

Rather than do an injustice to the Condensation Nuclei (CN) Detector, two recent reprints from Analytical Chemistry are attached to this letter. Having assured you of the best information available, the following constitutes a brief thumbnail sketch of the instrument and its manner of operation.

The CN Detector, was originally developed for the detection of condensation nuclei in the atmosphere. (Condensation Nuclei are particulate material ranging approximately from 0.001 to 0.1 μ .) These particles were admitted, under essentially 100% relative humidity, to the reactor chamber of the Detector, and the chamber is closed off. A pump evacuates an expansion chamber, and at the appropriate vacuum level, the gas in the reaction chamber is allowed to expand into it. This adiabatic expansion results in a marked lowering of the gas temperature. Accordingly, the water content of the initial gas has to be reduced to a new 100% relative humidity level for the new temperature condition. The water has to condense on the walls of the vessel or the condensation nuclei present. Self-condensation does not occur until at least a temperature of -39°C is attained (T.E. Hoffer, J. Meteor. 18, 766-78 (1961); V.J. Schaefer, Science 104, 457-59 (1946); B.M. Cwilong, Proc. Roy. Soc. (London) A190, 137-43 (1947)). Therefore, the particles grow through water condensation to sizes sufficiently large to be counted by light scattering techniques.

Since about 1957, the Laboratory has been engaged in efforts to convert the CN Detector into an analytical instrument. This work has involved the conversion of gaseous molecules, by selective reactions, into particulate matter that would serve the same function as the condensation nuclei as described above. Typical of the many reactions that have been investigated is that between ammonia and hydrogen chloride to produce ammonium chloride. Although this will be discussed more fully in a subsequent section, it would be well to briefly describe what occurs. Neither NH₃ or HCl, alone, will generate particles in the Detector. However, their interaction produces NH₄Cl particulates which act as condensation nuclei. In the detection of NH₃ by this method, a large excess of HCl is employed. This is done for essentially two reasons:

- 1) It ensures sufficient reagent is present to react with NH₃.
- 2) The large excess statistically ensures the formation of small particles the number of which is more readily correlatable with the ammonia.

The key to the successful application of the CN Detector as an analytical instrument lies in the ability to obtain a selective reaction with a gaseous molecule that will permit the formation of

discrete, particulate material upon which the saturated vapor will condense. To date, there has been a number of examples where this has been possible. However, it must be emphasized that the detected material must be gaseous.

The condensation nuclei leak detection technique is a method which allows for a rapid (2-3 seconds) sensitive ($10^{-6} \frac{\text{CC}}{\text{sec}}$) detection of leak of many of the working fluids of interest (see attached table).

The equipment is composed of a primary detector (the condensation nuclei detector) and a convertor for the specific vapor of the fluid to be detected. The condensation nuclei detector is a well developed equipment used by the military for many years. It can take many physical forms, the most readily available is that indicated in the attached report by G.F. Skala. Equipments can operate on either AC or DC power (300 watts). The condensation nuclei detector is about a \$4,500 piece of equipment. The actual price will depend upon the specific configuration.

The convertor which changes the vapor to particles can employ many different mechanisms. The following discussion indicates the technique which appears to be the best for each fluid. The ability to detect leaks of working fluid and not a tracer is an additional advantage of the concept. The conversion technique can be made specific so that NO₂ detector would not react to say UMDH and Hydrocarbons. However, NO₂O₄ would each respond with the same convertor. The convertor is generally a very small unit (30 in³), which can be attached to the inlet probe of the condensation nuclei detector. Cost of such a unit is \$10 to \$100.

The ability to change convertor units and be capable of detecting different fluids gives a good deal of flexibility to the concept. One condensation nuclei detector on a time share basis can be used to detect any vapor for which a convertor is available.

In the list submitted, a number of the materials are not gaseous, and the technique would not be applicable. These solid materials that cannot be detected are:

Beryllium

Beryllium hydride

Aluminum

Lithium

Lithium hydride

Lithium borohydride

Aluminum borohydride

Beryllium borohydride

However, as most of these materials are fuel additives, they represent some fraction of the material that would be escaping through a leak. The other component of the fuel most probably can be detected.

Apart from hydrogen and oxygen, for which no techniques are available, methods are suggested for the detection and analysis of the other materials on the submitted list. As is noted in the respective sections, our past experience has permitted us to assess detection levels to some of the materials. It should be pointed out that currently available equipment has been made more sensitive than the equipment used to determine the cited levels. Accordingly, we now are in a position to detect such materials at even lower concentration levels.

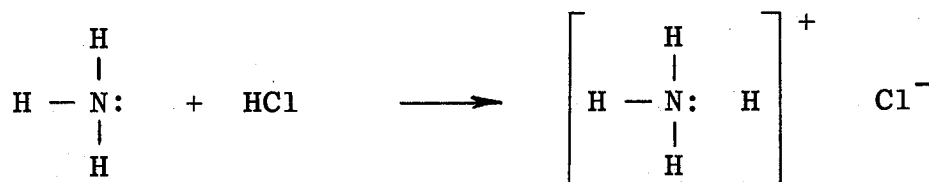
Petroleum Fractions

In this category are included RP-1, gasoline, and similar hydrocarbons. Materials such as these have been determined photochemically at concentrations of 0.1 ppm. The photochemical conversion involves modification of the basic CN Detector to the extent that ultraviolet light can be irradiated into the reaction chamber. Also, a trace of mercury is included in the chamber to assist in the photochemical reaction. Although products have not been isolated so that the precise nature of the reaction can be defined, sufficient evidence exists in the literature to speculate on what occurs under the cited conditions. Bogdanov (V.S. Bogdanov, Doklady Akad. Nauk SSSR 136, 121-4 (1961)) has exposed a number of hydrocarbons to radiolysis and has found that aerosols are formed. Studying the mercury-sensitized decomposition of 1, 5-hexadiene at 0-200 mm. at 2537A and found that several isomers of free radicals origin were derived. In the presence of air, the free radicals generated by such a process would be converted, at least in part, to oxygenated materials. It is also highly probable that such materials would form hydrates in the presence of the large quantities

of water. The subsequent adiabatic expansion would result in the condensation of water molecules on the hydrate nuclei, building the nuclei up to a sufficient size where they can be counted by conventional light scattering techniques.

Ammonia

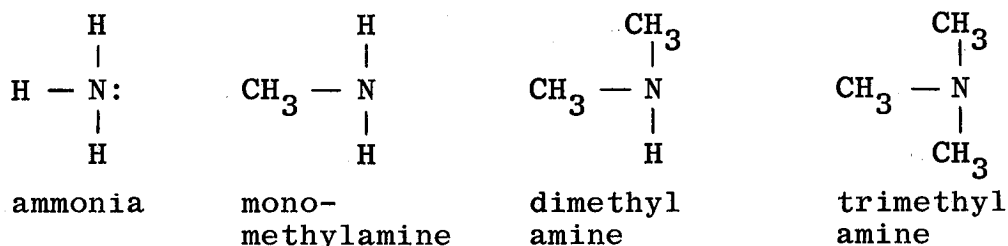
Ammonia, $\begin{array}{c} \text{H} \\ | \\ \text{H}-\text{N}: \\ | \\ \text{H} \end{array}$, has a free pair of electrons on the nitrogen atom which are available for further reaction. The ammonia molecule will react with hydrogen chloride, HCl, to form the salt NH_4Cl , ammonium chloride. This reaction occurs in accordance with the following reaction:



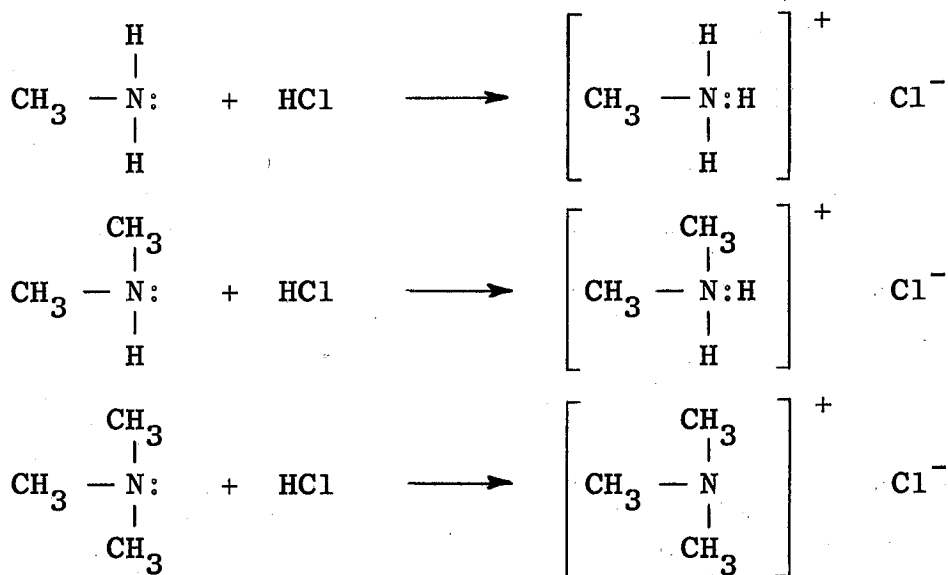
where the proton of the hydrogen chloride attaches itself to the ammonia molecule, converting it to the ammonium ion. The chlorine atom, in turn, retains the electron originally associated with the transferred proton to become a negative ion. Therefore, through this reaction a solid salt is formed from two covalent gases. In the detection of ammonia, the entrained gas is passed over a hydrochloric acid solution (which evolves HCl molecules) to form condensation nuclei which are particulate NH_4Cl . In the reactor chamber, these, together with the water vapor, are subjected to adiabatic expansion. As in the foregoing example, the water condenses on these nuclei to have them grow to a size sufficient to scatter light. This particular reaction can be applied to the detection of the acid as well as the ammonia. The detection limit for ammonia is at least at the 0.001 ppm. level. Current effort in the Laboratory is lowering this level markedly through improved techniques.

Diethylenetriamine and Mixed Amines

Amines may be considered merely as substituted ammonia molecules. For example, let us consider the various methyl amines and their relation to ammonia:

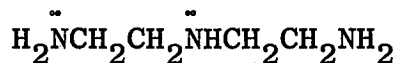


In this series of amines, the variation that exists from molecule to molecule is merely in the number of methyl groups substituted for the hydrogen atoms of the ammonia. All three amines have the free pair of electrons associated with them just as the ammonia molecule. Hydrogen chloride would react with the amines in exactly the same manner as it does with ammonia:



In this series of compounds, the basic properties of the nitrogen atom (in the Lewis theory of acids and bases, a base is a proton acceptor) increases with the increase in the number of methyl groups attached to the nitrogen atom. Accordingly, the amines would exhibit a stronger tendency to accept the proton and form the salts (as shown above) than ammonia itself. Accordingly, there is no difficulty in applying the technique described for ammonia to the detection and analysis of amines. Monoethylamine, $\text{CH}_3\text{CH}_2\text{NH}_2$, has been detected, with minimum effort, at 0.5 ppm.

Although no effort has been made to detect polyamines, no difficulties are anticipated in such a measurement. Diethylene-triamine, the compound of specific interest, has three amine groups in its molecule:



It is conceivable that each of these nitrogen atoms would react to form the trihydrochloride. However, this tendency would be minimized by the addition of each successive proton to the molecule. It may be that the actual salt species in this case would be the dihydrochloride. In any event, large excesses of hydrogen chloride are used, and calibration curves would determine the level of detection. It is presumed that it would be at least equivalent to the monoethylamine level.

Tetrafluorohydrazine

No work has been done on the detection of this molecular species. The following discussion is based on the work of others who have investigated properties and reactions of this compound. Tetrafluorohydrazine has been shown to exist in equilibrium with $\cdot\text{NF}_2$ free radicals (F.A. Johnson, Abstr. of Papers, pp. 17N-18N, 142nd Mtg., Amer. Chem. Soc., Atlantic City, Sept. 9-14 (1962)). Johnson (loc. cit.) has also shown that nitric oxide will react with the $\cdot\text{NF}_2$ free radical, and, further, that a gaseous equilibrium exists between NF_2NO and an $\text{NO-N}_2\text{F}_4$ mixture. Also, chlorine has been reacted with N_2F_4 to produce ClNF_2 . Although this latter reaction is slow at room temperature, it is greatly accelerated by ultraviolet light. It may be possible to produce a hydrate of either NONF_2 or ClNF_2 . However, a more profitable approach might consist of reacting the NF_2 free radicals with large organic free radicals (c.f. J.P. Freeman, Abstr. of Papers, 18N, 142nd Mtg., Amer. Chem. Soc., Atlantic City, Sept. 9-14 (1962)) to produce particulate material. Although no satisfactory technique is available for detection and analysis of this material, it appears that a technique, based on free radical reactions, could be developed subsequent to discussions with Rohm and Haas personnel stationed at Huntsville (i.e., Johnson and Freeman cited above).

In the highly fluorinated nitrogen compounds, such as N_2F_4 and NF_3 , no hydrochloride would be expected to form.

Nitrogen Trifluoride

Nitrogen trifluoride, NF_3 , has been employed in this Laboratory to make N_2F_4 . This has been accomplished by passing the NF_3 over copper turnings at elevated temperatures (ca. 500°C). Once N_2F_4 has been made from the NF_3 , the same detection and analysis approach as suggested for N_2F_4 (c.f. above) would apply.

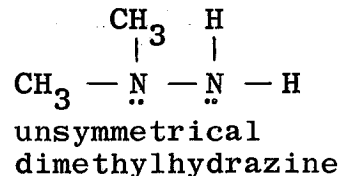
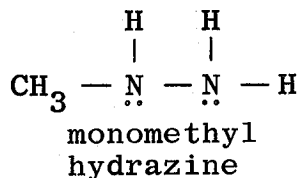
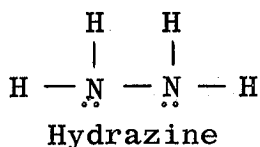
Nitric Acid

Work has been performed in this Laboratory for the U.S. Navy in which the CN Detector has been applied directly to the analysis of red fuming nitric acid. The detection limit for this analysis was found to be 0.5 ppm. with equipment that was available at that time (ca. 1957-8). Again, no analysis of the nuclei was made. However, pure nitric acid boils at $82.6 \pm 0.2^\circ\text{C}$ (J. Potier, Compt. rend. 78^e Congr. soc. savants Paris et dépts., Sect. sci. 1953, 457). Therefore, in the adiabatic expansion process, the nitric acid must be reduced to droplets, and water condenses on these to permit light scattering techniques to be applied.

A second method, i.e., reaction with ammonia to form ammonium nitrate, NH_4NO_3 , could be employed to produce solid condensation nuclei. This latter approach might permit greater sensitivity than the direct instrumental approach given above.

Hydrazine and Its Derivatives

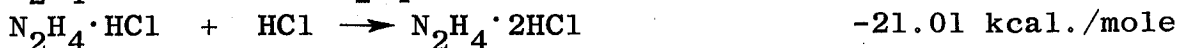
Hydrazine and its derivatives are related to ammonia in their chemical structure. The three chemical species of interest are:



Each of these compounds has two free pairs of electrons available for reaction with hydrogen chloride, and, in fact, these materials can form dihydrochlorides. If we use the heat of reaction as a criterion for reaction to occur, then the following heats of reaction have been calculated.

Reaction

ΔH_f°



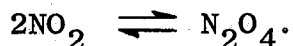
The highly exothermic character of the two reactions indicates that both materials would form, with the second reaction having a somewhat lowered tendency to occur. In the presence of a large excess of hydrogen chloride (as the CN Detector operates) it would be safe to assume that the particulate material would be the dihydrochloride salts of all three of these materials. The CN Detector technique has been applied to the unsymmetrical dimethylhydrazine and the detection limit was 0.1 ppm. In less precise work with hydrazine, itself, this same detection level was approached.

Hydrazine Hydrate

The properties of hydrazine hydrate, $\text{N}_2\text{H}_4 \cdot \text{H}_2\text{O}$, are not known to the writer to the extent that a positive statement can be made with respect to the capability of the CN Detector for detection and analysis. Its heat of formation, ΔH_f° , for the liquid state at 25°C is given as $-57.95 \text{ kcal./mole}$ (Rossini, F.D., et al., U.S. Bureau of Standards, Circular 500), indicating the compound is fairly stable. Lange's Handbook of Chemistry reports that the material has a m. pt. of -40°C , and a b. pt. of 118.5°C at 739.5 mm. In contrast, the b. pt. of hydrazine, itself, is given as 113.5°C . It would appear, from these data, that the hydrate maintains its integral composition in the vapor state. This hydrated molecule, then, would be expected to add hydrogen chloride to the unshared electron pair not involved in the hydrogen bonding with water. No serious difficulties are anticipated in detecting and analyzing hydrazine hydrate.

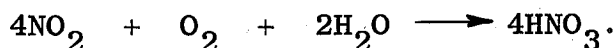
Nitrogen Dioxide and Nitrogen Tetroxide

These two materials, NO_2 and N_2O_4 , will exist as an equilibrium mixture which is fixed by the temperature and pressure. The equilibrium may be represented by



Increased pressure will force the reaction to the right, while temperature elevation drives the reaction to the left. Complete dissociation of N_2O_4 into NO_2 occurs at 140°C . At ordinary temperatures, some of both materials would exist. Accordingly, a method based on NO_2 alone would serve for the detection and analysis of both gases.

Again, work has not been performed on this material, per se. However, the reaction of nitrogen dioxide with water (the condensing medium in the CN Detector) in the presence of atmospheric oxygen to produce nitric acid is well known:



The nitric acid produced by this reaction would be capable of detection and analysis by either of the approaches discussed under nitric acid.

Nitric Oxide

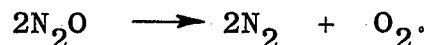
Nitric oxide, NO , is a highly reactive material. On contact with air, it would be converted to nitrogen dioxide by reaction with atmospheric oxygen:



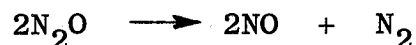
The product, NO_2 , can be analyzed by previously suggested methods.

Nitrous Oxide

Unfortunately, nitrous oxide, N_2O , is a fairly stable molecule. When cooled to -90°C , or exposed to pressures (30 atm. at 0°C ; 50 atm. at 15°C), it is converted to a liquid. Accordingly, it would not be liquified in the usual operation of the CN Detector. The latter usually attains a temperature of -12° to -14°C in normal operation. On heating, N_2O starts to decompose at approximately 520°C , and decomposition is complete at 900°C . At lower temperatures, the principal reaction is



At 1300°C , the reaction



also occurs. The latter reaction, however, occurs at such elevated temperatures that analysis based on it would appear unwarranted. A possible method is suggested below.

The application of corona to an air stream has been observed to produce nitrogen dioxide (personal comm., Dr. W.R. Browne) from the elements, nitrogen and oxygen. If corona were applied to a stream of N_2O in the presence of air, it would appear that this compound would be oxidized to NO and, subsequently, to NO_2 . (The decomposition reactions observed above were conducted without the presence of oxygen.) Further, the voltage required for this reaction might be expected to be lower than those required for synthesis from the elements, themselves, because the nitrogen is partially oxidized in the N_2O state. If the NO_2 is produced, then detection and analysis can be as described above. This approach appears to be a very reasonable one for detection of this material.

Boranes

No experience exists in the application of the equipment to boranes. However, there are approaches that would appear to merit consideration for detection of these materials. The first of these would be oxidative pyrolysis. In this approach, the air entraining the borane is carried into the equipment through a small chamber containing a platinum heating element. The borane would be oxidized to B_2O_3 , which would constitute a detectable particulate material. This approach may not be considered safe because of the heated platinum element. If such is the case, a possible approach to the detection of these materials could be made through interaction with amines. For example, trimethylboron and triethylamine react to form a white solid which melts between $-15^\circ C$ and $-13^\circ C$, with decomposition. The compound formed by reaction of trimethylboron and pyridine forms a much more stable adduct (H.C. Brown, H.I. Schlesinger, and S.Z. Cardon, J. Amer. Chem. Soc. 64, 328 (1942)), and would be the more preferred technique. Mikhailov and Bubnov (B.M. Mikhailov and Yu. N. Bubnov, Izvest. Akad. Nauk SSSR, Otdel, Khim. 1960, 1872-3) have reported the following reactions and product data:

<u>Reaction</u>	<u>Yield of Adduct, %</u>	<u>B. Pt. of Adduct, $^\circ C$</u>
$NH_3 + Bu_3B \rightarrow Bu_2BNH_2$	69.2	63-5, 15 mm.
$NH_3 + iso-Am_3B \rightarrow iso-Am_2BuNH_2$	74.7	74-5, 10 mm.
$Et_2NH + Pr_3B \rightarrow Pr_2BNEt_2$	91.9	119-22, 96 mm.

Accordingly, these products would at least form liquid nuclei that could provide means of detection and analysis. In such reactions, the $B \leftarrow N$ bond is the strongest formed, and becomes successively weaker as $B \leftarrow O$ and $B \leftarrow S$ dative bonds are formed. As the writer has no knowledge concerning the stability of the two boranes cited, i.e., B_2H_6 and B_5H_9 , the success of such an approach must remain purely speculative. However, the aluminum alkyls, which

dimerize and, in this sense, could be considered similar to the diborane, do form adducts with amines. Some of these adducts are cited below with available physical properties (N. Davidson and H.C. Brown, J. Amer. Chem. Soc. 64, 317 (1942)):

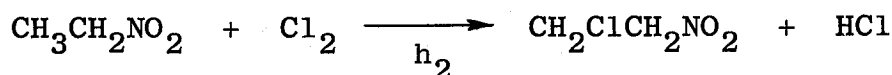
<u>Adduct</u>	<u>B.Pt., °C,</u> <u>Extrapolated</u>	<u>M.Pt., °C</u>
Me ₃ N:AlMe ₃		105
Me ₂ O:AlMe ₃	159	-29.9
Me ₃ P:AlMe ₃	189	62.5
Me ₂ S:AlMe ₃	141	

There is some justification for suspecting that boranes would react with electron-pair donors to form detectable adducts.

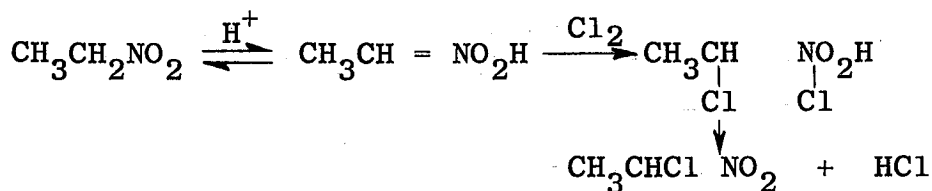
Aliphatic Nitro Compounds

The two aliphatic nitro compounds of interest are nitromethane, CH₃NO₂, and tetranitromethane. Both compounds would be liquids at room temperature: H₃CNO₂ - m.p. -29°C, b.p. 101.7°C; C(NO₂)₄ - m.p. 13°C, b.p. 126°C [H.B. Haas and E.F. Riley, Chem. Rev. 32, 387 (1943)]. The adiabatic expansion process associated with the operation of the CN Detector would appear to ensure the formation of droplets of both materials. The polar nature of the nitromethane especially should assist in the condensation of water on this molecule. However, this approach affords little selectivity in the measurement.

It would appear that the nitromethane, CH₃NO₂, could be determined by the introduction of chlorine with or without ultraviolet light. The review on the chemistry of nitroparaffins by Hass and Riley (loc. cit., p. 405) gives the following reactions with nitroethane:



However, in the presence of acid (HCl formed by the above reaction), a competing reaction can occur:



If the hydrogen chloride is formed by either mechanism, this material can produce ammonium chloride on addition of NH₃ (see discussion on ammonia).

Another reaction that might be employed is that between nitromethane and formaldehyde in the presence of a trace of base. This reaction would proceed as follows;



Ammonia may act as the base.

Other reactions are also possible. However, no previous effort has been made to detect such chemical species.

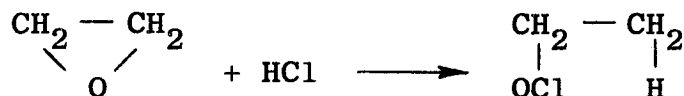
Ethylene Oxide

Ethylene oxide, $\text{CH}_2 - \text{CH}_2$, contains a three membered ring

which is subject to rupture under the influence of acidic or basic reagents:



This reaction would be anticipated from reactivity of epoxy resins.

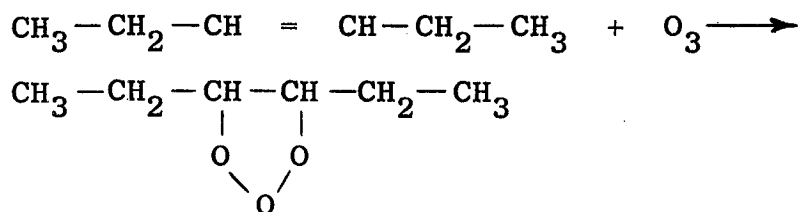


The ring rupture would be accelerated by the use of acid. Although hydrolysis might also be anticipated as occurring, this reaction should be significantly lower than the HCl reaction. The chlorohydrin would be expected to be detectable, but no data is available as to how this compound or ethylene oxide reacts in the CN Detector. The effects of these reactions can be easily assessed.

Ozone

The unsaturated hydrocarbons do not form particulate matter in the CN Detector without the employment of a conversion technique. Therefore, it appears that these materials could be employed for the development of a method for detection and analysis of ozone.

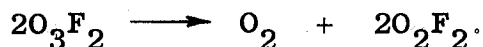
These materials would react with ozone to form the ozonide



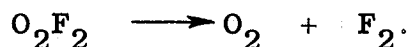
The subsequent hydrolysis of the ozonide (in the reactor chamber) would lead to the formation of two aldehyde molecules, $\text{CH}_3\text{CH}_2\text{CHO}$, and a molecule of hydrogen peroxide. This technique has not been applied previously, and experimentation would be required to determine the most satisfactory unsaturated material to use. The polar aldehyde would hydrate in the reactor through hydrogen bonding.

Ozone Fluoride

The properties of ozone fluoride, O_3F_2 , have been described by Kirshenbaum and Grosse [A.D. Kirshenbaum and A.V. Grosse, J. Amer. Chem. Soc. 81, 1277 (1959)]. This compound decomposes with heat evolution at 115°K according to the following equation:



At approximately 200°K , O_2F_2 dissociates quantitatively with the liberation of heat:



Therefore, the detection and analysis of this material would be essentially the same as fluorine, itself, which is described in a subsequent section.

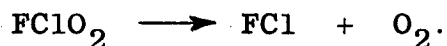
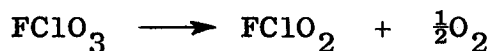
Oxygen Difluoride

A method for analysis and detection of oxygen difluoride would appear possible from the work of Peregud and Boikina [E.A. Peregud and B.S. Boikina, Zhur. Anal. Khim. 14, 141-2 (1959)]. These investigators have analyzed air for this material by passing the air through a solution of KBr. In the reaction, free bromine was liberated. This could be detected in the reactor through formation of ammonium bromide, through interaction of Br_2 , H_2O and NH_3 .

Perchloryl Fluoride

According to Mandell and Barth-Wehrenalp [H.C. Mandell, Jr., and G. Barth-Wehrenalp, J. Inorg. & Nucl. Chem. 12, 90-4 (1959)], ammonolysis of perchloryl fluoride is possible. They report that ClO_3F reacts with aqueous or liquid NH_3 to produce NH_4F and NH_4NHCO_3 . Although they employed sodamide, NaNH_2 , as a catalyst to accelerate this reaction, it would appear that the reaction would take place to some extent under the conditions usually employed to form ammonium salts in the CN Detector. It would appear that this reaction would be applicable to detection and analysis.

Decomposition at elevated temperatures (465° - 495°C) will decompose this material in accordance with the following equations [R. Gatti, J.E. Sicre and H.J. Schumacher, Z. physik. Chem. (Frankfurt) 23, 164-89 (1960)]:

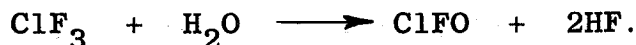


The FCl should be detectable in the same manner as proposed for F_2 (c.f. subsequent section on F_2).

Interhalogen Compounds

The interhalogen compounds chlorine trifluoride, ClF_3 , and bromine pentafluoride, BrF_5 , are included in this category. Chlorine trifluoride has a b.p. of 12°C while BrF_5 has a b.p. of 40°C . [R.B. Heslop and P.L. Robinson, Inorganic Chemistry, p. 375, Elsevier Publication Co., N.Y., N.Y., 1960].

Chlorine trifluoride reacts with water to produce a red liquid, ClFO , which crystallizes at -70°C . [H.J. Emeleus and J.S. Anderson, Modern Aspects of Inorganic Chemistry, p. 329, D. Van Nostrand Co., Inc., N.Y., N.Y., 1945]. It must be assumed that hydrogen fluoride is the other product of this reaction, i.e.,



This reaction would certainly take place in the CN Detector reactor. The HF would react with NH_3 to form ammonium fluoride.

Although no precise method is available for the analysis of BrF_5 , this compound is also very reactive [H.J. Emeleus and J.S. Anderson, loc. cit., p. 330]. It is assumed that this material, like ClF_3 , also will react with water to form HF, and that, through subsequent reaction with NH_3 , particulate NH_4Cl can be produced for detection and analysis of this material.

Fluorine

There appears to be a very simple procedure for the detection of fluorine. This gas reacts with water to produce hydrogen fluoride and oxygen, in accordance with the following equation;

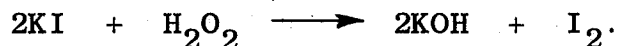


The hydrogen fluoride produced in this reaction (in the CN Detector reactor) will react with NH_3 to produce particulate NH_4F which would be detectable and permit analysis of fluorine.

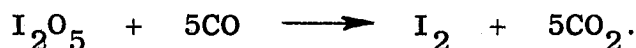
Hydrogen Peroxide

This oxidizer is decomposed by increasing temperature and several other factors [M.M. Roth, Jr., and E.S. Shanley, Ind. Eng. Chem. 45, 2343-9 (1953); see also Becco Chemical Division, Food Machinery and Chemical Corp., Bulletins 36 and 46]. The oxidation characteristics of H_2O_2 have long been used to detect the presence of this material. Partington [J.R. Partington, A Textbook of

Inorganic Chemistry, p. 302, Macmillan and Co., Ltd., London, England, 1937] reports that one part of peroxide in 25 million parts of water may be detected by the liberation of iodine from potassium iodide, and using starch to develop the blue color. The equation for this reaction is as follows:



By passing the gas entraining H_2O_2 through a KI solution, the iodine liberated in this reaction will be carried off by the air flowing through the system. Although not detected from this suggested type system, the CN Detector has been used to detect iodine levels in the application of the Schutze reagent. This latter material is I_2O_5 absorbed on silica gel, and is used to determine carbon monoxide, i.e.,



Although a number of methods have been suggested for the analysis of most of the list of materials submitted, it must be recognized that this list is far from exhausting the possibilities. The wide variation in detection possibilities merely has been indicated.

It is assumed that all of these materials would not be present at the same time. Rather, two of these materials would be present at one time. Under such circumstances, the CN Detector would provide the means for detection and analysis of the materials. If techniques and calibrations can be obtained for the materials listed of the same order as for ammonia, then detection limits would be of the order of 10^{-12} g/cc.

To develop a family of detectors for the fluids indicated in Table I would require the following steps.

1. A modification of the basic condensation nuclei detector to meet environment concentration. Portable units of 50 pounds or less could be designed. If a fixed installation is desired where only one condensation nuclei detector monitors many points, the presently designed equipment could be used.
2. The development and calculations of specific conversion units for the vapor to be detected would be required. In some cases this would be a minimum of effect since conversion methods are known such as for NO_2 - UDMH -- but for others such as Pentaborane basic investigation would be required to determine the conversion method and design the convertor.
3. Studies of the atmospheric ambients in which leak detection was desired would be necessary to be able to

provide a system and operating instructions which would be specific for this family of vapors and not affected by ambient particles or other vapors.

The duration of such a program would depend upon the specific application details. A minimum program could be completed in three months; a maximum one in six.

SUMMARY TABLE I

<u>Material</u>	<u>Detectable</u>	<u>Not Detectable</u>	<u>Limits of Detection (ppm)</u>
Petroleum Fractions	x		0.1
Hydrogen		x	---
Hydrazine	x		ca 0.1
Unsymmetrical Dimethyl- hydrazine	x		0.1
Aerозine	x		ca 0.1
Hydyne	x		ca 0.1
Ammonia	x		0.005
Diborane	x		?
Pentaborane	x		?
Aluminum Borohydride		x	---
Beryllium Borohydride		x	---
Lithium Borohydride		x	---
Hydrazine Hydrate	x		ca 0.1
Alcohols and Ethers	x		5.0
Ethylene Oxide	x		?
Mixed Amines	x		ca 0.01-1.0
Nitromethane	x		?
Aluminum		x	---
Beryllium		x	---
Beryllium Hydride		x	---
Lithium		x	---
Lithium Hydride		x	---
Oxygen		x	---
Ozone	x		ca 5.0
Hydrogen Peroxide	x		ca 0.1
Nitrogen Tetroxide	x		ca 0.5
Nitric Oxide	x		ca 0.5
Nitrogen Dioxide	x		ca 0.5
Nitrous Oxide	x		ca 0.5
Nitric Acid	x		0.5
Tetranitromethane	x		?
Fluorine	x		ca 1.0
Oxygen Difluoride	x		ca 1.0
Chlorine Trifluoride	x		ca 1.0
Bromine Pentafluoride	x		ca 1.0
Perchloryl Fluoride	x		ca 0.1
Nitrogen Trifluoride	x		?
Tetrafluorohydrazine	x		?
Ozone Fluoride	x		ca 1.0

Note: 1 ppm. sensitivity would allow for detection of a leak of 2×10^{-5} cc./sec if direct access to the leak were possible.

APPENDIX II

APPENDIX II

Condensation Nuclei, a New Technique for Gas Analysis

FRANK W. VAN LUIK, Jr., and RALPH E. RIPPERS¹

General Engineering Laboratory, General Electric Co., Schenectady, N. Y.

► A technique for measuring low concentrations of gas involves conversion of gas molecules to liquid or solid submicroscopic airborne particles which act as condensation nuclei. Water vapor is caused to condense on the particles. The opacity of the vapor is then measured and related by electrical signal to gas concentration. This procedure has many promising applications in air pollution control, toxic vapor detection, and continuous monitoring of chemical processes.

A NEW technique for measuring low gas concentrations by conversion of gas molecules to condensation nuclei has been developed. An understanding of the technique is dependent upon a knowledge of condensation nuclei and the capability of the condensation nuclei detecting instrument. A general description of the technique is given here, with a few of the possible instrument configurations that have been developed in the authors' laboratory and some performance test data on selected gases.

CONDENSATION NUCLEI

Condensation nuclei are liquid or solid submicroscopic airborne particles, each of which can act as the nucleus for the formation of a water droplet. Their size may vary from 0.001 to 0.1 micron in diameter.

Such nuclei are found in nature in concentrations ranging from a few hundred to hundreds of thousands per cubic centimeter of air. The nucleus derives its name from its triggering role in causing supersaturated water vapor to condense into droplets. Water vapor in air that contains no particles will not start to condense into droplets until the air is 800% supersaturated.

¹ Present address, Computer Department, General Electric Co., Sunnyvale, Calif.

Figure 1 indicates the amount of saturation required to cause a "particle" of water to act as its own condensation nucleus (1). While the major proportions of condensation nuclei are not water particles, once the growth process is triggered by a nucleus and water molecules start to attach themselves to it, the growing particle acts as if it were completely composed of water. Therefore, Figure 1 can serve as a guide in suggesting the amount of supersaturation required to condense water on particles of a given size.

The time required for the growth process—from nucleation at about 0.001-micron diameter to visible droplet about 1.0 micron in diameter—is about 7 milliseconds (7).

This speed of growth is an important factor in the instrumentation, and the growth in size of the particle provides an amplification factor which can be utilized to give extreme sensitivity to this method of measurement.

THE DETECTOR

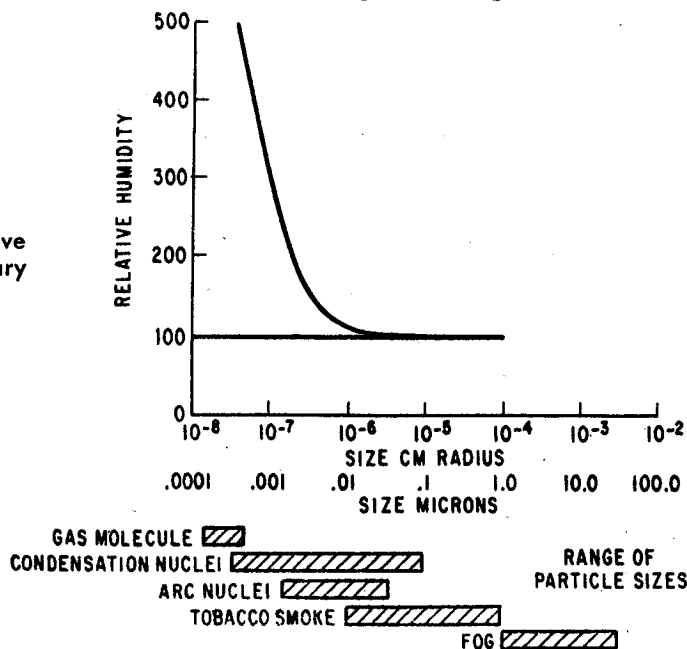
The condensation nuclei detector (CND) developed by General Electric Co. is shown schematically in Figure 2 (6). The power supplies, rotor driving mechanisms, and auxiliary equipment are omitted from the figure.

The air sample containing the particles to be detected and measured is drawn through the instrument by the vacuum pump. The sample first enters the humidifier, where its relative humidity is raised to 100% with water. The sample then passes through a rotating valve into the cloud chamber, where it is expanded adiabatically by the valving and transport system, causing the sample to cool and the relative humidity to rise to any desired supersaturation up to 400% (5).

This unstable condition can be relieved by three processes:

Condensation in which the nucleus of the droplet is a single water molecule;

Figure 1. Relative humidity necessary for condensation



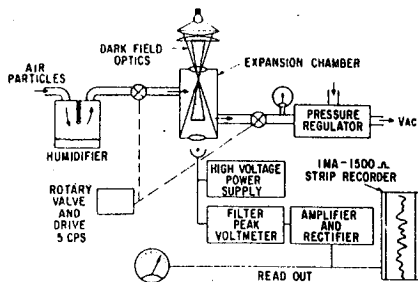


Figure 2. Condensation nuclei detector

this does not take place until the saturation has reached about 800%.

Condensation on the walls of the chamber; this affects relatively few of the water molecules in the sample because most of them are far away, in terms of molecular distances, from the walls.

Condensation on airborne particles in the sample; this is the primary and dominating effect.

The cloud of water droplets so formed, each containing an airborne nucleus, is measured in a dark-field optical system by scattering light on a multiplier phototube. The amount of light scattering is proportional to the number of droplets in the sample. This relationship holds because all the droplets after growth are the same size, a uniformity which eliminates the effect of particle size variation on the scattering of light (?).

The sample is then flushed out of the chamber through the rotation valve and discharged in the exhaust of the vacuum pump. This complete cycle may be varied from three to 10 times per second. Normal operation is at 5 cycles per second.

The complete sequence of events for any sample—from intake and humidifying, to expansion, measurement, and discharge; plus the time needed for instruments to respond—can be rapid, 1.5 seconds. That is the time constant of the detector to obtain 82% of full scale reading of a step input of condensation nuclei.

The electrical signal produced by the multiplier phototube (an RCA 931A tube) first passes through a filter designed to remove the 60-cycle flicker of the light source and to pass the 3- to 10-cycle frequency generated by the CND's own cycling rate. The filtered signal passes through a peak-reading voltmeter, is amplified, and comes to the readout device as a direct current proportional to the number of particles present in the sample.

The CND can detect concentrations as small as 10^1 or as large as 10^7 particles per cubic centimeter. Sample flow can be varied from 20 to several hundred cubic centimeters of gas per second by adjusting a critical orifice in the rotating valve.

Characteristics of Detector. Characteristics of the CND that are important to its use as a primary sensing element in gas analysis or detection are:

Extreme sensitivity. On a molecular basis this is about 10^4 molecules

of material in 10^{19} molecules of air, or 1 part in 10^{15} .

Good repeatability and stability of detection. Short-term stability is better than 5% of point and unaffected by the temperature of the sample or its moisture content.

An electrical output signal of 1 ma. into 1500 ohms.

Power supply: 60-cycle a.c., 115 volts, 300 watts.

Volume about 4 cubic feet and weight about 70 pounds.

Gas to Particle Conversion. Before the nuclei detector can be used to measure gas concentrations, the gas must be changed in form into a substance that will have a vapor pressure—at ambient temperature and pressure—such that the substance will be either a liquid or solid sub-microscopic particle.

Experiments have indicated that the particles formed do not have to be hygroscopic, polarized, or ionized to serve as condensation nuclei.

Many processes meet these criteria. Nine of these are: photochemical, pyrolysis, hydrolysis, acid-base reactions, reverse photochemical, ammonolysis, electrochemical, oxidation, and chemical. Many permutations and combinations of these processes are possible. One such combination is to obtain controlled conversion by one of the techniques and suppress this conversion by the introduction of another gas. This is in effect a reverse conversion which can be used for detection.

Perhaps the most readily understandable process is that used to measure the concentration of sulfur dioxide in air (3, 4). Here the conversion process is a photochemical reaction that takes place when SO_2 gas is subjected to ultraviolet light of a wavelength of 2537 Å. The SO_2 molecules break up and recombine as SO_3 , which in turn reacts with water vapor in the air and forms liquid particles of sulfuric acid—fine condensation nuclei.

The conversion processes may be classified into two groups: those which do not go to complete equilibrium (this may be a desirable factor for fast response), and those which reach equilibrium, as hydrolysis. In some cases a combination of reactions could be used.

MEASUREMENT SYSTEM REQUIREMENTS

A practical instrumentation system for measuring the concentration of a gas is composed of: a particle filter to remove any ambient condensation nuclei present in the sample, a reaction section where the nucleogenic process takes place, the CND with an appropriate readout device, a meter or recorder, and a pump which ejects the used sample and draws in succeeding ones.

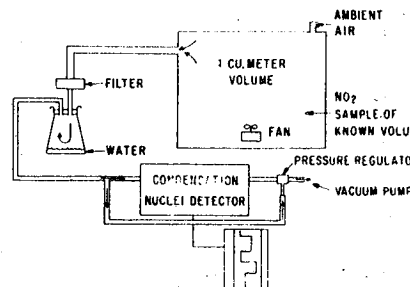


Figure 3. Test apparatus for measurement of NO_2

The function of the filter is most important, for without control of ambient nuclei consistent results would not be possible. The gas to be analyzed may be carried in air, in a carrier gas such as nitrogen, or in some other gaseous compound or mixture. Obviously, the less complex the carrier gas the more straightforward will be the construction of the filter and conversion equipment. The filter must not only be capable of removing ambient particles but it must also allow the gas to pass without undue adsorption or chromatographic effects. It is relatively easy to provide a filter which will reduce the ambient condensation nuclei to less than 50 particles per cc. Therefore, the sample entering the converter will contain essentially only the carrier gas and the gas to be measured.

The converter can use any of the nine processes listed above or combination thereof, but its prime function is to produce consistently a number of nuclei proportional to the concentration of the gas to be measured. The reaction need not go to completion because of the extreme sensitivity of the CND, and as long as the cycling time is so arranged that all samples enter the detector at the same relative point in the reaction.

In the detector itself, the sample is processed as previously described, producing an electrical signal proportional to the gas concentration, that can be calibrated in a variety of readout units such as parts per million.

Response time is in no way dependent on the concentrations being sampled. The converter and detector can be adjusted to measure concentrations all the way from fractions of a part per million up to several per cent.

INTERPRETATION OF RESULTS

The problem in the quantitative interpretation of results lies in the fact that the sensitivity and repeatability are dependent upon the size distribution and concentration of particles produced in the nucleogenic process. Both factors need to be known for a quantitative calibration to be made. Such a calibration has been considered, and some of the conditions which affect it are type of conversion process being used.

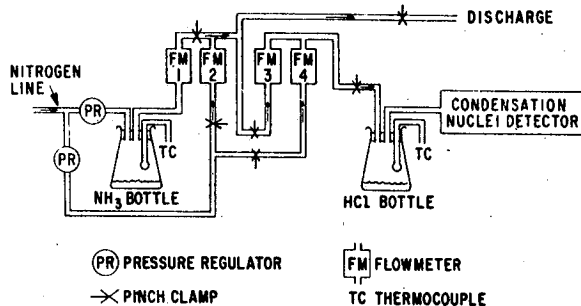


Figure 6. Test apparatus for measurement of ammonia

saturated ammonia gas leaving the bottle was determined.

Further detection was accomplished by dilution with N_2 . The flow was adjusted to match the requirement of the condensation nuclei detector (100 cc. per second). After dilution, the ammonia gas was passed through the HCl bubbler.

The concentration of ammonia in the gas entering the HCl bottle was computed from the vapor pressure and the flowmeter data and plotted against the nuclei reading (Figure 7). The HCl concentration is given in terms of the molar concentration of the liquid. When the HCl molar concentration was changed from 7 to 8%, a great increase in sensitivity was noted. The cause for this is unknown; however, at 8% molar,

the stoichiometric ratio was exceeded and an excess of HCl was present in the converter. Additional work is now under way to study this further.

OTHER GASES DETECTED

Table I indicates some types of gases which have been detected and the conversion mechanisms used. The sensitivities indicated are those which were readily obtained without extensive tests and do not indicate ultimate performance.

LITERATURE CITED

- (1) Das Gupta, N. N., Ghosh, S. K., *Rev. Mod. Phys.* **18**, 225-90 (1946).
- (2) Dunham, S. B., General Electric Co.,

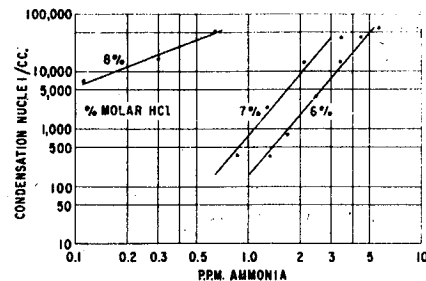


Figure 7. Concentration of ammonia vs. nuclei reading

- Schenectady, N. Y., private correspondence, 1960.
- (3) Dunham, S. B., *Nature* **188**, 51-2 (Oct. 1, 1960).
- (4) Gerhard, E. R., Johnstone, H. F., *Ind. Eng. Chem.* **47**, 972-6 (1955).
- (5) Nolan, P. J., Pollack, L. W., *Proc. Roy. Irish Acad.* **51A**, 9-31 (1946).
- (6) Rich, T. A., "Continuous Recorder for Condensation Nuclei," 4th International Symposium on Atmospheric Condensation Nuclei, Heidelberg, Germany, May 1961.
- (7) Skala, G. F., General Electric Co., Schenectady, N. Y., private correspondence, 1959.

RECEIVED for review April 23, 1962. Accepted September 7, 1962. Pittsburgh Conference on Analytical Chemistry and Applied Spectroscopy, Pittsburgh, Pa., March 6, 1962.

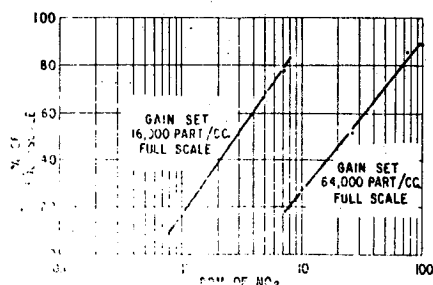


Figure 4. Calibration curve for NO₂ detection by hydrolysis

converter pressure and temperature, gas flow rate and dwell time in converter, and hygroscopicity of nuclei created.

One of the more important conditions is the dwell time between the creation of nuclei and the measurement of their concentration in the CND. The number of nuclei produced in the converter is generally large. Thousands of particles per cubic centimeter are normal. Since individual particles are continually growing by coagulation with adjacent particles, the size distribution is a rapidly changing factor unless steady-state condition can be obtained by controlling the dwell time within the converter. Tests utilizing diffusion chambers and electrical mobility measurements indicated that the nuclei produced are from 0.0008 to 0.02 micron in diameter for residence times up to a few seconds. Therefore, precise size distribution measurements are very difficult.

Because of the influence of such conditions, which are either not known or are difficult to measure, direct calibration has been used exclusively to obtain an empirical relationship between gas concentration and electrical output of the CND. Tests have indicated that when the converter temperature ($\pm 2^\circ$ C.), pressure (± 10 mm. of Hg), and gas flow rate ($\pm 2\%$) are controlled, consistent results are obtained. As an example, with NO₂ detection at the 5-p.p.m., level calibration over many days is within $\pm 5\%$ of point.

The effect of other gases in the atmosphere on the calibration is also of importance. Many tests have been conducted in ambient atmosphere and the difficulty encountered depends upon the gas being detected. SO₂ and NO₂ detection is influenced very little by other ambient gases present. However, an *unsym*-dimethylhydrazine detector will also detect ammonia or the amines. In general, this technique can be utilized to detect classes or related families of gas and, as are most techniques, is not completely selective in its response. Care in picking the type of conversion and controlling the operation of the converter can minimize the influence of other ambient gases.

Some of the practical difficulties encountered in using this new technique

stem from the extreme sensitivity of the detector. One must be very careful that the detector is not affected by nuclei other than those being produced in a controlled manner in the converter.

Also, extraneous reactions in the converter must be carefully avoided; the carrier gas must contain no substance or impurity that is also nucleogenic.

The adsorption of certain gases on the tubing passages or on the surface of the converter chamber may cause some difficulty, as it reduces the sensitivity of the instrument and delays the response time. If large quantities are adsorbed, it may take some time for the signal to diminish and stabilize for maximum sensitivity. The best design provides for having the gas enter the reaction zone immediately upon entrance into the apparatus and to have the reaction period as short as possible.

INSTALLATIONS

Despite the uncertainties, practical systems have been developed in the authors' laboratory, and several units have been installed in the field.

Nitrogen Dioxide Detection. Nitrogen dioxide may be readily detected after it has been converted to nitric acid particles by hydrolysis. Figure 3 is a schematic diagram of such a system.

The NO₂ gas is injected into a 1-cu. meter air-filled chamber in a known concentration by volume. The NO₂ and air pass through a Gelman Type E fiber glass filter and into the converter, a 500-ml. flask containing approximately 200 ml. of water at 76° F. The NO₂ reacts with the water to produce particles of nitric acid in the order of 0.002 micron in diameter.

The sample containing these particles is then passed into the condensation nuclei detector, which is adjusted to produce a supersaturation of about 375%.

The number of condensation nuclei so produced is indicated in Figure 4, where the two curves are for two different concentration levels. To make the transition in level, one merely has to change the sensitivity control on the detector. Total flow rate through the filter and converter was 1 cu. foot per minute.

As an indication of the response times obtained, Figure 5 represents a typical response when approximately 6 feet of $\frac{1}{4}$ -inch Tygon tubing was used to connect the filter-converter and the nuclei detector.

A delay of about 10 seconds was observed from the time the NO₂ was injected into the intake chamber until the detector indicated full scale. This response time was primarily a function of the flow rate and the total volume of chamber, tubing, and converter. It can be changed by adjusting the system

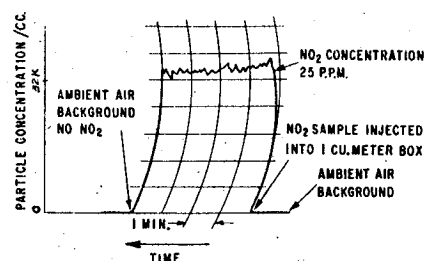


Figure 5. NO₂ detection

flow rate. This does not affect the operation of the detector, since most of the air bypasses the instrument.

Ammonia Detection. Detection of ammonia gas (2) involves an acid-base reaction to form particles. The tests were conducted with the apparatus sketched in Figure 6.

The ammonia gas was carried in dry nitrogen. The converter was composed of a Fisher-Milligan gas washing bottle filled with a solution of HCl of varying molarity. The ammonia reacted with HCl to produce ammonium chloride.

A known ammonia solution was placed in a similar gas washing bottle and its temperature measured. With these two values the vapor pressure was determined and the concentration of

Table I. Some Types of Gases Detected

Substance	Type of conversion	Concentrations utilized, p.p.m.
Aluminum iodide	Hydrolysis	0.01
Ammonia	Acid-base	0.005
Benzene	Photochemical	2
Carbon dioxide	Electrochemical	5
Carbon monoxide	Chemical	1
Chlorine	Chemical	1
Ethyl alcohol	Reverse photochemical	5
Freon 12-21	Pyrolysis	2
Fuming nitric acid	Hydrolysis	0.5
Hydrochloric acid	Hydrolysis	0.5
Hydrocarbons	Photochemical	0.1
Methyl mercaptan	Oxidation	0.01
Monoethylamine	Chemical	0.5
Mercury	Photochemical	0.001
Metallic carbonyl	Hydrolysis	0.001
Nitrogen dioxide	Hydrolysis	0.5
Naphtha	Reverse photochemical	5
Octane	Photochemical	2
Sulfur dioxide	Photochemical	0.001
Sulfur hexafluoride	Pyrolysis	1
Sulfuric acid	Hydrolysis	2
Solvesso 100	Reverse photochemical	1
Toluene	Reverse photochemical	1
<i>Unsym</i> -Di-methylhydrazine	Chemical	0.1

APPENDIX III

APPENDIX III

A New Instrument for the Continuous Measurement of Condensation Nuclei

GEORGE F. SKALA

Advanced Technology Laboratories, General Electric Co., Schenectady, N. Y.

► An instrument is described which provides a continuous measurement of airborne particle concentrations in the size range down to 0.001 micron. The concentration range of the instrument is from 10 to 10^7 particles per cubic centimeter with a response time in the order of 1 to 2 seconds. The instrument is designed for continuous unattended operation and employs a unique dual beam, single phototube optical system in which the reference beam passes through the same optical elements as the measuring beam.

THE FIRST experiments which demonstrated the existence of nuclei as centers of condensation can be traced back as early as 1841 to the work of Espy (6). Further investigations were conducted by Aitken (1), who concluded that, except for the presence of nuclei, there would be no fog, no clouds, no mist, and probably no rain. He is also credited with making the first instrument for the measurement of nuclei concentrations (2). In recognition of his contributions to the investigations of condensation nuclei, these particles are often referred to as Aitken nuclei.

Typical nuclei concentrations range from 500 per cc. at mid-ocean to 500,000 per cc. in metropolitan traffic conditions.

While conducting experiments based on the works of Aitken and others on the expansion of air saturated with water vapor, Wilson devised his famous cloud chamber for the detection of radioactivity (15).

It was not until 1938 that photoelectric cells were mentioned as being applied to the measurement of condensation nuclei, by Bradbury and Meuron (3). About the same time, L. W. Pollak applied the photocell to a photoelectric counter of his design, and together with P. J. Nolan described its calibration (9).

With the improvements that have been made in this counter, and the accumulated knowledge of its performance, it has become a very useful laboratory instrument and serves in many instances as a calibration standard.

A smaller, battery operated, portable counter which employs an expansion into a partially evacuated chamber has been described by Rich (10). This device is now being manufactured commercially by Gardner Associates, Schenectady, N. Y.

All the counters referred to above are manually operated, and are capable of a single measurement at a time. A number of investigators have constructed automated versions of various counter configurations in which electrically operated valves substitute for the human operator. Cycling rates have varied from one reading every 15 minutes (13) to as many as four a minute (8). These have generally served their purpose, but because of the cyclic nature of the output, they present problems of read out and recording. Also, zero stability and adequate water supply can be problems for long term unattended operation.

A counter in which hydrogen chloride gas is used to achieve a continuous supersaturation, making it capable of reading continuously, is described by Holl and Mühleisen (7). However, because of the low flows employed, the response time is of the order of 1 minute.

A nuclei counter which achieves a continuous reading by rapidly cycling the expansion ratio was described in 1949 by Vonnegut (14). An improved version, employing a different expansion system, was described by Rich (11). The counter of this paper is based on

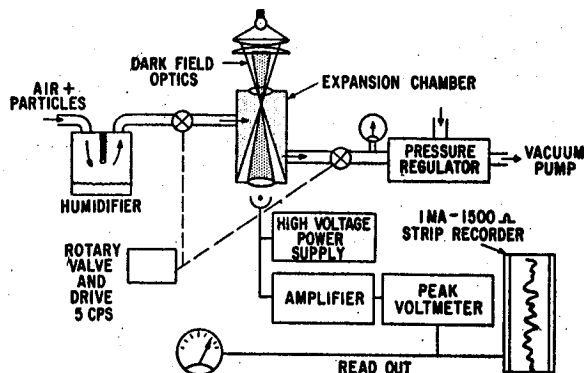


Figure 1. Schematic condensation nuclei counter

the one developed by Rich, with modifications such as transistorized circuitry and improved stability.

CONTINUOUS CONDENSATION NUCLEI COUNTER

The basic condensation nuclei (CN) counter is shown schematically in Figure 1. The sample, at a flow rate of about 100 cc. per second, is drawn in through a humidifier to bring it to 100% relative humidity. It then passes through the first section of a rotary, motor driven, valve into the expansion chamber. After a brief dwell period, the second section of the rotary valve opens the expansion chamber to a source of regulated vacuum.

The sudden expansion results in adiabatic cooling of the sample, causing the relative humidity to rise above 100%. Water will then condense on nuclei present, and the resulting droplets soon grow to a size where they can scatter light. The expansion chamber contains a dark field optical system which produces no light on the multiplier phototube in the absence of fog droplets. With droplets present in the chamber, they cause light to be scattered to the phototube. The amount of light is proportional to the number of droplets (each containing one nucleus) and to their scattering area.

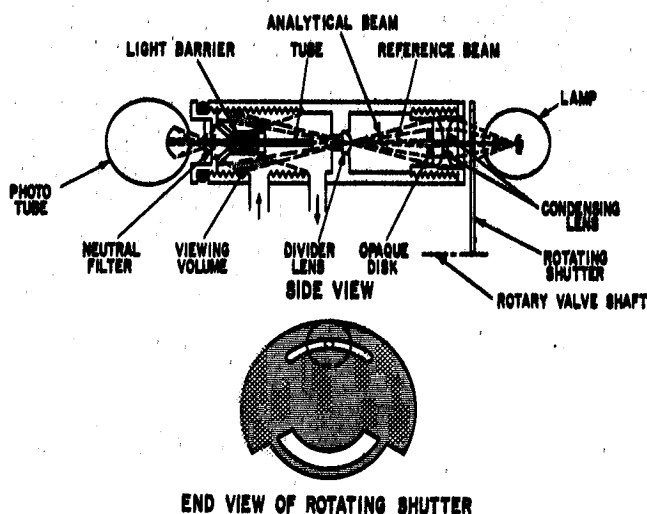


Figure 3. Expansion chamber details

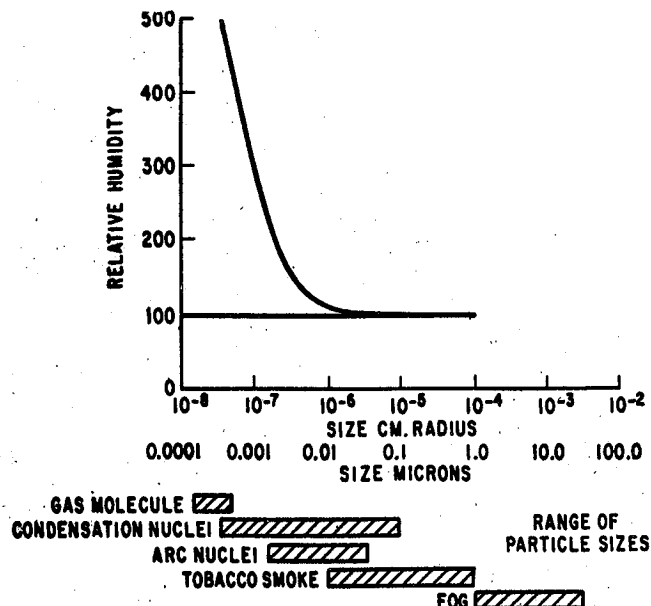


Figure 2. Relative humidity necessary for condensation

Figure 2 indicates the amount of supersaturation required for a water droplet of a given size to serve as a condensation nucleus (4). Although most nuclei of interest are not water, they appear to behave in a similar manner, and once condensation starts the growing particle behaves like a water droplet.

For most applications the vacuum is regulated to give an underpressure expansion of 8 inches of mercury. This results in a supersaturation of about 400%. According to Figure 2, condensation on nuclei 0.001 micron and larger will occur. This is adequate for most uses, but higher expansions can be employed for special applications. However, if the expansion is raised much over 10 inches, a sudden increase in reading will result because of spontaneous nucleation on gas or water molecules.

The valve cycling rate is five times a second, producing an essentially continuous measurement of nuclei con-

centration. The response time is about 1 second, due in part to flow delays, particularly in the humidifier. For applications requiring long inlet lines, it is possible to connect the vacuum regulator by-pass flow to the sample inlet line through a T connection. This increases the flow through the sample line to about 500 cc. per second, reducing the transport delay, and at the same time minimizing coagulation and diffusion losses in the sample line.

Stabilizing Methods. To provide a stable reading, consideration must be given to the large effects of lamp and multiplier phototube supply voltages. This can be done in a number of ways, including the "brute force" regulation of lamp and phototube supplies; the use of coupling circuits whereby an increase in lamp voltage reduces the phototube voltage by an amount which is adjusted to maintain constant over-all gain; compensation using a second phototube to monitor the lamp and vary the high voltage to both phototubes to maintain constant gain, and compensation whereby suit-

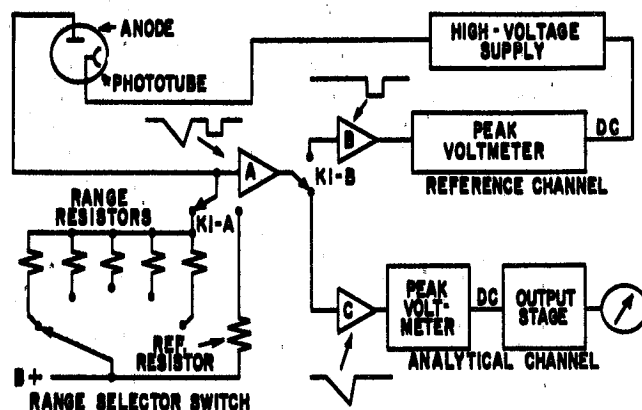


Figure 4. Block diagram, stabilized CN counter

able switching means are employed to use the same phototube for the analytical and reference function. All of these methods have been employed in CN counters developed by the author's company. However, because it is the only one capable of correcting for changes in phototube characteristics, as well as changes in the optical properties of the expansion chamber, the last method was chosen for this application because of the desirability of long term stability.

Figure 3 shows the details of the expansion chamber optics. A small opening is provided in the center of the opaque section of the condensing lens that is used to form the cone of the dark field optics. This allows light to pass through the tube in the light barrier, and on to the multiplier phototube. The purpose of the tube is to reduce stray light from illuminated portions of the divider lens. A small diameter neutral density filter located in the center of the viewing window attenuates the reference beam to prevent saturation of the phototube.

A rotating shutter on the same shaft as the rotary valve contains sectors which alternately block all light, block the central portion of the condensing lens, block all light again, and then expose only the central portion of the condensing lens. The shutter is synchronized with the rotary valve so that the expansion takes place while the central portion of the lens is blocked. This cuts off the reference beam, but illuminates the viewing volume inside the expansion chamber. Between expansions, the central portion of the lens is exposed. This allows the attenuated reference beam to pass through the chamber to the phototube. The solid sectors of the shutter provide a zero-light standard to which the light signal produced by the reference beam is compared.

A simplified block diagram of the complete CN counter is shown on Figure 4. A switch synchronized with the rotary valve controls relays which separate the analytical and reference signals. One set of relay contacts, *K1-A* introduces alternately one of the range resistors during the expansion cycle, and a fixed reference resistor during the reference cycle in the anode circuit of the phototube. The value of range resistance is determined by the full scale nuclei concentration as set by the range selector switch. The combined signals are amplified by *A*, and separated by relay contact *K1-B*, which switches at the same time as *K1-A*.

After further amplification in *B* and *C*, both signals go to peak voltmeters which convert the five cycle pulses into d.c. levels proportional to the respective peak light signals. The output of the reference channel peak voltmeter is fed to a variable high voltage supply where it is compared with the voltage across a Zener diode. If the reference voltage is too low, the output of the high voltage supply is increased to raise the gain of the photomultiplier. In this manner, the output of the reference channel is maintained at a con-

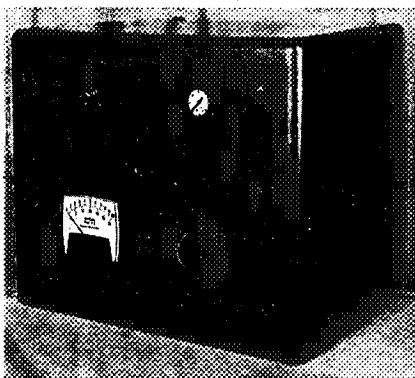


Figure 5. Condensation nuclei counter

stant level in spite of changes in lamp output, lens conditions, or phototube characteristics. Because the gain of the analytical channel also is determined by these elements, it too will remain constant. Amplifier *A* is common to both channels, so any changes in its gain will be cancelled out. However, changes in gain between amplifiers *B* and *C*, and the peak voltmeters, would affect the over-all gain. To avoid this, the amplifiers and peak voltmeters are identical, and employ negative feedback for maximum stability. To provide additional stabilization, the lamp is supplied by a constant voltage transformer to eliminate the effects of rapid line fluctuations which the circuit may be too slow to correct for because of the necessary filtering time constants. The use of a regulated voltage on the lamp will also prolong its life, particularly since it is only 70% of the rated lamp voltage.

Other factors which could change counter sensitivity are rotary valve speed, expansion pressure, and temperature. An induction motor is used for the valve drive, and provides adequate speed control. A synchronous motor would be more constant, but would have less torque. The expansion pressure is controlled by a diaphragm type vacuum regulator which maintains constant vacuum over wide variations in air flow or pump output. The temperature is maintained within desired limits by thermostatically controlled heaters in the casting which houses the humidifier, valve, and expansion chamber. A fan is used to dissipate the heat generated by the vacuum pump.

Design Features. Consideration has been given throughout the over-all design to the need for long operating life and stability, and capability for unattended operation.

All circuits are transistorized, only two different types being employed for all functions.

An important feature is the combining of the humidifier, valve, and expansion chamber into one casting to reduce temperature differentials. If the humidifier becomes warmer than other parts of the flow system, condensation can occur, with the result that bulk water will enter the expansion chamber and cause noise to appear on the phototube. If the humidifier is

cooler than the expansion chamber, a loss in relative humidity would affect the sensitivity and calibration.

The humidifier and an additional reservoir hold enough water for over 100 hours of operation. If desired, the counter can be connected directly to a source of water. Water flow to the humidifier is controlled by a solenoid valve, with a thermistor used as level sensor. Freezing will not cause damage, and heaters in the casting are used to provide rapid melting if the counter should be turned on while the temperature is below freezing.

The relays used to switch between analytical and reference channels employ mercury wetted contacts. They are controlled by a switch magnetically synchronized to the rotary valve shaft. This switch is of the hermetically sealed reed type, held closed by a permanent magnet. A disk sector of permeable material on the valve shaft passes between the magnet and switch, alternately shunting the magnetic flux, and allowing the switch to open and close in synchronism with shaft rotation.

A photograph of a prototype instrument is shown on Figure 5.

RESULTS

Measurements indicate that, once the required supersaturation is achieved, the start of the growth process is virtually instantaneous (less than one milli-second delay). The rate of droplet growth in a small dry-wall chamber was measured by observing the forward scattered light signal after air at 100% relative humidity containing condensation nuclei was rapidly expanded. Filters were used so that the growing particles were illuminated by light of a narrow spectral spread. The resulting phototube signal contained peaks characteristic of the Mie scattering theory. By knowing the particle size corresponding to each peak, it was possible to obtain a droplet growth relationship as plotted on Figure 6 at various expansions. As indicated by this plot, the increase in droplet area is proportional to time. As an example of the magnitudes of size and time involved, if an under pressure expansion of 8 inches of mercury is used, a 0.001-micron droplet will grow to a diameter of 5 microns in about 26 milliseconds. This represents an increase of 25×10^6 in its area, or over 10^{11} increase in volume. The increase in scattered light is also of the order of 10^{11} because of the low scattering coefficient for particles very much smaller than the wavelength of light. Because of this large increase in diameter, the size of the original nucleus has negligible effect on the final droplet size, providing the supersaturation is initiated rapidly enough so that all droplets start growing at the same time. At the 5-micron size, the droplet is readily detectable by optical means.

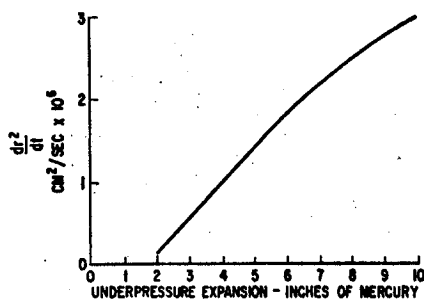


Figure 6. Droplet growth in dry wall chamber

As discussed earlier, the light signal on the phototube is proportional to the product of droplet concentration and the scattering area of each droplet. Also, at any one instant of time all droplets, once they are large enough to scatter light, will be virtually the same size. The scattering area of these larger droplets is proportional to the square of their radius. Also, from Figure 6, the droplet growth is such that the radius squared increases linearly with time. Therefore, as the droplets grow, the output signal of the phototube will increase linearly with time, with a slope proportional to nuclei concentration.

This growth cannot continue indefinitely, however. It will cease when the relative humidity, at the temperature of the expanded sample, drops back to 100% as a result of the excess water being used up by the growing drops. When this happens, the light signal will stop increasing and remain constant (if we neglect evaporation). The overall light signal is then a ramp function as shown on Figure 7, which assumes that the growth rate remains essentially constant as the excess water is consumed.

The initial slope is proportional to nuclei concentration N , and the peak value to $N^{1/3}$. This can be readily shown as follows:

To determine scattered light *vs.* N where the final droplet size is determined by water available, let:

- W = Water available for growth, gm./cc.
- r = Final droplet radius
- N = Nuclei concentration, number/cc.
- K = Scattering coefficient
- ρ = Density of water
- L = Scattered light

$$\text{Total droplet volume} = \frac{4}{3} \pi r^3 N \quad (1)$$

therefore

$$W = \frac{4}{3} \pi r^3 N \rho \quad (2)$$

$$L = K \pi r^2 N \quad (3)$$

Solving for r from Equation 2

$$r = \left(\frac{3W}{4\pi N \rho} \right)^{1/3} \quad (4)$$

Substituting in Equation 3

$$L = K \pi \left(\frac{3W}{4\pi N \rho} \right)^{2/3} N \quad (5)$$

$$L = K \pi^{1/3} \left(\frac{3W}{4\rho} \right)^{2/3} N^{1/3} \quad (5)$$

The location of the knee is a function of the rate of growth, excess water available as a result of supersaturation, and N .

If the valve cycle time is such that the droplets are flushed out of the expansion chamber before the excess water has been used up, the output of the CN counter will be proportional to N . If the droplets cease growing before they are flushed out, the output re-

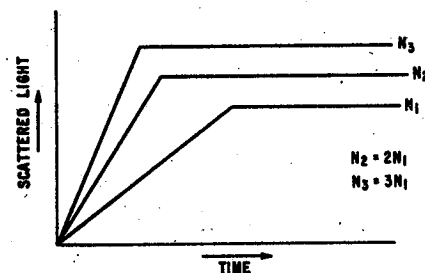


Figure 7. Scattered light vs. time at different nuclei concentrations

sponse will be proportional to $N^{1/3}$. For this application, it was decided to make the response linear up to a value of N of 100,000 nuclei per cc., with an expansion pressure of 8 inches. The necessary growth time can be calculated from the known growth rate, if a constant rate is assumed.

To determine the time required to use all water available, for $N = 10^5$, let:

t = Time, sec.

\dot{r}^2 = Rate of change of r^2

From equation 4

$$r^2 = \left(\frac{3W}{4\pi N \rho} \right)^{2/3} \quad (6)$$

$$t = \frac{r^2}{\dot{r}^2} = \left(\frac{3W}{4\pi N \rho} \right)^{2/3} \quad (7)$$

From Figure 6, for $8'' \Delta P$, $\dot{r}^2 = 2.43 \times 10^{-6} \text{ cm.}^2/\text{sec.}$

From a pseudoadiabatic diagram, for an $8'' \Delta P$, starting at 25°C.

$W = 6.5 \times 10^{-6} \text{ gm./cc.}$

$$t = \left(\frac{3 \times 6.5 \times 10^{-6}}{4\pi \times 10^5} \right)^{2/3} = 25.5 \times 10^{-3} \text{ sec.} \quad (8)$$

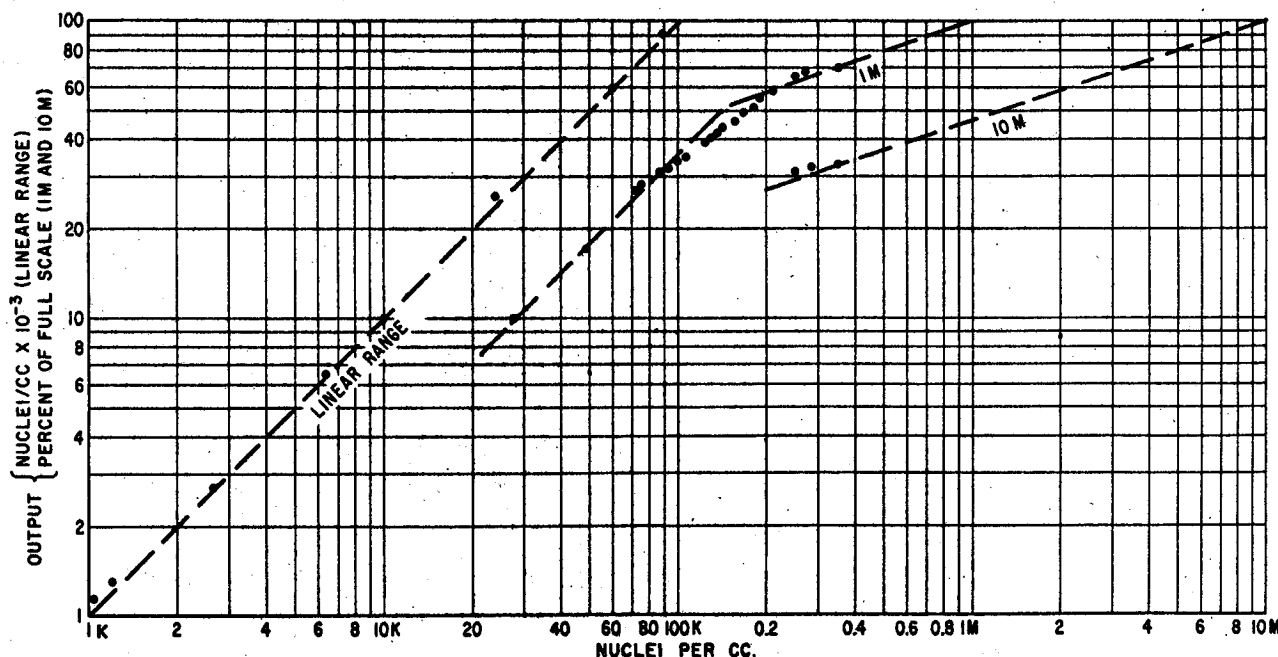


Figure 8. Counter calibration

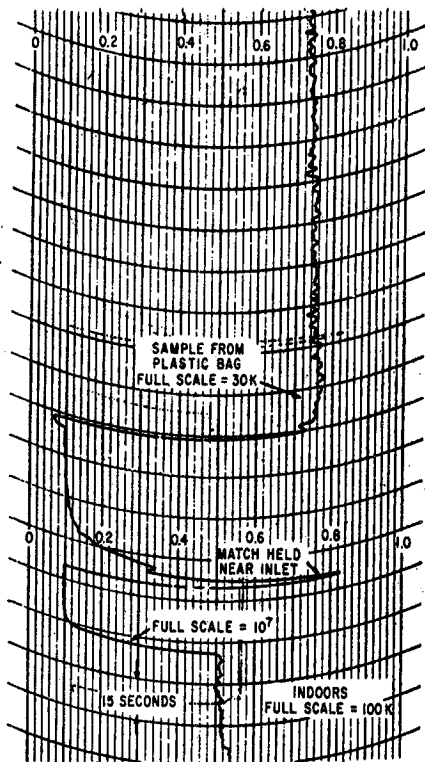


Figure 9(a). Chart record, indoors

The rotary valve was designed to produce the required expansion dwell time of 25.5 milliseconds. The linear portion of the counter response is divided into full scale ranges of 300, 1000, 3000, 10,000, 30,000, and 100,000 nuclei per cc. Two nonlinear ranges having full scale values of 10^6 and 10^7 nuclei per cc. are also provided. A typical calibration is shown on Figure 8. The response is linear up to 100 K, and then follows a line having a slope of $1/2$, above about 200 K. The effects of decreasing droplet growth rate as the humidity approaches 100% is indicated by the plotted points which lie below both lines in the transition region between 100 K and 200 K.

Most applications where the accuracy and resolution of the linear range are needed will be for concentrations below 100,000. With higher concentrations the level is likely to be variable, and subject to uncertain errors such as coagulation losses, so that a compressed exponential scale will be more useful.

The standard against which the instrument is calibrated is a Pollak counter of the kind mentioned earlier. Its calibration, in turn, has been compared against a photographic cloud chamber

in which the droplets in a known volume of air were photographed immediately after growth.

Typical chart records are shown on Figure 9. These illustrate inside and outdoor readings, at widely differing chart speeds.

DISCUSSION

At this point, we can only speculate as to all the possible applications of systematic condensation nuclei measurements to the problems of air pollution. Because nuclei play an important role in atmospheric physics by making possible condensation in the air, they can be significant factors in determining the effects of a given amount of atmospheric pollutants. A distinct possibility exists that some of the physiological effects of pollution, such as eye irritation, are aggravated by the concentration of polluting agents on condensation centers (8). The onset of fog or smog can no doubt be related to the nuclei concentration.

The usefulness of the CN counter is further extended by the application of gas conversion techniques. These are processes by which gases are converted to condensation nuclei by any of several mechanisms. These techniques make possible the real time detection of trace gases such as NO_2 or SO_2 at parts per million, or even parts per billion sensitivities (12). Therefore, by serving as a sensitive analyzer, either of particulates or trace gases, the CN counter is ready to play a significant role in air pollution, both in control enforcement and in research.

LITERATURE CITED

- (1) Aitken, John, "On Dust, Fogs, and Clouds," Royal Society of Edinburgh, Proceedings, p. 14, Dec. 20, 1880.
- (2) Aitken, John, "On the Number of Dust Particles in the Atmosphere," Royal Society of Edinburgh, Proceedings, Vol. 35, 1887-1888.
- (3) Bradbury, N. E., Meuron, H. J., "The Diurnal Variation of Atmospheric Condensation Nuclei," Terr Magn, Vol. 43, p. 231, 1938.
- (4) Das Gupta, N. N., Ghosh, S. K., "A Report on the Wilson Cloud Chamber and Its Applications in Physics," Reviews of Modern Physics, p. 225, April, 1946.
- (5) Epsy, James Pollard, "The Philosophy of Storms," Boston, Charles C. Little and James Brown, 1841.
- (6) General Electric Co. Instruction Manual GEI 45015A, on secondary standard detector, Cat. 112L959, Jan., 1959.
- (7) Holl and Mühleisen, "A New Condensation Nuclei Counter with Con-

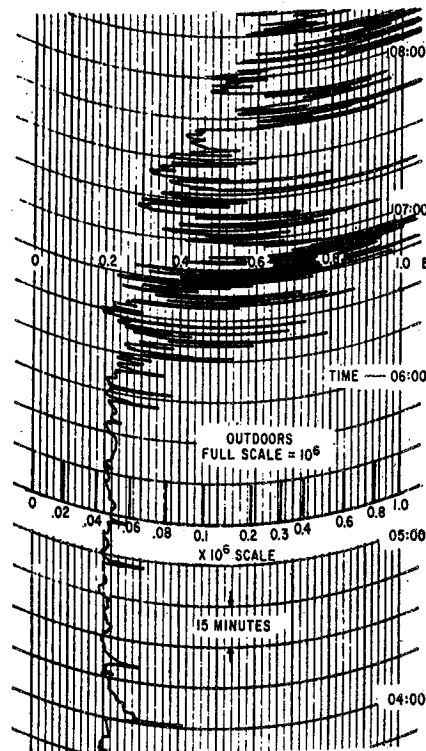


Figure 9(b). Chart record, outdoors

tinuous Over-Saturation," *Geofis. Pura Appl.*, 31, 21, 1955.

- (8) Leighton, P. A., "Photochemistry of Air Pollution," p. 276, Academic Press, N. Y., London, 1961.
- (9) Nolan, P. J., Pollak, L. W., "The Calibration of a Photo-Electric Nucleus Counter," *Proc. Roy. Irish Acad.*, p. 9, July, 1946.
- (10) Rich, T. A., "A Photo-Electric Nucleus Counter with Size Discrimination," *Geofis. Pura Appl.*, Instituto Geofisico Italiano, Milan, Italy, 31, 60, 1955.
- (11) Rich, T. A., "A Continuous Recorder for Condensation Nuclei," 4th International Symposium for Atmospheric Condensation Nuclei, Heidelberg, Germany, May, 1961.
- (12) Van Luik, F. W., Rippere, R. E., *ANAL. CHEM.*, 34, 1617, 1962.
- (13) Versar, F., "Continuous Record of Atmospheric Condensation Nuclei and of Their Retention in the Respiratory Tract," *Geofis. Pura Appl.*, 31, 183, 1955.
- (14) Vonnegut, B., "A Continuous Recording Condensation Nuclei Meter," reprinted from *Proc. First National Air Pollution Symposium*, Los Angeles, 1949, pp. 36-44.
- (15) Wilson, C. T. R., "On the Condensation Nuclei Produced in Gases by the Action of Roentgen Rays, Uranium Rays, Ultra-Violet Light and Other Agents," Royal Society of London, Philosophical Transactions, Ser. A, p. 403, 1899.

RECEIVED for review November 5, 1962. Accepted February 27, 1963. Division of Water and Waste, 142nd Meeting, ACS, Atlantic City, N. J., September 1962.

APPENDIX IV

Appendix IV
LEAKAGE UNITS CONVERSION TABLES

The following three tables and instructions are for conversion of leakage rates of different units.

TABLE IV-1

LEAKAGE CONVERSION FACTORS

micron x cc	1	1.0x10 ³	5.2x10 ⁴	7.6x10 ⁵	16	1.6x10 ⁴	8.5x10 ⁵	1.2x10 ⁷	29	2.9x10 ⁴	1.5x10 ⁶	2.2x10 ⁷	1.0x10 ³	1.0x10 ⁶	5.2x10 ⁷	7.6x10 ⁸	2.8x10 ⁴	2.8x10 ⁷	1.5x10 ⁹	2.1x10 ¹⁰
torr x cc	1.0x10 ⁻³	1	52	7.6x10 ²	1.6x10 ⁻²	16	8.5x10 ²	1.2x10 ⁴	2.9x10 ⁻²	29	1.5x10 ³	2.2x10 ⁴	1.0	1.0x10 ³	5.2x10 ⁴	7.6x10 ⁵	28	2.8x10 ⁴	1.5x10 ⁶	2.1x10 ⁷
psi x cc	1.9x10 ⁻⁵	1.9x10 ⁻²	1	15	3.1x10 ⁻⁴	0.31	16	2.4x10 ²	5.6x10 ⁻⁴	0.56	29	4.4x10 ²	1.9x10 ⁻²	19	1.0x10 ³	1.5x10 ⁴	0.53	5.3x10 ²	2.8x10 ⁴	4.1x10 ⁵
atm x cc	1.3x10 ⁻⁶	1.3x10 ⁻³	6.8x10 ⁻²	1	2.1x10 ⁻⁵	2.1x10 ⁻²	0.11	16	3.8x10 ⁻⁵	3.8x10 ⁻²	0.20	29	1.3x10 ⁻³	1.3	68	1.0x10 ³	3.6x10 ⁻²	36	1.9x10 ³	2.8x10 ⁴
micron x in ³	6.1x10 ⁻²	61	3.2x10 ³	4.6x10 ⁴	1	1.0x10 ³	5.2x10 ⁴	7.6x10 ⁵	1.8	1.0x10 ³	9.4x10 ⁴	1.4x10 ⁶	61	6.1x10 ⁴	3.2x10 ⁶	4.6x10 ⁷	1.7x10 ³	1.7x10 ⁶	8.8x10 ⁷	1.3x10 ⁹
torr x in ³	6.1x10 ⁻⁵	6.1x10 ⁻²	3.2	46	1.0x10 ⁻³	1	52	7.6x10 ²	1.8x10 ⁻³	1.8	96	1.4x10 ³	6.1x10 ⁻²	61	3.2x10 ³	4.6x10 ⁴	1.7	1.7x10 ³	8.8x10 ⁴	1.3x10 ⁶
psi x in ³	1.2x10 ⁻⁶	1.2x10 ⁻³	6.1x10 ⁻²	0.89	1.9x10 ⁻⁵	1.9x10 ⁻²	1	15	3.4x10 ⁻⁵	3.4x10 ⁻²	1.8	26	1.2x10 ⁻³	1.2	61	8.9x10 ²	3.2x10 ⁻²	32	1.7x10 ³	2.5x10 ⁴
atm x in ³	7.9x10 ⁻⁸	7.9x10 ⁻⁵	4.1x10 ⁻³	6.1x10 ⁻²	1.3x10 ⁻⁶	1.3x10 ⁻³	6.8x10 ⁻²	1	2.3x10 ⁻⁶	2.3x10 ⁻³	0.12	1.8	7.9x10 ⁻⁵	7.9x10 ⁻²	4.1	61	2.2x10 ⁻³	2.2	1.2x10 ²	1.7x10 ³
micron x fl.oz.	3.4x10 ⁻²	34	1.7x10 ³	2.6x10 ⁴	0.55	5.5x10 ²	2.9x10 ⁴	4.2x10 ⁵	1	1.0x10 ³	5.2x10 ⁴	7.6x10 ⁵	34	3.4x10 ⁴	1.8x10 ⁵	2.6x10 ⁷	9.6x10 ²	9.6x10 ⁵	4.9x10 ⁷	7.3x10 ⁸
torr x fl.oz.	3.4x10 ⁻⁵	3.4x10 ⁻²	1.7	26	5.5x10 ⁻⁴	0.55	29	4.2x10 ²	1.0x10 ⁻³	1	52	7.6x10 ²	3.4x10 ⁻²	34	1.8x10 ³	2.6x10 ⁴	0.96	9.6x10 ²	4.9x10 ⁴	7.3x10 ⁵
psi x fl.oz.	6.4x10 ⁻⁷	6.4x10 ⁻⁴	3.4x10 ⁻²	0.49	1.0x10 ⁻⁵	1.0x10 ⁻²	0.55	8.1	1.9x10 ⁻⁵	1.9x10 ⁻²	1	14.7	6.4x10 ⁻⁴	0.64	34	4.9x10 ²	1.8x10 ⁻²	18	9.6x10 ²	1.4x10 ⁴
atm x fl.oz.	4.4x10 ⁻⁸	4.4x10 ⁻⁵	2.3x10 ⁻³	3.4x10 ⁻²	7.2x10 ⁻⁷	7.2x10 ⁻⁴	3.7x10 ⁻²	0.55	1.3x10 ⁻⁶	1.3x10 ⁻³	6.8x10 ⁻²	1	4.4x10 ⁻⁵	4.4x10 ⁻²	0.23	34	1.2x10 ⁻³	1.2	65	9.6x10 ²
micron x liters	1.0x10 ⁻³	1.0	52	7.6x10 ²	1.6x10 ⁻²	16	8.3x10 ²	1.2x10 ⁴	2.9x10 ⁻²	29	1.5x10 ³	2.2x10 ⁴	1	1.0x10 ³	5.2x10 ⁴	7.6x10 ⁵	28	2.8x10 ⁴	1.5x10 ⁶	2.2x10 ⁷
torr x liters	1.0x10 ⁻⁶	1.0x10 ⁻³	5.2x10 ⁻²	0.76	1.6x10 ⁻⁵	1.6x10 ⁻²	0.83	12	2.9x10 ⁻⁵	2.9x10 ⁻²	1.5	22	1.0x10 ⁻³	1	52	7.6x10 ²	2.8x10 ⁻²	28	1.5x10 ³	2.2x10 ⁴
psi x liters	1.9x10 ⁻⁸	1.9x10 ⁻⁵	1.0x10 ⁻³	0.15	3.0x10 ⁻⁷	3.0x10 ⁻⁴	1.6x10 ⁻²	0.24	5.5x10 ⁻⁷	5.5x10 ⁻⁴	2.9x10 ⁻²	0.43	1.9x10 ⁻⁵	1.9x10 ⁻²	1	14.7	5.5x10 ⁻⁴	0.55	28	4.3x10 ²
atm x liters	1.3x10 ⁻⁹	1.3x10 ⁻⁶	6.8x10 ⁻⁵	1.0x10 ⁻³	2.1x10 ⁻⁸	2.1x10 ⁻⁵	1.1x10 ⁻³	1.6x10 ⁻²	3.8x10 ⁻⁸	3.8x10 ⁻⁵	1.9x10 ⁻³	2.9x10 ⁻²	1.3x10 ⁻⁶	1.3x10 ⁻³	6.8x10 ⁻²	1	3.8x10 ⁻⁵	3.8x10 ⁻²	1.9	28
micron x ft ³	3.5x10 ⁻⁵	3.5x10 ⁻²	1.8	27	5.8x10 ⁻⁴	0.58	30	4.4x10 ²	1.0x10 ⁻³	1.04	54	7.9x10 ²	3.5x10 ⁻²	35	1.8x10 ³	2.7x10 ⁴	1	1.0x10 ³	5.2x10 ⁴	7.6x10 ⁵
torr x ft ³	3.5x10 ⁻⁸	3.5x10 ⁻⁵	1.8x10 ⁻³	2.7x10 ⁻²	5.8x10 ⁻⁷	5.8x10 ⁻⁴	3.0x10 ⁻³	0.44	1.0x10 ⁻⁶	1.0x10 ⁻³	5.4x10 ⁻²	0.79	3.5x10 ⁻⁵	3.5x10 ⁻²	1.8	27	1.0x10 ⁻³	1	52	7.6x10 ²
psi x ft ³	6.7x10 ⁻¹⁰	6.7x10 ⁻⁷	3.5x10 ⁻⁵	5.1x10 ⁻⁴	1.1x10 ⁻⁸	1.1x10 ⁻⁵	5.8x10 ⁻⁴	9.9x10 ⁻³	1.9x10 ⁻⁸	1.9x10 ⁻⁵	1.0x10 ⁻³	1.5x10 ⁻²	6.7x10 ⁻⁷	6.7x10 ⁻⁴	3.5x10 ⁻²	0.51	1.9x10 ⁻⁵	1.9x10 ⁻²	1	15
atm x ft ³	4.6x10 ⁻¹¹	4.6x10 ⁻⁸	2.4x10 ⁻⁶	3.5x10 ⁻⁵	7.5x10 ⁻¹⁰	7.5x10 ⁻⁷	3.9x10 ⁻⁵	5.8x10 ⁻⁴	1.4x10 ⁻⁹	1.4x10 ⁻⁶	7.1x10 ⁻⁵	1.0x10 ⁻³	4.6x10 ⁻⁸	4.6x10 ⁻⁵	2.4x10 ⁻³	3.5x10 ⁻²	1.3x10 ⁻⁶	1.3x10 ⁻³	6.8x10 ⁻²	1

This Table Is Reprinted
From "Studies of Special
Topics in Sealing"; Work
Done Under NASA Contract
7-102.

To convert leakage rate units, find the starting pressure x volume units on the left hand side of the chart. Move horizontally on that line, to the column which is 1 for those units. Move vertically to the line which contains the desired new units. Multiply the old leakage rate by the new units to obtain a new pressure x volume.

To convert the time units, obtain the time conversion factors in the above described manner and divide the leak rate by the appropriate conversion factor.

Example: Convert 5 psi x ft³/month to atm x cc/sec

$$5 \text{ psi x ft}^3/\text{month} \times 1.9 \times 10^3 \text{ atm x cc/psi x ft}^3 \times 1/2.6 \times 10^6 \text{ sec/month} = 3.7 \times 10^{-3} \text{ atm-cc/sec}$$

seconds	1	60	3.6x10 ³	8.6x10 ⁴	6.1x10 ⁵	2.6x10 ⁶	3.1x10 ⁷
minutes	1.7x10 ⁻²	1	60	1.4x10 ³	1.0x10 ⁴	4.3x10 ⁴	5.2x10 ⁵
hours	2.8x10 ⁻⁴	1.7x10 ⁻²	1	24	1.7x10 ²	7.2x10 ²	8.8x10 ³
days	1.2x10 ⁻⁵	6.9x10 ⁻⁴	4.2x10 ⁻²	1	7	30	3.7x10 ²
weeks	1.6x10 ⁻⁶	9.8x10 ⁻⁵	5.9x10 ⁻³	0.14	1	4.3	52
months	3.8x10 ⁻⁷	2.3x10 ⁻⁵	1.4x10 ⁻³	3.3x10 ⁻²	0.23	1	12
years	3.2x10 ⁻⁸	1.9x10 ⁻⁶	1.1x10 ⁻⁴	2.8x10 ⁻³	1.9x10 ⁻²	0.83	1

TABLE IV-2

LEAKAGE UNIT CONVERSION

atm cc	1	1.3	3.7×10^{-20}	2.2×10^4	2.2×10^7	6.4×10^5	1.0×10^7
torr liters	0.76	1	2.8×10^{-20}	1.7×10^4	1.7×10^7	4.8×10^5	7.7×10^6
molecules	2.7×10^{19}	3.5×10^{19}	1	6.0×10^{23}	6.0×10^{26}	1.7×10^{25}	2.7×10^{26}
gram-moles	4.5×10^{-5}	5.9×10^{-5}	1.7×10^{-24}	1	10^3	28	4.5×10^2
kilogram-moles	4.5×10^{-8}	5.9×10^{-8}	1.7×10^{-27}	10^{-3}	1	2.8×10^{-2}	0.45
oz-moles	1.6×10^{-6}	2.1×10^{-6}	5.9×10^{-26}	3.5×10^{-2}	35	1	16
lb-moles	1.0×10^{-7}	1.3×10^{-7}	3.7×10^{-27}	2.2×10^{-3}	2.2	6.3×10^{-2}	1

The weight leakages are stated in weight-mole units, i.e. the number of moles of the material expressed in the stated weight units. To obtain the weight of material, multiply the weight-mole by the molecular weight of the material.

The conversions between volume and weight or molecular numbers are made for a gas temperature of 0°C. To convert volume to a weight at any other temperature, multiply result of calculation at 0°C by $\frac{273}{273+T}$. Where T is the temperature in degrees centigrade.

Example:

Convert 5×10^{-4} atm cc of air at 100°C to grams:

$$(5 \times 10^{-4}) \times (4.5 \times 10^{-5}) \times 29 \times (273/373) = 4.78 \times 10^{-7} \text{ GRAMS}$$

$$(\text{ATM CC}) \times \frac{(\text{GRAM-MOLES})}{(\text{ATM CC})} \times (\text{MOLECULAR WT.}) \times (\text{TEMPERATURE CORRECTION}) = (\text{GRAMS})$$

TABLE IV-3

Gasoline	100	Nitrous Oxide	44
Hydrogen	2	Nitric Acid	63
Hydrazine	32	Tetranitromethane	196
UDMH	60	Fluorine	38
Monomethylhydrazine	46	Oxygen Difluoride	54
Ammonia	17	Chlorine Difluoride	92
Diborane	26	Bromine Pentafluoride	175
Pentaborane	59	Perchloryl Fluoride	102
Hydrazine Hydrate	50	Nitrogen Trifluoride	71
Ethylene Oxide	42	Tetrafluorohydrazine	104
Nitromethane	61	Ozone Fluoride	86
Oxygen	32	Water	18
Ozone	48	Argon	40
Hydrogen Peroxide	34	Chlorine	31
Nitrogen Tetroxide	92	Nitrogen	28
Nitric Oxide	30	Helium	4
Nitrogen Dioxide	46	Air	29

APPENDIX V

APPENDIX V

CREEP STUDY REPORT

Prepared By
BATTELLE MEMORIAL INSTITUTE
505 King Avenue
Columbus, Ohio 43201

ABSTRACT

A design procedure is developed for predicting the relaxation or time to leakage for separable tube connectors, including bolted-flanged and threaded types. The procedure is based upon the steady-state creep law, revised to account for the effects of primary creep. Sample calculations are provided for René 41 at 1500 F. The analysis includes the effects of external loads and temperature differentials. René 41 is selected as the best material currently available for use at 1440 F.

TABLE OF CONTENTS

	<u>Page</u>
INTRODUCTION	1
SUMMARY	2
RECOMMENDATIONS	3
NOMENCLATURE	4
CREEP AND RELAXATION	6
MATERIALS	7
Introduction	7
Material Properties	7
Material Selection	11
Design Properties of René 41	15
DESIGN PROCEDURE	17
Basis for Design Procedure	17
Bolted-Flanged Connectors	17
Threaded Connectors	21
External Loads	24
Temperature Differentials	24
Retightening	25
Relaxation Data	25
Redesign Considerations	26
DISCUSSION OF SAMPLE CALCULATIONS	27
REFERENCES	29

APPENDIX A

SAMPLE CALCULATIONS	A-1
Loose-Type Bolted Flange	A-1
Integral-Type Bolted Flange	A-4
Threaded Connector	A-5
External Loads	A-8
Bolt-Flange Temperature Differential	A-8

APPENDIX B

DERIVATION OF EQUATIONS	B-1
-----------------------------------	-----

TABLE OF CONTENTS
(Continued)

	<u>Page</u>
Flange Flexibility	B-1
Bolt Creep	B-2
Flange Creep	B-2
Intercept Stress Reduction	B-3
Bolt Relaxation	B-4
External Loads	B-6
Bolt-Flange Temperature Differential	B-7

APPENDIX C

SECONDARY EFFECTS	C-1
Stress Concentrations	C-1
Creep Bending of Bolt	C-1
Dynamic Creep	C-1
Gasket Creep	C-2
Flange Rotations	C-2

APPENDIX D

TUBE DESIGN	D-1
-----------------------	-----

LIST OF FIGURES

Figure 1. Typical Creep Curve	(Figures appear at end of report)
Figure 2. Steady-State Creep	
Figure 3. Primary Creep	
Figure 4. Creep-Relaxation Comparison (Copper at 165 C)	
Figure 5. Master Creep Curve for René 41 Bar	
Figure 6. Creep Rate of René 41 at 1440 F and 1500 F	
Figure 7. Design Creep Properties of René 41	
Figure 8. Typical Flange Geometry	
Figure 9. Threaded Connector Model	
Figure 10. Inwardly Projecting Flange	
Figure 11. Loose-Type Flange Geometry (René 41-1500 F)	
Figure 12. Integral-Type Flange Geometry (René 41-1500 F)	

LIST OF FIGURES (Continued)

	<u>Page</u>
Figure 13. Residual Bolt Load Versus Time for Bolted-Flanged Connector (Shown in Figure 11)	
Figure 14. Leakage Pressure Versus Time for Bolted-Flanged Connector (Shown in Figure 11)	
Figure 15. Effect of Life Factor on Initial Stress ($\sigma_{BT} = 65,400$ psi)	
Figure 16. Effect of Initial Bolt Stress on Relaxation (Flange Geometry of of Figure 11)	
Figure 17. Threaded-Connector Geometry	
Figure 18. Residual Nut Load Versus Time for Threaded Connector (Shown in Figure 17)	
Figure 19. Intercept Stress Reduction	
Figure 20. Creep of Flange and Bolt	
Figure 21. Creep Bending of Rectangular Section ($n = 6$)	
Figure 22. Combined Creep and Fracture Stress Range Diagram for 6.3% Mo-Waspaloy at 1500 F	

LIST OF TABLES

Table 1. Nominal Compositions of Superalloys	9
Table 2. Properties of Superalloys at 1700 F.	10
Table 3. Properties of Superalloys at 1400-1500 F	12

RELAXATION DESIGN OF SEPARABLE TUBE CONNECTORS

by

L. M. Cassidy, E. C. Rodabaugh, D. B. Roach,
and T. M. Trainer

INTRODUCTION

The design of separable tube connectors for operating below the temperature which produces significant creep of the metal used in the connector may be based on conventional elastic analysis methods. For example, the ASME Unfired Pressure Vessel Code^{(1)*} gives a widely accepted method for designing bolted-flanged joints, including an approximation of the required bolt load and an elastic analysis of the flanges to insure adequate flange strength for carrying the required bolt load.

Even at temperatures where creep does not occur, the design of a conventional separable tube connector is not simply a strength problem, since the usual criterion of failure is leakage and leakage may occur without necessarily overstressing any part of the connector. In practice, conventional connectors are initially loaded (tightened bolts in a bolted-flanged connector, tightened nut in a threaded connector) so that the elastically stored forces in the connector are sufficient to prevent separation of the connector parts due to the subsequently applied service loads arising from internal pressure or loads on the attached pipe or tubing. Accordingly, not only the stresses but also the strains or displacements are significant in connector design.

At operating temperatures where significant creep occurs, the design method for the connector must take into account the relaxation of the elastically stored forces which occur as a result of the plastic flow of the metal components. In bolted-flanged joints designed in accordance with the ASME Code⁽¹⁾, this relaxation effect is taken into account in an indirect and approximate manner by the use of allowable stresses which are based on creep or stress-to-rupture properties of the material. These allowable stresses, however, do not necessarily reflect the relaxation characteristics of bolted-flanged joints in general, and use of the method may result in excessively conservative design or inadequate performance over the desired service life.

There have been previous discussions and simplified analyses^(2,3,4,5,6,7) of relaxation in bolted joints. Unfortunately, a practical solution considering primary creep does not appear to have been developed. The method of analysis presented in this report is intended as a workable approach to the design of separable tube connectors at temperatures where creep or relaxation occurs.

The only known published data on the elevated-temperature testing of separable connectors in order to study leakage is a very comprehensive set of tests^(8,9,10) by the British Pipe Flanges Research Committee on bolted-flanged joints. The results of these tests indicate a definite relation between the time to leakage and the temperature. However, the results are not amenable to a theoretical analysis because of the lack of sufficient specimen creep or relaxation data on the materials used in the test.

*Numbers in raised parentheses designate References on page 29.

Material properties are, of course, interrelated with the design procedure. Accurate information of material properties (such as yield strength, modulus of elasticity, and creep or relaxation rates) are needed to apply the design procedure. Accordingly, this report includes a discussion of material properties and tabulation of properties for various materials with desirable high-temperature properties. The section of the report on material properties leads to a selection of an optimum material for use in connector design for aerospace application at 1440 F operating temperature.

SUMMARY

Materials were evaluated for use at 1440 F, with the result that René 41 is the material choice for the connector design. René 41 is equivalent in strength to the other candidate materials at 1440 F, and has a greater amount of data available. In addition, René 41 is readily available and has seen considerable research and service experience. Nevertheless, the lack of a suitable family of creep curves at 1440 F led to the recommendation that creep or relaxation data be generated for René 41.

With the expectation that relaxation data will not be available for most materials, the design method is directed primarily toward the utilization of creep data, with a discussion on the use of relaxation data. The widespread scatter in creep data as well as possible secondary effects, such as those discussed in Appendix C, led to the use of a design factor of safety.

The design procedure utilizes the steady-state or power law of creep with an assumed zero time reduction in stress to account for primary creep. This approach is conservative for short times, the degree of conservatism depending upon the amount of primary creep exhibited by the material at the design temperature. A comparison is shown for predicting relaxation from creep data for various creep theories.

Both bolted-flanged and threaded connectors are included in the relaxation design, and sample calculations are provided to illustrate the design method for each type of connector. The effect of temperature differentials and external loads on the leakage pressure* is considered. Secondary effects such as stress concentrations, creep bending of bolt, dynamic creep, gasket creep, and flange rotations are discussed briefly, but are not included as an integral part of the design procedure.

The design method is suitable for hand calculations, but could be expedited and easily adapted for solution on a high-speed computer. The optimum (minimum weight) design for a given value of leakage pressure can be determined only after calculating a wide range of geometries. A suitable number of calculations enables the static** design to be rated in accordance with various combinations of leakage pressure and time. The detailed gasket design is not considered herein, since Reference (11) is quite comprehensive in this respect.

*Leakage pressure refers to the value of uniform internal pressure at or below which tolerable leakage rates occur, and should not be confused with the value of gasket pressure required for (1) initially seating the gasket or (2) residual pressure required on the gasket in order to prevent excessive leakage rates. The determination of these gasket pressures is not covered in this report.

**Static design refers to a conventional-type design such as the ASME Boiler Code⁽¹⁾, which is not time dependent.

Various methods of analyses are discussed for the creep design of tubes. The data available indicate that a suitable approach for the tube design is to design for the tangential (hoop) stress on the basis of uniaxial tensile creep data.

RECOMMENDATIONS

On the basis of the subject design study, the following recommendations are made in support of the over-all design effort for separable tube connectors:

- (1) Creep and/or relaxation data on René 41 at 1440 F, preferably relaxation data, should be generated.
- (2) It is recommended that a design factor of safety of 2.0 be used. However, one or more René 41 connectors should be tested at 1440 F in order to substantiate this factor of safety.
- (3) Avoid yielding of the connector components due to stresses incurred during installation.
- (4) Even though retightening of the connector compensates for the bolt or nut relaxation, care must be taken not to incur excessive deformations in the component parts which could lead to rupture.
- (5) In order to be conservative, the cycle time should be measured from the start of the heating cycle to the end of the cooling cycle.
- (6) Consideration should be given to various design configurations. For example, loose-type bolted flanges may offer certain advantages over integral-type flanges which would not be realized in a static design.

NOMENCLATURE*

α	= mean coefficient of thermal expansion, in/in/°F
A	= area of bolt, gasket, tube, or flange, in.
c	= inner radius of flange or tube, in.
C_1	= coefficient in steady-state creep law
C_2	= coefficient in intercept stress law
d	= outer radius of flange or tube, in.
δ	= deflection, in.
e	= moment arm for flange bending, in.
ϵ	= normal strain, in/in.
$\dot{\epsilon}$	= strain rate = $\frac{de}{dt}$, in/in/hr
E	= modulus of elasticity, psi
F_B	= bolt flexibility, in/lb
F'_B	= bending flexibility of the "bolt" (threaded connector), in/lb
F_F	= flange flexibility at bolt circle, in/lb
F.S.	= design factor of safety
g	= radius to centerline of gasket, in.
h	= flange thickness, in.
θ	= rotation, radians
K_B	= creep rate of bolts, in/hr
K'_B	= bending creep rate of the "bolt" (threaded connector), in/hr
K_F	= creep rate of flanges, in/hr
L	= influence coefficient from Page 138, Paragraph UA-47, of the ASME Code ⁽¹⁾
L_B, L_F	= effective length of bolt and flange, respectively, in.
m	= exponent in intercept stress law

*The nomenclature of the ASME Code⁽¹⁾ is used exclusively in the sample Code calculations on pages A-1 and A-4, and is used elsewhere in the report where necessary for clarity.

- M = flange bending moment = Pe , in-lb
 ν = Poisson's ratio
 n = exponent in steady-state creep law
 p = uniform internal pressure, psi
 P = total bolt load, lb
 P'_t = design value for residual bolt load = $\frac{P_t}{F.S.}$, lb
 r_F = flexibility ratio = F_F/F_B
 r'_F = flexibility ratio = F'_B/F_B
 r_K = creep ratio = K_F/K_B
 r'_K = creep ratio = K'_B/K_B
 R = life factor = $\frac{1 + r_F}{1 + r_K}$ (bolted-flanged connector) or $\frac{1 + r_F + r'_F}{1 + r_K + r'_K}$ (threaded connector)
 σ = normal stress, psi
 t = time, hr
 ΔT = temperature differential, °F
 V = influence coefficient from Figure UA-51.3, Page 144, Paragraph UA-51 of the ASME Code⁽¹⁾
 w = width of gasket, in.

Subscripts

- | | |
|------------------------------|--|
| A = axial load | r = radial direction in tube |
| B = bolt | R = room temperature |
| c = creep | t = time |
| e = elastic | T = tube or design temperature |
| F = flange | ϕ = circumferential direction in tube |
| G = gasket | y = yield |
| M = bending moment | z = axial direction |
| o = intercept or zero time | |

CREEP AND RELAXATION

Creep and relaxation are closely related, even though they are not necessarily interchangeable in a stress-analysis problem. These phenomena play an important role in the behavior of a separable connector operating at elevated temperatures, and are best illustrated by mechanical models.

Creep is the tendency for a material to exhibit time-dependent strains at a constant stress level, typical of metals at elevated temperatures. Figure 1 shows a typical creep curve (neglecting tertiary creep) and the corresponding Maxwell-Kelvin model. Figure 1 is obtained by superposition of the Maxwell and Kelvin models of Figures 2 and 3, representing the steady-state and primary creep, respectively. The enclosed design procedure utilizes an equivalent Maxwell model, shown as the dashed curve in Figure 1. The total strain is made up of an instantaneous strain and a time-dependent (steady-state) strain. The instantaneous or intercept strain ϵ_0 includes the elastic strain ϵ_e plus an additional strain $C_2\sigma_0^m$ which conservatively accounts for the primary creep period.

Relaxation is the reduction or relaxation of stress in time under a constant strain. Elastic strains are replaced by creep strains, causing a progressive reduction in stress. The models in Figures 1-3 can be considered relaxation models by assuming a constant total strain rather than a constant stress.

There has been considerable literature written on how to predict relaxation from creep data, few agreeing on the best creep theory to use. Although there are very few test data available on the same material to enable a comparison of various theories, Finnie and Heller⁽⁷⁾ made a comparison of copper at 165 C with an initial stress of 13,500 psi. Figure 4 shows that the steady-state creep law with the intercept stress reduction used herein is conservative for short times and shows good agreement with the experimental results for longer times. Of course, the time scale would be quite reduced for a superalloy at 1440 F.

The most basic form of a separable connector would be flexible bolting in a pair of rigid flanges, in which case the model of Figure 1 would suffice for a relaxation analysis. The tightness of the joint would be dependent on the ability of the bolt to resist creep deformations. However, the flange assembly can also be represented by a Maxwell model in parallel with the bolt assembly. The flange can increase or decrease the rate of bolt relaxation, depending upon the characteristics of the flange geometry. A properly designed flange assembly should be superior to a rigid flange in that the flange elastic recovery as a spring will retard the bolt relaxation.

MATERIALS

At the initiation of the program, it was thought that the connector might be exposed to service temperatures in the range from 70 F to a maximum of 1700 F. The upper temperature limit was subsequently changed to 1440 F. Consequently, material properties are evaluated at both 1700 F and 1440 F, and a material selection made at 1440 F.

Introduction

At the initiation of the materials survey, it was apparent that certain material properties were of major importance in establishing the optimum connector design. Strength over the desired temperature range was the prime criterion. In addition, because of the continued requirement to design space vehicles with minimum weight, density (or strength-to-density ratio) was a major consideration. Also, because service conditions involve cycling from maximum temperature to room temperature, thermal shock, embrittlement, and oxidation were also considered important criteria.

Of the various strength parameters, creep strength and resistance to relaxation were considered of utmost importance. In the installation of a separable connector, the connector is tightened to a given stress. To prevent leakage during service, this stress should remain sufficiently high during service. Relaxation or creep during service will tend to loosen the joint and may give rise to leakage. In addition, good rupture strength and ductility are deemed necessary to insure against complete, catastrophic failure of the connector. Also, because the connector will be installed and tightened at room temperature, consideration must be given to thermal expansion of the connector during heating to the maximum temperature. Variations in thermal expansion of different materials comprising the tubing and the connector could lead to tightening of the connector and undue stress, or to loosening of the connector and leakage.

In addition, consideration was given to the availability, fabricability, machinability, and weldability of the various candidate materials. Of particular importance was the general engineering "know-how" in the handling and use of the various alloys. Finally, since the connector should be capable of being loosened or tightened periodically, consideration was given to bonding or self-welding of the various candidate materials under service conditions.

Material Properties

As indicated above, candidate alloys for separable connectors must have good creep, rupture, and relaxation strengths over the anticipated service-temperature range. Good resistance to thermal shock, oxidation, and embrittlement during cyclic service is also required. These requirements are almost identical to those involved in selection of alloys for turbine-bucket application in aircraft gas turbines. Turbine-bucket materials, however, are not selected on the basis of relaxation resistance, although rupture strength and creep resistance are major requirements. At the present time, turbine-bucket materials are selected on the basis of rupture strength and

thermal-shock resistance. Thus, it was evident that the requirements for separable connectors were sufficiently similar to those of turbine buckets that a summary of the various turbine-bucket materials would likely yield those alloys having the most desired combination of properties for the design of high-temperature separable connectors.

A survey of published property data for various nickel- and cobalt-based superalloys was conducted. Emphasis was placed on creep and rupture strength at 1700 F, and on short-time tensile properties over the service-temperature range. A search of the literature revealed that relaxation data were not available for the bulk of the alloys of interest. On the basis of this survey, the following alloys were selected for more thorough examination:

Wrought Alloys

- (1) Astroloy
- (2) Nimonic 105
- (3) Nimonic 115
- (4) René 41
- (5) Udimet 700
- (6) Unitemp 1753
- (7) Waspaloy

Cast Alloys

- (8) GMR 235
- (9) IN-100
- (10) Inco 713C
- (11) Nicrotung
- (12) SM 200
- (13) SM 302
- (14) SM 322

These alloys have the highest strength at 1700 F. All have been, or, are being considered for use as turbine buckets in gas-turbine engines. Not all of these alloys are readily available, and not all are weldable.

In addition, three more common, lower strength superalloys on which extensive experience in fabrication and usage is available were studied for comparison purposes. These were:

- (15) Inconel X
- (16) N 155
- (17) S 816

Typical compositions for these 17 alloys are given in Table 1.

Alloys for Use at 1700 F

The typical properties of the 17 candidate alloys are given in Table 2. It will be noted in this table that short-time tensile and rupture data were available for the bulk of the alloys. Creep data at 1700 F were quite often lacking. Where creep data were

TABLE 1. NOMINAL COMPOSITIONS OF SUPERALLOYS

Alloy	Form		C	Cr	Co	Fe	Ni	Mo	W	Al	B	Ti	Zr	Other
	Wrought	Cast												
Astroloy	X		0.10	15.0	15.5	—	Balance	5.0	—	4.2	0.03	4.0	—	—
Nimonic 105	X		0.15	15.0	20.0	—	Balance	5.0	—	4.7	—	1.2	—	—
Nimonic 115	X		—	—	—	—	—	—	—	—	—	—	—	—
Rene' 41	X		0.09	19.0	—	—	Balance	10.0	—	1.5	0.005	3.5	—	—
Udimet 700	X	X	0.10	15.0	18.5	—	Balance	5.2	—	4.3	0.008	3.5	—	—
Unitemp 1753	X		0.24	16.0	7.5	9.5	Balance	1.6	8.4	1.9	0.008	3.2	0.06	—
Waspaloy	X		0.08	19.0	13.5	—	Balance	4.5	—	1.3	0.008	3.0	0.08	—
GMR-235		X	0.14	16.0	—	10.0	Balance	5.5	—	3.0	0.05	2.0	—	—
IN 100		X	0.18	10.0	15.0	—	Balance	3.0	—	5.5	0.015	5.0	0.05	—
Inco 713C		X	0.14	12.0	—	—	Balance	4.5	—	6.0	0.012	0.5	0.05	2.0 Cb
Nicrotung		X	0.10	12.0	10.0	—	Balance	—	8.0	4.0	0.05	4.0	0.05	—
SM-200		X	0.15	9.0	10.0	1.5	Balance	—	12.5	5.0	0.015	2.0	0.05	1.0 Cb
SM-302		X	0.85	21.5	Balance	0.8	—	—	—	10.0	0.005	—	0.2	9.0 Ta
SM-322		X	1.00	21.5	Balance	1.5	—	—	—	9.0	—	0.75	2.25	4.5 Ta
Inconel X	X		0.06	16.0	—	7.0	Balance	—	—	0.60	—	2.5	—	1.0 Cb
N-155	X	X	0.15	21.0	20.0	Balance	20.0	3.0	—	—	—	—	—	1.0 Cb + 2.5 V
S-816	X		0.40	20.0	44.0	Balance	20.0	4.0	4.0	—	—	—	—	4.0 Cb

TABLE 2. PROPERTIES OF SUPERALLOYS AT 1700 F

Alloy	0.2% Yield Strength, ksi							Elongation, %, at 1700 F	Stress Rupture, ksi, for Indicated Hours at 1700 F			Creep, %	Stress, ksi, for Indicated % Creep and Indicated Hours at 1700 F			Modulus of Elasticity, ksi x 10 ⁻⁶			Coefficient of Thermal Expansion, in./in./F x 10 ⁻⁶			Density, lb/cu in.
	R.T.	1000 F	1200 F	1400 F	1600 F	1700 F	1800 F		10	100	1000		10	100	1000	1600 F	1700 F	1800 F	80 to 1600 F	80 to 1700 F	80 to 1800 F	
Astroloy (W)	157	153	148	140	—	—	—	—	—	24	14	—	—	—	—	22	20	16.7	—	—	—	0.286
Nimonic 105 (W)	—	132 ^(a)	144 ^(b)	—	58 ^(f)	—	24 ^(g)	—	—	24 ^(f)	13.5 ^(f)	—	—	—	—	—	—	—	—	—	—	—
Nimonic 115 (W)	122	118	119	113	82	64	—	18	37	24.5	16.5	1.0	35	21.5	13	—	—	—	8.9	9.2	9.6	0.284
Rene 41 (W) ^(j)	120	117	116	107	70	46	—	29	25	8	—	0.2	17	14	—	23.0	22.0	—	8.7	9.0	9.3	0.298
Rene 41 (W) ^(k)	154	146	144	136	80	50	—	26	23	12	—	0.2	13	10	—	23.0	22.0	—	8.7	9.0	9.3	0.298
Udimet 700 (W)	140	—	124	120	92	68	44	31	40	28	16	1.0	27.3	17.5	9.6	21.5	19.7	17.5	8.9	9.3	9.6	0.287
Unitemp 1753 (W)	129	126	128	120	90	62	—	21	—	18.5	12	1.0	33 ^(f)	23 ^(f)	—	22.8 ⁽ⁱ⁾	21.9 ⁽ⁱ⁾	20.4 ⁽ⁱ⁾	8.2	8.6	—	0.305
Waspaloy (W)	115	106	100	99	76	50	—	35 ^(e)	32 ^(f)	18 ^(f)	12 ^(f)	1.0	36 ^(d)	25 ^(d)	14 ^(d)	20	18.5	17	9.1	9.3	9.7	0.296
GMR-235 (C)	102	94	89	78	40	30	—	—	28	18	13	1.0	20	9	—	21.7	20.7	19.5	8.5	8.8	9.1	—
IN 100 (C)	123	123	123	120	108	80	61	5	54	38	27	—	—	—	—	—	—	—	—	—	—	0.275
Inco 713C (C)	105	104	104	103	89	62	48	10	—	30	23	0.2	8	6	4	22	—	—	8.7	8.9	9.2	0.286
Nicrotung (C)	120	106	102	96	77	64	52	4.5	43	32	20	—	—	—	—	25.7 ⁽ⁱ⁾	25 ⁽ⁱ⁾	—	8.3	8.5	8.8	0.300
SM-200 (C)	120	124	125	123	109	87	67	3.5	52	40	—	—	—	—	—	—	—	—	—	—	—	0.304
SM-302 (C)	100	74	66	56	45	39	33	13.5	26	18.5	13.5	—	—	—	—	—	—	—	8.3	8.5	8.7	0.333
SM-322 (C)	91	63	57	51	—	—	—	—	32	28	21	—	—	—	—	—	—	—	8.3	8.5	8.7	0.322
Inconel X (W)	90	88	80	70	30	20	—	—	—	8	3	1.0	16 ^(e)	12 ^(e)	—	20 ^(c)	—	—	9.2	—	—	0.298
N-155 (W)	57	48	43	36	25	—	—	—	17.5 ^(f)	10 ^(f)	7.3 ^(f)	—	—	—	—	21	—	—	10.0	10.1	10.2	0.300
S-816 (W)	55	46	44	40	35	—	22	18.5	23 ^(e)	16 ^(e)	9 ^(e)	—	9.8 ^(e,h)	—	—	26 ^(e,i)	—	—	8.8	8.9	9.0	0.313

Note: W = wrought; C = cast.

(a) 930 F.

(g) 1830 F.

(b) 1290 F.

(h) 0.001%/hr.

(c) 1400 F.

(i) Dynamic.

(d) 1500 F.

(j) Sol. tr. 2150 F, 2 hr; AC. Aged 1650 F, 4 hr; AC.

(e) 1600 F.

(k) Sol. tr. 1950 F, 4 hr; AC. Aged 1400 F, 16 hr; AC.

(f) 1650 F.

not available at 1700 F, information on the creep strength at lower temperatures was included.

On the basis of yield strength at 1700 F and creep and rupture strengths at 1700 F, it is evident in Table 2 that the cast alloys have significantly higher strength than the wrought alloys. Of the 17 candidate alloys, SM 200, IN 100, Nicrotung, and Udimet 700 are the highest strength alloys at 1700 F. Of these only Udimet 700 is a wrought material. Of the wrought materials, the order of decreasing strength at 1700 F may be listed as Udimet 700, Nimonic 115, Unitemp 1753, René 41, and Waspaloy.

In general, it was found that the cobalt-based alloys were of lower strength than the nickel-based alloys.

It will be noted that the coefficients of thermal expansion of these alloys were quite similar in the temperature range from 1600 to 1800 F. Likewise, the density values for the nickel-base alloys were quite similar. Those alloys containing significant amounts of tungsten, of course, had slightly higher density values than those containing little tungsten. Because the density values were so similar, there was little merit in comparing the alloys on a strength-to-density basis.

Alloys for Use at 1440 F

It was subsequently decided that the maximum operating temperature for the connector should be reduced from 1700 to 1440 F. Consequently, a survey of the properties of the 17 alloys listed in Table 1 was made to ascertain the most promising alloys at this reduced temperature. The properties of the alloys at 1400 and 1500 F are summarized in Table 3. Where possible, values at 1440 F were interpolated.

The data given in Table 3 show that the wrought alloys compare more favorably with the cast alloys at this temperature than they did at 1700 F. It will be noted that on the basis of yield strength at 1400 to 1500 F, René 41 and Astroloy (Udimet 700) compare favorably with SM 200 and IN 100. On the basis of stress for rupture in 10 hours at 1400 F, SM 200, Udimet 700, Nimonic 115, and René 41 have very similar strengths. For longer times at 1400 F and at 1500 F, René 41 compares less favorably with these other alloys. It will be noted that at 1500 F and above, Waspaloy has strength properties equal to René 41. In the range of 1400 to 1500 F, René 41 has appreciably better short-time tensile properties and higher short-time (10-hour) rupture and creep strengths than Waspaloy.

Material Selection

On the basis of the material properties cited in the preceding section, SM 200, Udimet 700, Nimonic 115, IN 100, and René 41 appear to have the highest strength at 1440 F. SM 200 is a cast alloy which is used principally as the turbine bucket material in the J57 engine. Extensive experience in its use and handling has not been gained as yet. In addition, it is not normally considered a weldable alloy. Udimet 700 has gained appreciable usage, and many shops are familiar with forging and machining the alloy. It is not readily rolled and is not considered weldable. The Nimonics are British alloys not readily available in the United States, and extensive data and experience are not

TABLE 3. PROPERTIES OF SUPERALLOYS AT 1400-1500 F

Alloy	0.2% Yield Strength, ksi			Elongation, %			Stress Rupture, ksi						Creep, %	Stress for Indicated % Creep, ksi						Modulus of Elasticity, ksi x 10 ⁻⁶			Coefficient of Thermal Expansion, in./in. °F x 10 ⁻⁶		
							Hours at 1400 F			Hours at 1500 F				Hours at 1400 F			Hours at 1500 F								
	1400 F	1440 F	1500 F	1400 F	1440 F	1500 F	10	100	1000	10	100	1000		10	100	1000	10	100	1000	1400 F	1440 F	1500 F	1400 F	1440 F	1500 F
Astroloy (W)	140	139	136	—	—	5	—	67	54	—	52	39	—	—	—	—	—	—	23.8	23.5	23.0	—	—	—	
Nimonic 105 (W)	—	—	102 ^(a)	—	—	—	—	72.8 ^(b)	60.5 ^(b)	—	44.8	31.6	—	—	—	—	—	—	—	—	—	—	—	—	
Nimonic 115 (W)	117	—	100	25	23	20	98	77	62	76	55	42	1.0	96	74	57	66	47	34	—	—	—	8.4	8.5	8.6
Rene 41 (W) ^(e,g)	107	103	97	11	12	14	92	68	50	65	45	29	0.2	67	45	30	44	29	18	24.8	24.4	24.0	8.2	8.3	8.5
Rene 41 (W) ^(e,g)	136	130	118	11	11.5	14	90	64	40	60	38	24	0.2 1.0	61 —	39 —	22 —	39 70	17 40	4 25	24.8	24.4	24.0	8.2	8.3	8.5
Udimet 700 (W)	120	116	110	23	25	29.5	94	78	64	76	58	43	1.0	—	—	—	—	46	29	24.0	23.5	22.8	8.3	—	8.6
Unitemp 1753 (W)	120	115	110	15	—	15	—	—	—	60	47	34	1.0	—	—	—	52	42	—	24.2 ^(d)	—	23.5 ^(d)	7.8	7.9	8.0
Waspaloy (W)	98	95	90	28	28.3	29	79	60	42	58	40	26.5	1.0	—	—	—	36	25	14	22.5	22.0	21.3	8.6	8.7	8.8
GMR-235 (C)	78	74	60	—	—	—	—	—	—	52	38	25	1.0	50	43	36	39	31	22	23.6	23.3	22.7	8.1	8.2	8.3
IN-100 (C)	120	118	115	6	5.5	5	—	—	—	85	72	59	—	—	—	—	—	—	—	—	—	—	—	—	—
Inco 713C (C)	103	101	97	5	5	5	—	81	72	70	55	41	0.2	36	29	22	28	22	15	27.1	26.5	25.0	8.2	8.3	8.5
Nicrotung (C)	96	94	90	6	4	3	—	—	—	—	65	—	1.0	—	—	—	75	62	50	—	—	—	—	—	—
SM-200 (C)	123	122	121	3.2	3	3	92	90	—	81	73	—	—	—	—	—	—	—	—	—	—	—	—	—	—
SM-302 (C)	56	54	52	8	8.5	9.5	—	—	—	49	—	40	—	—	—	—	—	—	—	—	—	—	8.0	8.1	8.1
SM-322 (C)	51	50	—	6	—	—	61	48	36	49	38	26	—	—	—	—	—	—	—	—	—	—	—	—	—
Inconel X (W)	70	—	60	10	—	20	45 ^(c)	36 ^(c)	—	35	28	18	0.2	—	—	—	32	27	16	21	—	18	8.7	—	9.0
N-155 (W)	36	—	30	31	—	32.5	36 ^(b)	28 ^(b)	22 ^(b)	26	17.5	15	1.0	—	—	—	—	15	13	22.1	—	21.1	9.7	—	9.8
S-816 (W)	40	—	38	25	—	21	43	32.5	25	31.2	23.7	16.5	—	—	—	—	—	—	—	26.2	—	25.8	8.8	—	8.9

Note: W = wrought; C = cast.

(a) 1470 F.

(e) Sol. tr. 2150 F, 2 hr; AC. Aged 1650 F, 4 hr; AC.

(b) 1350 F.

(f) Sol. tr. 1950 F, 4 hr; AC. Aged 1400 F, 16 hr; AC.

(c) 1425 F.

(g) Modulus of Elasticity E = 32 x 10⁶ psi at 70 F.

(d) Dynamic.

available on Nimonic 115. IN 100 has gained little commercial acceptance, and little is known of the alloy other than the properties cited.

Extensive experience, on the other hand, has been gained in the use of René 41. The alloy is available as forgings, billets, bar, and sheet from several sources. It has excellent strength properties over the temperature range from 70 to 1500 F. In fact, it was for this temperature range that René 41 was specifically designed. It was not designed to be used at temperatures above 1500 F.

For these reasons, René 41 was selected as the most promising material for high-temperature separable connectors. Table 3 cites the short-time-tensile and the available creep-rupture properties of René 41. Complete time-deformation curves during creep testing are required in designing connectors for high-temperature use. To obtain specific data for design purposes, a family of complete creep curves at a number of stresses at 1440 F is required. Such curves were not available in the literature. In most creep testing, loads are usually selected to produce rupture in 1000 hours or less. Such loads can result in 0.2 to 0.3 per cent deformation on loading. At lower stress levels where smaller per cent deformation on loading occurs, rupture lives of several thousand hours will result. Such tests are seldom run, and if they are, complete creep data are not reported. Nevertheless, a few complete creep curves for René 41 in the temperature range of interest were uncovered in References (12, 13).

Relaxation data on René 41 were not available in the literature.

René 41 is a precipitation-hardenable nickel-base alloy. The material is usually supplied in the solution-annealed condition. Hardening is accomplished by aging the alloy at 1400 or 1650 F. This causes precipitation of a complex nickel-titanium-aluminum phase (called the gamma-prime phase) and produces excellent strength over the temperature range of interest.

René 41 is readily forged and considerable experience has been accumulated by many forge shops in working the alloy. Like most high-strength nickel-base alloys, René 41 work hardens rapidly during machining and is considered difficult to machine. Nevertheless, it is machined by many shops on a production basis.

René 41 is considered a weldable alloy. Nevertheless, as is the case with all high-strength precipitation-hardenable alloys, welding may be somewhat of a problem. Welding in the solution-annealed condition (the low-strength condition) is recommended. After welding, the part should be reannealed and aged to obtain the properties cited. Welding in the aged condition, particularly under conditions of stress, is not recommended. This is true of all precipitation-hardenable nickel-base alloys. In general, it has been found that the greater the aluminum plus titanium content, the higher is the strength and the more difficult are the welding operations. The use of a significantly more weldable material will consequently entail a very appreciable reduction in strength and a sizable weight penalty.

Two specific heat treatments have been developed for René 41: one to develop maximum short-time strength and one to develop maximum long-time creep and rupture strengths. The former treatment involves solution treating at 1950 F for 4 hours, air cooling, and aging at 1400 F for 16 hours. This treatment yields good short-time tensile properties and acceptable 10-hour rupture and creep strengths. The latter treatment, involving solution treating at 2150 F for 2 hours, air cooling, and aging at

1650 F for 4 hours, produces somewhat reduced short-time tensile properties but significantly improved long-time creep and rupture strength. As indicated previously, René 41 should be welded in the solution-treated condition. Recent welding studies have revealed problems in weld metal cracking for material welded after the high-temperature treatment (2150 F). The use of the lower temperature treatment (1950 F) has reportedly eliminated weld-metal-cracking problems. For this reason, a solution-treatment temperature of 1950 F and an aging treatment of 1400 F are recommended. With such a heat treatment, high short-time tensile properties and good 10-hour rupture and creep properties will be obtained. A sacrifice in long-time creep and rupture strength will result. Long-time strength is not a prime requirement for the present application.

René 41 has excellent oxidation resistance over the specified service-temperature range. It is not known to become embrittled in this temperature range. While comparative data on resistance to thermal shock are not available, it is believed that the alloy has comparable or better resistance to thermal shock than the other candidate materials.

Finally, it is not anticipated that René 41 will show a tendency to bonding or self-welding during service. Alloys which contain appreciable amounts of chromium, aluminum, and titanium are exceedingly difficult to bond. Bonding is accomplished only in atmospheres capable of reducing the stable spinel-type oxide on the surface of the alloy and under conditions of high temperature, high stress, and relative metal flow at mating surfaces. Consequently, self-welding of connectors of this alloy is not to be expected. If sticking of the connector is encountered, oxidation of the mating surfaces of the connector should reduce, if not eliminate, the problem. Heating the connector at about 1800 F in an atmosphere containing a low oxygen content should produce a hard, thin oxide layer which is exceedingly difficult to remove. Such an oxide film should prevent self-welding of the connector. If self-bonding persists, the deposition of a very thin layer of titanium or aluminum on the mating surfaces of the connector is recommended. The thin film should be diffused into the connector and oxidized by heating to high temperatures, such as solution treating at 1950 F. This should prevent self-welding.

In summation, René 41 has been selected as the material of construction for high-temperature separable connectors operating from room temperature to 1440 F. Certain other alloys have better creep strength than René 41; however, the combination of properties obtainable in René 41, as well as the availability and experience gained on this alloy, strongly recommends it.

This survey and the recommendations were made with limited knowledge of the tubing material that will be used with the René 41 connector. If the connector is to be welded to the tubing, knowledge of the tubing material is required before the weldability and the compatibility of the connector and the tubing can be ascertained. Welding dissimilar materials is often a major problem. While it is not the purpose herein to select a tubing material, consideration was given to various tubing materials capable of being employed with René 41 connectors. René 41 tubing is not currently commercially available. The high-temperature tubing materials capable of being employed in this application and currently commercially available are Inconel X, Hastelloy X, Inconel 718, and Waspaloy. Inconel X, Hastelloy X, and Inconel 718 are of significantly different composition than René 41. In addition, these alloys have significantly lower strength at the design temperature than René 41, and the heat treatments employed to strengthen these alloys are not compatible with that recommended for René 41. In

comparison, Waspaloy is quite similar in composition to René 41, and has similar physical and mechanical properties. The heat treatment of René 41 is compatible with that of Waspaloy, and welding René 41 connectors to Waspaloy tubing is feasible.

It is therefore suggested that Waspaloy be given full consideration as the tubing material for use with René 41 connectors. Both the tubing and the connector should be in the solution-treated condition for welding. After welding, the assembly must be completely heat treated. The heat treating sequence recommended is as follows:

- (1) Solution treat at 1975 F for 4 hours, air cool
- (2) Stabilize at 1550 F for 24 hours, air cool
- (3) Age at 1400 F for 12 hours, air cool.

This heat treatment is recommended for Waspaloy. The René 41 connectors, when subjected to this heat treatment, will have properties comparable to those reported herein.

Design Properties of René 41

The minimum or steady-state creep rates are determined from the master creep curve of Reference (14), shown in Figure 5. The data of Figure 5 are replotted in Figure 6 for 1440 and 1500 F. The straight dashed lines in Figure 6 are a conservative fit to the data at the two temperatures. The corresponding constants are:

At 1440 F,

$$C_1 = 4.23 \times 10^{-28} ,$$

$$n = 4.97.$$

At 1500 F,

$$C_1 = 1.30 \times 10^{-26} ,$$

$$n = 4.82.$$

A rapid method for determining the constants C_1 and n from creep data, using the creep law $\dot{\epsilon} = C_1 \sigma^n$, is as follows:

Determine the strain rates $\dot{\epsilon}_1$ and $\dot{\epsilon}_2$ for the stresses σ_1 and σ_2 , respectively. From the steady-state creep law, $\dot{\epsilon}_1 / \dot{\epsilon}_2 = (\sigma_1 / \sigma_2)^n$, where n is the only unknown, and is easily solved. After calculating n , the constant C_1 can be determined from $\dot{\epsilon}_1 = C_1 \sigma_1^n$.

The constants C_2 and m for the intercept stress were obtained from the test data and plotted curves of Reference (13). Since the intercept data of Reference (13) are not very consistent, the following constants are considered only approximate in magnitude. This is one reason for the recommendation that creep data be generated for René 41 at 1440 F.

At 1440 F,

$$C_2 = 1.25 \times 10^{-8},$$

$$m = 1.00.$$

At 1500 F,

$$C_2 = 3.93 \times 10^{-11},$$

$$m = 1.57.$$

The design data for René 41 at 1440 F and 1500 F are plotted in Figure 7 for various stress levels.

Other design properties of René 41 are obtained from Tables 2 and 3.

The yield strength $\sigma_y = 120,000$ psi at 70 F,

$$\sigma_y = 103,000 \text{ psi at } 1440 \text{ F},$$

$$\sigma_y = 97,000 \text{ psi at } 1500 \text{ F}.$$

The modulus of elasticity $E_R = 32.0 \times 10^6$ psi at 70 F,

$$E_T = 24.4 \times 10^6 \text{ psi at } 1440 \text{ F},$$

$$E_T = 24.0 \times 10^6 \text{ psi at } 1500 \text{ F}.$$

The mean coefficient of thermal expansion $\alpha = 8.3 \times 10^{-6}$ in/in/°F at 1440 F,

$$\alpha = 8.5 \times 10^{-6} \text{ in/in/°F at } 1500 \text{ F}.$$

DESIGN PROCEDURE

Basis for Design Procedure

The design procedure considers only the elastic and creep behavior of the bolts and flange assembly. Secondary effects such as flange rotation due to internal pressure, creep of the gasket, creep of the threads, creep bending of the bolt, and dynamic creep are not included in the design procedure, but are discussed in Appendix C. The design factor of safety is intended to account for these secondary effects in addition to the scatter in material properties.

The gasket (seal) design for mechanical fittings is not included in the design procedure, but is discussed in Reference (11), where it was concluded that plastic yielding of seal surfaces is desirable for effective sealing. An initial seating stress as high as 2.75 times the yield strength of the metal gasket material was considered necessary to achieve the desired degree of yielding in order to keep the leakage rate of helium below the tolerable level⁽¹¹⁾.

It is assumed that the bolts are flexible compared to the gasket in order that the application of internal pressure results in negligible bolt-load changes. It is not necessary that the gasket be the only load path through the assembly.

The design procedure is intended primarily as a method for calculating relaxation of the connector assembly, and does not include a failure analysis of the component parts. It is assumed that the material possesses sufficient ductility to withstand the progressive deformation incurred if the connector assembly is retightened after each cycle. Various methods of analysis available for predicting the tube strains are discussed in Appendix D. These methods are intended for the tube design at locations sufficiently removed from discontinuities such as the connector assembly.

The detailed design procedure for bolted-flanged and threaded connectors is described step-by-step for the purpose of obtaining a curve of leakage pressure versus time (or a time to leakage for a specific value of the design pressure). The effects of external loads, temperature differentials, and retightening, and the use of relaxation data are discussed separately from the basic design procedure.

The equations used in the design procedure are derived in Appendix B.

Bolted-Flanged Connectors

The basic design procedure for a bolted-flanged connector consists of nine specific steps in order to arrive at a curve of leakage pressure versus time. Figure 8 shows a typical flange geometry.

(1) Design Conditions

Establish the design temperature, design pressure, nominal connector diameter, tube geometry, life requirements, and temperature differentials.

(2) Material Properties

Determine the yield strength σ_y and the modulus of elasticity E at both room temperature and the design temperature, and the coefficient of thermal expansion α at the design temperature.

From a family of creep curves at the design temperature, determine the constants C_1 , C_2 , m , and n to fit the following equation:

$$\epsilon = \epsilon_e + C_2 \sigma_o^m + C_1 \sigma_o^n t \quad (1)$$

The creep constants should be selected to give the best fit to the experimental data in the range of stress levels expected in the design*.

(3) ASME Code Design

The design procedure can be applied to any arbitrary design. However, it is desirable to use the ASME Boiler and Pressure Vessel Code⁽¹⁾ for the initial static design in order to establish a balanced design. Also, the Code-rated flange can subsequently be rated on a life basis for comparison.

Using the rules of the ASME Code⁽¹⁾, establish either a loose-type or integral-type flange geometry for an appropriate value of internal pressure. This pressure, of course, should be at least as high as the design pressure multiplied by the ratio of the cold-to-hot modulus of elasticity, and multiplied by the design factor of safety. The initial gasket seating load will be dependent on the type seal used and the maximum permissible leakage rate, and need not follow the rules of Reference (1). The allowable Code stress is assumed to equal two-thirds of the room-temperature yield strength in order to avoid yielding of the assembly during the bolt-up operation.

The ASME Code will establish a static design at room temperature. The initial bolt load and bolt stress at room temperature are designated as P_{BR} and σ_{BR} , respectively.

(4) Flexibility Equations

Determine the bolt flexibility F_B (bolt deflection due to a unit bolt load):

$$F_B = \frac{L_B}{A_B E_T} \quad (2)$$

*Further details on the creep constants and the intercept stress reduction are given on pages 6, 15, and B-3.

where

L_B = effective length of the bolt, usually taken as the total length between the nut bearing surfaces plus one nominal bolt diameter,

A_B = total bolt area based on root diameter.

Determine the flange flexibility F_F (total deflection of two flanges at the bolt circle due to a unit bolt load).

For a loose-type flange,

$$F_F = \frac{3.82 e^2}{E_T h^3 \ln d_F / c_F} \quad (3)$$

For an integral-type flange,

$$F_F = \frac{1.29 V e^2}{L \sqrt{c_F} (d_T - c_T)^{5/2} E_T} \quad (4)^*$$

(5) Creep Equations

Calculate the rate of creep deflection of the bolts K_B and the rate of creep deflection of the two flanges at the bolt circle, K_F :

$$K_B = \frac{C_1 P_t^n L_B}{A_B^n}, \quad (5)$$

and

$$K_F = \frac{4 \sigma_{Ft}^n C_1 e c_F}{h}, \quad (6)$$

where

$$\sigma_{Ft} = \left(\frac{h}{2 c_F} \right)^{\frac{1}{n}} \left(\frac{P_t e}{2 \pi} \right) \left[\frac{\left(2^{1+\frac{1}{n}} \right) \left(1 - \frac{1}{n} \right) \left(2 + \frac{1}{n} \right)}{\left(d_F^{1-\frac{1}{n}} - c_F^{1-\frac{1}{n}} \right) h^{2+\frac{1}{n}}} \right]$$

Equation (6) applies only to a loose-type flange. The creep rate of an integral-type flange is assumed equal to that of the loose-type flange, provided the maximum design stresses according to Reference (1) are equal. The procedure for an integral-type flange is to calculate the maximum design stress by Reference (1). Then determine the thickness of a loose-type flange with the same flange inner and outer radii, moment arm, and maximum design stress as the integral-type flange; this results in an equivalent strength loose-type flange. Using the loose-type flange geometry, calculate the creep rate from Equation (6), assuming this to be the creep rate of the integral-type flange.

*The terms V and L in Equation (4) conform to the nomenclature of Reference (1).

(6) Flexibility and Creep Ratios

Calculate the life factor R for the purpose of conveniently evaluating a flange geometry on a life basis:

$$R = \frac{1 + r_F}{1 + r_K} \quad , \quad (7)$$

where

$$r_F = \text{flexibility ratio} = F_F/F_B \quad ,$$

$$r_K = \text{creep ratio} = K_F/K_B \quad .$$

Equations (5) and (6) should be calculated in terms of the bolt load P_t , in order that the creep ratio r_K be calculable.

(7) Intercept Stress Reduction

Calculate the bolt stress, σ_{BT} . The initial room-temperature bolt stress σ_{BR} is reduced to a new value σ_{BT} at the design temperature due to the change in modulus of elasticity:

$$\sigma_{BT} = \sigma_{BR} \left(\frac{E_T}{E_R} \right) \quad . \quad (8)$$

Calculate a further reduction in bolt stress from σ_{BT} to a value σ_o due to the effects of primary creep:

$$\sigma_o = \sigma_{BT} - \frac{E_T C_2 \sigma_o^m}{R} \quad . \quad (9)$$

Equation (9) is conveniently solved for σ_o by trial and error. The bolt stress σ_o or corresponding bolt load P_o represents the actual starting point in the life calculations.

(8) Bolt Relaxation

Calculate the time t required for the bolt stress to relax from an initial value σ_o to a new value σ_t :

$$t = \frac{R}{C_1 E_T^{(n-1)}} \left[\frac{1 - \left(\frac{\sigma_t}{\sigma_o} \right)^{n-1}}{\sigma_t^{n-1}} \right] \quad . \quad (10)$$

(9) Leakage Pressure

Solve Equation (10) successively in order to obtain a curve of residual bolt stress σ_t or load P_t versus time. Convert these results to an allowable leakage pressure versus time curve by the successive solution of Equation (11):

$$P_t' = P_p + P_G \quad , \quad (11)$$

where

$$P_t' = \frac{P_t}{F.S.} \quad ,$$

$$P_p = \text{bolt load due to pressure} = \pi p g^2 \quad ,$$

P_G = residual gasket load (or load across flange face) required to prevent excessive leakage (the determination of this load is not included in this report).

In Equation (11), P_t' is established directly from the P_t versus t curve by applying a suitable factor of safety to the load rather than the time scale. The value P_G is dependent on the type of gasket used, and may or may not be a function of the internal pressure p .

Threaded Connectors

The design procedure for threaded connectors commences with Step 1 (design conditions) and Step 2 (material properties) of the bolted-flanged connector design procedure. Six additional steps are then required for the threaded connector in order to obtain a leakage pressure versus time curve.

Reference (15) can be used for the static design of a threaded connector. The nomenclature for the parts of the threaded connector is based on the functional analogy to the parts of the bolted-flanged connector and is not to be taken as a literal description of the parts. A threaded connector model is shown in Figure 9. The nut is considered the "bolt" member of the analysis, and contributes both axial and bending deformations. The flange and union members in Figure 9 are considered the "flange" member of the analysis with axial deformation only.

(1) "Bolt" Flexibility

Calculate the "bolt" flexibility F_B , which represents the axial flexibility of the nut and has the same form as Equation (2):

$$F_B = \frac{L_B}{A_B E_T} \quad , \quad (12)$$

where L_B and A_B are the effective nut length and area, respectively.

Calculate the bending flexibility of the "bolt" F_B' by using the development on pages 194-197 of Reference (15) for inwardly projecting flanges (see Figure 10):

$$F_B' = e^2 \left(\frac{\theta}{M} \right) \quad , \quad (13)$$

where

$$\frac{\theta}{M} = \frac{3(1-\nu^2)}{\pi d_T \beta (d_T - c_T)^3 E_T \left[\frac{(1-\nu^2)}{2\beta d_T} \left(\frac{h}{d_T - c_T} \right)^3 \ln \frac{d_T}{c_F} + 1 + \frac{\beta h}{2} \right]}$$

and

$$\beta = \sqrt[4]{\frac{3(1-\nu^2)}{d_T^2 (d_T - c_T)^2}} .$$

(2) "Flange" Flexibility

Calculate the axial flexibility of the "flange", F_F :

$$F_F = \frac{L_F}{A_F E_T} . \quad (14)$$

The effective length L_F can be considered equal to L_B in Equation (12). A_F is the cross-sectional area of the "flange".

(3) "Bolt" Creep

Calculate the axial creep rate of the "bolt", K_B :

$$K_B = \frac{C_1 P_t^n L_B}{A_B^n} . \quad (15)$$

Calculate the bending creep rate of the "bolt", K'_B , in a manner similar to an integral-type flange*, except that the maximum design stress is determined from Reference (15) for an inwardly projecting flange.

The longitudinal hub stress S_H , radial ring stress S_R , and tangential ring stress S_T , respectively, are

$$S_H = \frac{3M}{\pi d_T (d_T - c_T)^2 \left[\frac{(1-\nu^2)}{2\beta d_T} \left(\frac{h}{d_T - c_T} \right)^3 \ln \frac{d_T}{c_F} + 1 + \frac{\beta h}{2} \right]} ,$$

$$S_R = \frac{3(1 + \frac{\beta h}{2})M}{\pi d_T h^2 \left[\frac{(1-\nu^2)}{2\beta d_T} \left(\frac{h}{d_T - c_T} \right)^3 \ln \frac{d_T}{c_F} + 1 + \frac{\beta h}{2} \right]} , \quad (16)$$

*See procedure on page 19 for integral-type flanges.

$$S_T = \frac{3(1-\nu^2)hM}{2\pi d_T c_F (d_T - c_T)^3 \beta \left[\frac{(1-\nu^2)}{2\beta d_T} \left(\frac{h}{d_T - c_T} \right)^3 \ln \frac{d_T}{c_F} + 1 + \frac{\beta h}{2} \right]},$$

$$\text{where } \beta = \sqrt[4]{\frac{3(1-\nu^2)}{d_T^2 (d_T - c_T)^2}}.$$

The maximum stresses from Equations (16) should be combined according to the method of Reference (1). For a threaded connector, Equation (6) herein should be used with a constant of two rather than four because there is one rather than two flange members.

(4) "Flange" Creep

Calculate the axial creep of the "flange", K_F , which has the same form as Equation (15):

$$K_F = \frac{C_1 P_t^n L_F}{A_F^n} \quad (17)$$

(5) Flexibility and Creep Ratios

Calculate the life factor R:

$$R = \frac{1 + r_F + r'_F}{1 + r_K + r'_K}, \quad (18)$$

where

$$r_F = F_F/F_B, \quad r'_F = F'_B/F_B,$$

$$r_K = K_F/K_B, \quad r'_K = K'_B/K_B.$$

(6) Nut Relaxation

Determine the relaxation of the nut from Equation (10), but using the life factor R from Equation (18). Use Equation (11) to calculate the leakage pressure versus time.

External Loads

Determine the effect of external loads on the leakage pressure by revising Equation (11) to read:

$$P'_t = P_p + P_G + P_A + P_M \quad , \quad (19)$$

where P_A and P_M include the effects of external thrusts and moments, respectively:

$$P_A = \pi p K_A c_T^2 \quad , \quad (20)$$

$$P_M = \frac{\pi p K_M c_T^2 (d_T^2 + c_T^2)}{2 d_T g}$$

Solve Equation (19) successively in order to obtain a leakage pressure versus time curve.

The constants K_A and K_M are used to define the magnitude of the stress due to tube thrusts (σ_A) and moments (σ_M), respectively, in terms of the axial tube stress (σ_T) due to internal pressure:

$$K_A = \frac{\sigma_A}{\sigma_T} \quad , \quad K_M = \frac{\sigma_M}{\sigma_T} \quad ,$$

where

$$\sigma_T = \frac{p c_T^2}{(d_T^2 - c_T^2)} \quad .$$

Temperature Differentials

The analysis of temperature differentials is limited herein to the case of components at uniform temperatures, but at a different average temperature from another component of the assembly. In one case, the bolt is assumed to be at a different average temperature than the flange and tube assembly, probably the more critical case. In the other case, the flange and bolt assembly is assumed to be at a different average temperature than the tube. The change in material properties with temperature change is neglected in the thermal calculations. It is also assumed that the temperature differentials are of a short-time nature, occurring almost instantaneously for the purpose of analysis. A more refined analysis would be required for temperature differentials varying considerably with time.

Bolt-Flange Differential

Letting a positive value of ΔT represent the flange at a higher average temperature than the bolt, calculate the change in bolt stress $\Delta \sigma_B$:

$$\Delta \sigma_B = \frac{\alpha(\Delta T) E_T}{1 + r_F} \quad . \quad (21)$$

For a threaded connector, the change in "bolt" (nut) stress is

$$\Delta\sigma_B = \frac{\alpha(\Delta T) E_T}{1 + r_F + r'_F} \quad (22)$$

The change in bolt or nut load in Equations (21) and (22) should be evaluated in a different manner, depending upon the nature of the differential. A positive temperature differential at the start of the cycle would lead to an increase in the bolt load. This increase should be used to guard against overstressing of the bolt (or other connector components), and neglected for short-time differentials in the relaxation analysis. If a negative temperature differential should occur near the end of the operating cycle, the reduction in bolt load should be added to Equation (11) to determine a reduced leakage pressure:

$$P'_t = P_p + P_G + P_T \quad , \quad (23)$$

where $P_T = \Delta\sigma_B A_B$ (bolt-load change due to temperature differential).

Flange-Tube Differential

The analysis by Dudley⁽¹⁶⁾ or an extension of the equations presented by Rodabaugh in discussion of Reference (17) can be used to evaluate bolt-load changes due to the tube and flange assembly being at different average temperatures. The method of Rodabaugh⁽¹⁷⁾ is preferred, since it is consistent with the basic equations of the ASME Code⁽¹⁾. At the start of the operating cycle the tube will possibly be hotter than the remaining assembly, thus causing a reduction in the bolt load. The opposite effect may occur upon cooling down the assembly. An increase in the bolt load should be used to guard against overstressing the connector assembly, whereas a decrease in the bolt load should be used in Equation (23).

Retightening

If the assembly is not retightened between operating cycles, a continuous operating cycle is assumed, consisting of the total time of the individual cycles. This procedure is consistent with the assumption that creep strains are irreversible in nature.

In the event that retightening is contemplated, each cycle is reanalyzed according to the creep design procedure (not repeating static design) as though it were the first cycle. This is a conservative approach because the flange life will probably improve on subsequent cycles to the extent that the primary creep strains are nonrecurring, as evidenced by the British Flange Tests⁽⁹⁾.

Relaxation Data

The design procedure is based on the assumption that only creep data are available. Of course, relaxation data are preferred. Relaxation data should be available as a

family of curves, starting from various initial stress levels, sufficient to cover the range of initial stress levels expected in the design.

Since the relaxation test is usually run with no elastic follow-up ($R = 1$), the time required for a connector assembly bolt or nut stress to relax from an initial stress σ_0 to a final value σ_t is obtained directly from the relaxation test data, multiplied by the life factor R determined from Equation (7) or (18). If the relaxation tests are run with elastic follow-up, the relaxation time is determined by multiplying the test data (time) by the ratio of the life factor R of the connector to that of the test assembly. Interpolation of the test data may be required for specific values of the initial stress σ_0 not available in the test data. The use of a direct ratio for various values of the life factor is based on the assumption that the life factor is a constant in the analysis. Baumann⁽²⁾ justifies this approach, regardless of the creep law observed by the material.

The direct use of relaxation data results in a residual stress versus time curve, similar to that yielded by Equation (10). In generating relaxation data, it would be desirable to run at least one test with sufficient elastic follow-up to simulate the life factor of a connector assembly.

Redesign Considerations

The designer may find that the calculated connector life for a particular design pressure is less than the required design life. If the temperature and material have already been fixed, the only changes that can be made in order to obtain an improved life are geometry changes. Ordinarily, the connector inner diameter, bolt geometry, and gasket geometry will be kept constant during a redesign. Therefore, the logical changes to make if the life factor R in Equation (10) is to be improved are changes in the flange thickness, flange width, and moment arm.

Changes in the moment arm e can have an appreciable effect on the life factor R . Of course, an increase in the moment arm will have to be compensated for by changes in the flange width and/or thickness (or hub geometry for an integral-type flange) in order that the flange stresses be maintained at an acceptable level. It is recommended that improvements in the connector life be made by simultaneous changes in the moment arm for flange bending, the flange width, and the flange thickness. Effects of changes in the length of the bolt L_B (perhaps with the use of a rigid bolt collar) should also be investigated.

If the desired connector life is not attained by the changes described above, the next logical step would be to redesign the bolt geometry and gasket geometry in order to allow for greater percentage reductions in the initial bolt load before leakage occurs.

DISCUSSION OF SAMPLE CALCULATIONS

The sample calculations are presented in order to adequately demonstrate the design procedure, and not to arrive at optimum design connectors. An optimum design can be determined only after calculating a wide range of connector geometries, thus enabling the selection of a minimum-weight design for a given combination of design (leakage) pressure and life.

The loose-type and integral-type flange geometries of Figures 11 and 12, respectively, have nearly the same initial stress σ_0 , and the life factor R differs by only 10 per cent. Therefore, the results in Figures 13 and 14 for the loose-type flange very nearly apply for the integral-type flange. The loose-type flange is heavier. This will not always be the case since the loose-type flange can frequently have a much higher flexibility than the equivalent integral-type flange.

The factor of safety used in Figure 13, together with the intercept stress reduction and the bolt load reduction due to change in elastic modulus, leads to a maximum design pressure of 2980 psi in Figure 14, assuming no external loads or temperature differentials. It is shown that a temperature difference between the bolt and flange assembly of -100 F severely affects the leakage pressure and establishes a limiting life of 38 hours. The curves of Figure 14 indicate that, up to approximately 0.5 hour, there is negligible change in the leakage pressure. This would infer that, for accumulated life cycles totaling 0.5 hour or less, retightening after each cycle would not be very beneficial.

René 41 at 1500 F does not exhibit a great deal of primary creep, as shown by the relative insensitivity of the initial stress σ_0 to the life factor R in Figure 15. For some materials, the effect of the life factor on the reduced intercept stress would be a strong influence in choosing an optimum design. The life factor R is a convenient measure of the relative merits of various designs with the same initial bolt stress because it is essentially a geometry-dependent constant in the relaxation equation, all other constants in Equation (10) being a function only of the material and temperature.

It is usually considered desirable to preload the bolt or nut as high as possible without yielding any portions of the connector assembly. The high preload is intended to delay the relaxation of stress or load. Various values of the initial bolt stress were used in the relaxation equation (27). The results in Figure 16 indicate that, for design lives over 1-2 hours, there is very little advantage gained by higher prestressing. In fact, the initial prestress σ_0 of 45,000 psi would be more desirable for longer lives since it will provide greater safety against yielding. The initial stress of 90,000 psi at 1500 F for René 41 would be difficult to obtain because of the intercept stress reduction, the elastic modulus change, and the limitation imposed on the room-temperature bolt preload to avoid yielding.

Results of the threaded-connector geometry of Figure 17 are shown in Figure 18. The geometry of Figure 17 does not represent a well-balanced design. As a result, the axial nut stress σ_{BR} is limited to 40,000 psi (room-temperature prestress) to avoid over-stressing the inwardly projecting flange. The low prestress results in the relatively slow relaxation of the nut load shown in Figure 18.

It is quite possible that the optimum static design will also provide a good design for relaxation, depending upon the material and design temperature. However, for some combinations of material and temperature, the sound static design approach may not suffice because of the importance of the interaction of bolt and flange creep and flexibility ratios. For a static design, the integral-type bolted flange is usually lighter than the loose-type flange. This may not be true for relaxation design. In some cases, loose-type flanges offer advantages in the way of increased flexibility and the ability to better withstand certain types of temperature differentials.

REFERENCES

- (1) ASME Boiler and Pressure Vessel Code, Section VIII, "Rules for Construction of Unfired Pressure Vessels", New York (1962).
- (2) Baumann, K., "Some Considerations Affecting Future Developments of the Steam Cycle", Engineering, 130, 597-599, 661-664, 723-727 (1930).
- (3) Bailey, R. W., "The Utilization of Creep Test Data in Engineering Design", Proceedings of the Institution of Mechanical Engineers, 131, 131-349 (1935).
- (4) Bailey, R. W., "Flanged Pipe Joints for High Pressures and Temperatures", Engineering, 144, 364-365, 419-421, 490-492, 538-539, 615-617, 674-676 (1937).
- (5) Waters, E. O., "Analysis of Bolted Joints at High Temperature", Transactions of the ASME, 60, 83-86 (1938).
- (6) Marin, J., Mechanical Properties of Materials and Design, McGraw-Hill Book Co., Inc., New York (1942).
- (7) Finnie, I., and Heller, W. R., Creep of Engineering Materials, McGraw-Hill Book Co., Inc., New York (1959).
- (8) Gough, H. J., "First Report of the Pipe Flanges Research Committee", Proceedings of the Institution of Mechanical Engineers, 132, 201-340 (1936).
- (9) Tapsell, H. J., "Second Report of the Pipe Flanges Research Committee", Proceedings of the Institution of Mechanical Engineers, 141, 433-471 (1939).
- (10) Johnson, A. E., "Pipe Flanges Research Committee - Third Report", Proceedings of the Institution of Mechanical Engineers, 168, 423-463 (1954).
- (11) Rathbun, F. O., Jr., "Design Criteria for Zero-Leakage Connectors for Launch Vehicles, Vol 3, Sealing Action at the Seal Interface", General Electric Advanced Technology Laboratories Report No. 63GL43 (March 15, 1963).
- (12) Aarnes, M. N., and Tuttle, M. M., "Presentation of Creep Data for Design Purpose", ASD Technical Report 61-216 (June, 1961).
- (13) Gluck, J. V., and Freeman, J. W., "Effect of Creep - Exposure on Mechanical Properties of René 41", ASD Technical Report 61-73 (August, 1961).
- (14) Sachs, G., and Pray, R. F., "Air Weapons Materials Application Handbook - Metals and Alloys", ARDC Report TR 59-66.
- (15) Rodabaugh, E. C., et al., "Development of Mechanical Fittings", Edwards Air Force Base Report No. RTD-TDR-63-1115 (December, 1963).
- (16) Dudley, W. M., "Deflection of Heat Exchanger Flanged Joints as Affected by Barreling and Warping", Transactions of the ASME, Series B, 83, 460-466 (November, 1961).

- (17) Wesstrom, D. B., and Bergh, S. E., "Effect of Internal Pressure on Stresses and Strains in Bolted-Flanged Connections", Transactions of the ASME, 73, 121-136 (1951).
- (18) Timoshenko, S., "Strength of Materials - Part II", D. Van Nostrand Co., Inc. (1956).
- (19) Marin, J., "Stresses and Deformations in Pipe Flanges Subjected to Creep at High Temperatures", Journal of the Franklin Institute, 226, 645-657 (1938).
- (20) MacCullough, G. H., "An Experimental and Analytical Investigation of Creep in Bending", Transactions of the ASME, Journal of Applied Mechanics, 55, 55-60 (1933).
- (21) Tapsell, H. J., and Johnson, A. E., "An Investigation of the Nature of Creep Under Stresses Produced by Pure Flexure", Journal of the Institute for Metals, 57 (2), 121-140 (1935).
- (22) Davis, E. A., "Creep of Metals at High Temperature in Bending", Transactions of the ASME, Journal of Applied Mechanics, 60, A-29-A-31 (March, 1938).
- (23) Findley, W. N., and Poczatek, J. J., "Prediction of Creep - Deflection and Stress Distribution in Beams From Creep in Tension", Transactions of the ASME, 77 (1955).
- (24) Hult, J., "Mechanics of a Beam Subject to Primary Creep", Transactions of Chalmers University of Technology, Gothenburg, Sweden (256) (1962).
- (25) Voorhees, H. R., Freeman, J. W., and Herzog, J. A., "New Investigations Relating to Stress Concentrations Under Creep Conditions", Transactions of the ASME, Journal of Basic Engineering, 84, 207-213 (June, 1962).
- (26) Lazan, B. J., "Dynamic Creep and Rupture Properties of Temperature Resistant Materials Under Tensile Fatigue Stress", ASTM Proceedings, 49, 757-787 (1949).
- (27) Vitovec, F. H., and Lazan, B. J., "Fatigue, Creep, and Rupture Properties of Heat Resistant Materials", WADC Technical Report 56-181, ASTIA AD 97240 (August, 1956).
- (28) Langenecker, B., "Acoustic Radiation Damage in Materials", Presented at Leak-Tight Separable Fluid Connector Design Conference at Huntsville, Alabama (March 24-25, 1964).
- (29) Finnie, I., "Steady-State Creep of a Thick-Walled Cylinder Under Combined Axial Load and Internal Pressure", ASME Paper No. 59-A-57.
- (30) Finnie, I., "An Experimental Study of Multiaxial Creep in Tubes", 1963 Joint International Conference on Creep.
- (31) Rimrott, F.P.J., Mills, E. J., and Marin, J., "Prediction of Creep Failure Time for Pressure Vessels", Transactions of the ASME, Journal of Applied Mechanics, 27, 303-308 (June, 1960).

- (32) Davis, E. A., "Creep Rupture Tests for Design of High-Pressure Steam Equipment", Transactions of the ASME, Journal of Basic Engineering, 82, 453-461 (June, 1960).
- (33) Rattinger, I., and Padlog, J., "Design Implications of Creep in Pressurized Cylindrical Shells", Aerospace Engineering, 20, 95-108 (March, 1961).
- (34) Coffin, L. F., Jr., Shepler, P. R., and Cherniak, G. S., "Primary Creep in the Design of Internal-Pressure Vessels", Transactions of the ASME, 71, 229-241 (1949).

LMC:ECR:DBR:TMT/all

APPENDIX A

SAMPLE CALCULATIONS

APPENDIX A

SAMPLE CALCULATIONS

The sample calculations are all performed on René 41 at 1500 F. The following design values apply to René 41 at room temperature and at 1500 F*.

The yield strength:

$$\sigma_y = 120,000 \text{ psi at } 70 \text{ F,}$$

$$\sigma_y = 97,000 \text{ psi at } 1500 \text{ F.}$$

The modulus of elasticity:

$$E_R = 32.0 \times 10^6 \text{ psi at } 70 \text{ F,}$$

$$E_T = 24.0 \times 10^6 \text{ psi at } 1500 \text{ F.}$$

The mean coefficient of thermal expansion $\alpha = 8.5 \times 10^{-6} \text{ in/in/}^\circ\text{F}$ at 1500 F.

The creep and intercept constants at 1500 F are:

$$C_1 = 1.30 \times 10^{-26},$$

$$C_2 = 3.93 \times 10^{-11},$$

$$n = 4.82,$$

$$m = 1.57.$$

The ASME Code calculations are based on an internal pressure of 10,000 psi. This corresponds to a reduced value of the design pressure equal to 10,000 (E_T/E_R) (1/F.S.) = 3750 psi for a factor of safety equal to two. Therefore, the maximum possible value of the design pressure is 3750 psi, and will be further reduced due to the effects of primary creep.

Loose-Type Bolted FlangeASME Code Design**

The allowable stress for use in Reference (1) equals $2/3 (120,000) = 80,000 \text{ psi}$. The geometry is shown in Figure 11.

The tube thickness can be determined from other considerations, such as discussed in Appendix D, to equal 0.210 in.

For the purpose of the bolt design, assume that a residual gasket stress of 3P (P = 10,000 psi, the ASME Code design pressure) is required to maintain the gasket

*Material properties for René 41 are given on pages 15-16.

**Use the nomenclature of the ASME Code⁽¹⁾.

seal. Also, assume that the gasket plating material has a yield strength of 10,000 psi and that it requires a gasket stress of three times the yield strength ($y = 60,000$ psi) to seat the metallic gasket. For a gasket width $2b = 0.125$ in. (assume full width is effective),

$$H_P = 2b \times 3.14G \times 3P = 45,900 \text{ lb},$$

$$H = 0.785 G^2 P = 119,000 \text{ lb},$$

$$W_{m1} = H + H_P = 164,900 \text{ lb},$$

$$W_{m2} = 3.14bGy = 45,900 \text{ lb}.$$

The design bolt load $W = 164,900$ lb.

The required bolt area is

$$A_{m1} = \frac{164,900}{80,000} = 2.06 \text{ in}^2.$$

Use 10-9/16-in.-diameter bolts with a total root area equal to 1.89 in^2 . The bolt stress is

$$S_a = \frac{164,900}{1.89} = 87,300 \text{ psi}.$$

For the flange design,

$$h_G = h_T = 0.663 \text{ in.}, \quad h_D = 0.813 \text{ in.},$$

$$H_D = 0.785 B^2 P = 102,000 \text{ lb},$$

$$H = 0.785 G^2 P = 119,000 \text{ lb},$$

$$H_G = W - H = 45,900 \text{ lb},$$

$$H_T = H - H_D = 17,000 \text{ lb},$$

$$M_D = H_D h_D = 82,800 \text{ lb},$$

$$M_T = H_T h_T = 11,300 \text{ lb},$$

$$M_G = H_G h_G = 30,500 \text{ lb},$$

$$M_O = M_D + M_T + M_G = 124,600 \text{ in-lb},$$

$$S_T = 80,000 \text{ psi},$$

$$K = A/B = 1.90.$$

From Figure UA-51.1 of Reference (1), $Y = 3.3$.

Then,

$$t = \sqrt{\frac{Y M_o}{B S_T}} = 1.20 \text{ in.}$$

Flexibility and Creep

From the equations on pages 18-20,

$$F_B = 1.78/E_T, \quad F_F = 1.51/E_T,$$

$$K_B = 0.157 C_1 P_t^{4.82},$$

$$\sigma_{Ft} = 0.215 P_t,$$

$$K_F = 2.405 \times 10^{-3} C_1 P_t^{4.82},$$

$$r_F = 0.849, \quad r_K = 0.0153,$$

$$R = 1.82.$$

Bolt Relaxation

From Equations (8) and (9),

$$\sigma_{BT} = 87,300 \left(\frac{24 \times 10^6}{32 \times 10^6} \right) = 65,400 \text{ psi},$$

$$\sigma_o = \sigma_{BT} - \frac{E_T C_2 \sigma_o^m}{R} \quad (24)$$

Solving Equation (24) by trial and error, $\sigma_o = 52,100$ psi. It is convenient to solve Equation (24) for various values of R in order to construct Figure 15, thus saving considerable calculating time when optimizing the flange geometry. For a rigid flange ($R = 1$), σ_o would equal 46,000 psi.

From Equation (10), the bolt relaxation equation becomes

$$t = 1.53 \times 10^{18} \left[\frac{\left(\frac{\sigma_t}{\sigma_o} \right)^{n-1}}{\sigma_t^{n-1}} \right] \quad (25)$$

With $\sigma_o = 52,100$ psi, the successive solution of Equation (25) results in the residual bolt-load curve of Figure 13.

Leakage Pressure

In order to convert residual bolt load to leakage pressure assume a factor of safety F.S. = 2.0 on the residual load, establishing the design curve of Figure 13. For example, if it is assumed that leakage will occur when the gasket pressure reaches a value of $3p$, Equation (11) becomes

$$P_t' = \pi p g^2 + 3pA_G. \quad (26)$$

The solution of Equation (26) for various values of the internal pressure p results in the leakage pressure versus time curve ($K_A = K_M = 0, \Delta T = 0$) of Figure 14. For example, at $p = 2000$, $P_t' = 33,000$ lb. The time t from Figure 13 for 33,000 lb is 4.9 hours.

Effect of Initial Stress

The relaxation equation for the geometry of Figure 11 is

$$t = 1.53 \times 10^{18} \left[\frac{1 - \left(\frac{\sigma_t}{\sigma_0} \right)^{n-1}}{\sigma_t^{n-1}} \right]. \quad (27)$$

The effect of varying the bolt stress σ_0 in Equation (27) is shown in Figure 16.

Integral-Type Bolted Flange

ASME Code Design*

An integral-type flange was designed in accordance with Reference (1). The gasket geometry, moment arm, outer flange radius, tube geometry, and design bolt load are the same as for the loose-type flange of Figure 11. The integral-type flange geometry is shown in Figure 12:

$$h_T = 0.868 \text{ in.}, \quad h_G = 0.663 \text{ in.}, \quad h_D = 0.863 \text{ in.}$$

From page A-2,

$$W = 164,900 \text{ lb,}$$

$$H = 0.785 G^2 P = 119,000 \text{ lb,}$$

$$H_D = 0.785 B^2 P = 74,500 \text{ lb,}$$

$$H_G = W - H = 45,900 \text{ lb,}$$

$$H_T = H - H_D = 44,500 \text{ lb,}$$

*Use the nomenclature of the ASME Code(1).

$$M_D = H_D h_D = 64,200 \text{ lb},$$

$$M_T = H_T h_T = 38,600 \text{ lb},$$

$$M_G = H_G h_G = 30,500 \text{ lb},$$

$$M_O = M_D + M_T + M_G = 133,300 \text{ in-lb.}$$

Using an allowable stress of 80,000 psi and a design moment of 133,300 in-lb, the thickness of an integral-type flange is calculated from Reference (1) to be 0.95 in.

Flexibility and Creep

From Equations (2) and (5),

$$F_B = 1.35/E_T,$$

$$K_B = 0.118 C_1 P_t^{4.82}.$$

Since the flange design stress of 80,000 psi is the same as that of the equivalent loose-type flange, the flange creep rate is assumed to equal that of the loose-type flange:

$$K_F = 2.405 \times 10^{-3} C_1 P_t^{4.82}.$$

The flexibility of the integral-type flange from Equation (4) is

$$F_F = 1.43/E_T.$$

Then

$$r_F = 1.06, \quad r_K = 0.0204,$$

$$R = 2.02.$$

Bolt Relaxation

From Figure 15, $\sigma_o = 52,900$ psi. The bolt relaxation equation becomes

$$t = 1.69 \times 10^{18} \left[\frac{1 - \left(\frac{\sigma_t}{\sigma_o} \right)^{n-1}}{\sigma_t^{n-1}} \right]. \quad (28)$$

Equation (28) does not yield results significantly different from Equation (25) for a loose-type flange.

Threaded Connector

Figure 17 shows a threaded-connector geometry, which represents an arbitrary set of dimensions rather than an optimum static design. The design procedure is used to

calculate the design life of the geometry of Figure 17, based on René 41 at 1500 F. Figure 9 is a guide for the proper dimensions to use in the analysis.

Bolt Flexibility

$$A_B = \pi(1.05^2 - 0.90^2) = 0.91 \text{ in.}^2,$$

$$L_B = 1.60 - 0.45 = 1.15 \text{ in.}$$

The axial flexibility of the bolt is

$$F_B = \frac{L_B}{A_B E_T} = 1.26/E_T.$$

The bending flexibility of the bolt is

$$= F'_B = e^2 \left(\frac{\theta}{M} \right) = 1.14/E_T,$$

where

$$\frac{\theta}{M} = 19.8/E_T,$$

and

$$e = \frac{1.05 + 0.90}{2} - \frac{0.86 + 0.60}{2} = 0.24 \text{ in.}$$

Flange Flexibility

$$L_F = L_B = 1.15 \text{ in.},$$

$$A_F = \pi(0.86^2 - 0.50^2) = 1.54 \text{ in.}^2,$$

$$F_F = \frac{L_F}{A_F E_T} = 0.75/E_T.$$

Bolt Creep

The axial creep of the bolt is

$$K_B = \frac{C_1 P_t^n L_B}{A_B^n} = 1.82 C_1 P_t^{4.82}.$$

In order to obtain the bending creep rate of the bolt, the stresses for an inwardly projecting flange are calculated from Reference (15). The critical combination of these stresses by the ASME Boiler Code⁽¹⁾ is

$$\frac{S_H + S_T}{2} = 9.18 M.$$

For a maximum design stress equal to $2/3 \sigma_y = 80,000$ psi, the design moment equals $80,000/9.18$, or $M = 8710$ in-lb. With a moment arm $e = 0.24$ in., this corresponds to an initial nut design load of 36,300 lb. In this case, the initial load of 36,300 lb is not limited by the axial stress in the nut, but by the stress in the inwardly projecting flange.

The thickness of an equivalent loose-type flange is determined from Reference (1) using the basic geometry of the inwardly projecting flange of Figure 17. The equivalent thickness equals 0.575 in. The creep rate of the equivalent loose-type flange, calculated from Equation (6), is

$$K'_B = \frac{2\sigma_{Ft}^n C_1^{ec} F}{h} = 1.26 C_1 P_t^{4.82},$$

where

$$\sigma_{Ft} = 1.21 P_t.$$

Flange Creep

$$K_F = \frac{C_1 P_t^n L_F}{A_F^n} = 0.145 C_1 P_t^{4.82}.$$

Flexibility and Creep Ratios

$$r_F = 0.595, \quad r'_F = 0.905,$$

$$r_K = 0.0796, \quad r'_K = 0.693,$$

$$R = \frac{1 + r_F + r'_F}{1 + r_K + r'_K} = 1.41.$$

Intercept Stress Reduction

The initial bolt stress is

$$\sigma_{BR} = P/A_B = 36,300/0.91 = 40,000 \text{ psi},$$

$$\sigma_{BT} = 40,000 \left(\frac{E_T}{E_R} \right) = 30,000 \text{ psi}.$$

From Equation (9),

$$\sigma_o = 24,700 \text{ psi,}$$

or

$$P_o = \sigma_o A_B = 22,500 \text{ lb.}$$

Nut Relaxation

From Equation (10),

$$t = 1.18 \times 10^{18} \left[\frac{1 - \left(\frac{\sigma_t}{\sigma_o} \right)^{n-1}}{\sigma_t^{n-1}} \right] \quad (29)$$

The relaxation curve is shown in Figure 18.

External Loads

It is assumed that $K_A = K_M = 0.50$ in this example. The leakage criterion used in Equation (26) is used in Equation (19) to calculate a leakage pressure versus time curve. For example (for the connector shown in Figure 11), at a pressure p of 2000 psi, from Equation (26),

$$P_p + P_G = 33,000 \text{ lb.}$$

From Equation (20),

$$P_A = 7440 \text{ lb,}$$

$$P_M = 5920 \text{ lb.}$$

Then, from Equation (19),

$$P'_t = 33,000 + 7440 + 5920 = 46,360 \text{ lb.}$$

The design curve of Figure 13 gives $t = 0.37$ hour. The results are shown in Figure 14 ($K_A = K_M = 0.50, \Delta T = 0$).

Bolt-Flange Temperature Differential

It is assumed that at the beginning of the cooling-down cycle, the bolt assembly is hotter than the flange assembly, or

$$\Delta T = -100 \text{ F.}$$

From Equation (21) and the geometry of Figure 11,

$$\Delta \sigma_B = \frac{\alpha (\Delta T) E_T}{1 + r_F} = 11,000 \text{ psi.}$$

The reduction in bolt load due to the thermal gradient is

$$P_T = (11,000)(1.89) = 20,800 \text{ lb.}$$

From Equation (23),

$$P'_t = P_p + P_G + P_T. \quad (30)$$

From Equations (26) and (30), at a pressure $p = 1500$ psi,

$$P'_t = \pi(1500)(1.95^2) + 3(1500)(1.53) + 20,800 = 45,580 \text{ lb.}$$

From Figure 13, $t = 0.52$ hour.

The results of the analysis are shown in Figure 14 ($K_A = K_M = 0$, $\Delta T = -100$ F).

APPENDIX B

DERIVATION OF EQUATIONS

APPENDIX B

DERIVATION OF EQUATIONSFlange FlexibilityLoose Type

Timoshenko⁽¹⁸⁾ gives the flange rotation θ_F due to a flange moment M as

$$\theta_F = \frac{12M}{2\pi E_T h^3 \ln d_F/c_F} . \quad (31)$$

Since

$$M = Pe,$$

and the flange deflection at the bolt circle is

$$\delta_F = e\theta_F, = \frac{1.91Pe^2}{E_T h^3 \ln d_F/c_F} \quad (32)$$

then,

$$F_F = \frac{2\delta_F}{P} = \frac{3.82e^2}{E_T h^3 \ln d_F/c_F} . \quad (33)$$

Integral Type

Wesstrom and Bergh⁽¹⁷⁾ present an equation for the flange rotation:

$$\theta_F = \frac{0.645 VM}{L \sqrt{c_F} (d_T - c_T)^{5/2} E_T} . \quad (34)^*$$

Since the total flange moment $M = Pe$, and the deflection $\delta_F = \theta_F e$,

$$F_F = \frac{2\delta_F}{P} = \frac{1.29 Ve^2}{L \sqrt{c_F} (d_T - c_T)^{5/2} E_T} . \quad (35)^*$$

*The terms V and L in Equations (34) and (35) conform to the nomenclature of Reference (1).

Bolt Creep

From the steady-state creep law,

$$\epsilon_B = C_1 \sigma_B^n t, \quad (36)$$

or, the bolt deflection is

$$\delta_B = \frac{C_1 P_t^n t L_B}{A_B^n}, \quad (37)$$

where

$$\sigma_B = \frac{P_t}{A_B}.$$

Then,

$$K_B = \frac{\delta_B}{t} = \frac{C_1 P_t^n L_B}{A_B^n} \quad (38)$$

Flange Creep

Marin⁽¹⁹⁾ developed equations for the steady-state creep of a circular ring of rectangular cross section subjected to uniform moments. The flange rotation and maximum stress on the inner surface are

$$\theta_F = \left[\left(\frac{P_t e}{2\pi} \right) \frac{\left(2^{1+\frac{1}{n}} \right) \left(1 - \frac{1}{n} \right) \left(2 + \frac{1}{n} \right)}{\left(d_F^{1-\frac{1}{n}} - c_F^{1-\frac{1}{n}} \right) h^{2+\frac{1}{n}}} \right]^n C_1 t, \quad (39)$$

$$\sigma_{Ft} = \left(\frac{h}{2c_F} \right)^{\frac{1}{n}} \left(\frac{P_t e}{2\pi} \right) \left[\frac{\left(2^{1+\frac{1}{n}} \right) \left(1 - \frac{1}{n} \right) \left(2 + \frac{1}{n} \right)}{\left(d_F^{1-\frac{1}{n}} - c_F^{1-\frac{1}{n}} \right) h^{2+\frac{1}{n}}} \right]. \quad (40)$$

Equations (39) and (40) are based on the steady-state creep law $\epsilon = C_1 \sigma^n t$ and assume the creep stress distribution in the flange. There exists sufficient test and theoretical data on the creep bending of beams^(20, 21, 22, 23, 24) to justify that:

- (1) Plane sections remain plane.
- (2) The creep deflections can be predicted on the basis of the steady-state creep law.

- (3) Individual fibers of the beam creep at a rate equivalent to that predicted by a tensile creep test.
- (4) The creep stress distribution is attained shortly after the commencement of the test and does not change for the remainder of the test. This is analytically confirmed by Hult⁽²⁴⁾. Because of the like nature of the beam and ring deformations, the above assumptions are also assumed to hold true for the creep deflection of a flange.

From Equations (39) and (40),

$$\theta_F = \frac{2\sigma_{Ft}^n C_1 c_{Ft}}{h} . \quad (41)$$

Then,

$$K_F = \frac{2e\theta_F}{t} = \frac{4\sigma_{Ft}^n C_1 e c_F}{h} . \quad (42)$$

Intercept Stress Reduction

It is assumed that the initial stress σ_{BT} is reduced in zero time to a new value σ_o which has a total intercept strain ϵ_o equal to the initial bolt stress σ_{BT} divided by the modulus of elasticity E_T . From Figure 19,

$$\epsilon_o = \epsilon_e + C_2 \sigma_o^m , \quad (43)$$

or

$$\sigma_{BT} = \sigma_o + E_T C_2 \sigma_o^m . \quad (44)$$

The constants C_2 and m are determined by a best fit to the intercept data from a family of creep curves at the design temperature.

For a flexible flange, the interaction of the flange and bolt has to be accounted for. The primary creep of the bolt can be represented by

$$\delta_{Bc} = C_2 \sigma_o^m L_B . \quad (45)$$

The change in bolt stress is determined by the elastic bolt recovery:

$$\sigma_o = \sigma_{BT} - \frac{\delta_{Be} E_T}{L_B} . \quad (46)$$

From Figure (20), in order to maintain compatibility of bolt and flange,

$$\delta_{\text{TOTAL}} = \delta_{\text{Fe}} - \delta_{\text{Fc}} = \delta_{\text{Bc}} - \delta_{\text{Be}} . \quad (47)$$

By definition,

$$r_F = \frac{\delta_{\text{Fe}}}{\delta_{\text{Be}}} , \quad r_K = \frac{\delta_{\text{Fc}}}{\delta_{\text{Bc}}}$$

$$R = \frac{1 + r_F}{1 + r_K} ,$$

and Equation (47) becomes

$$\delta_{\text{Be}} (r_F + 1) = \delta_{\text{Bc}} (r_K + 1), \quad (48)$$

or

$$\frac{\delta_{\text{Be}}}{\delta_{\text{Bc}}} = \frac{1 + r_K}{1 + r_F} = \frac{1}{R} . \quad (49)$$

Substituting (45) and (46) in (49),

$$\sigma_o = \sigma_{\text{BT}} - \frac{E_T C_2 \sigma_o^m}{R} . \quad (50)$$

For a rigid flange ($R = 1$), Equation (50) is identical to Equation (44). The development of Equation (50) for a flexible flange assumes that the creep ratio r_K is the same for primary creep as it is for steady-state creep.

Bolt Relaxation

The analysis of bolt relaxation is similar to that of References (2,6). The nomenclature is defined as follows:

L_F = original length between nut bearing surfaces

L_B = length of bolt if it is relieved of stress before creep occurs

$\delta' = L_F - L_B$ = initial flange deflection plus bolt extension (or total initial relative movement between nut and bolt)

$K_F t = \delta_{\text{Fc}}$ = creep deflection of flanges

$K_B t = \delta_{\text{Bc}}$ = creep deflection of bolts

$F_F P = \delta_{\text{Fe}}$ = elastic flange deflection

$F_B P = \delta_{\text{Be}}$ = elastic bolt deflection.

In order that the flange and bolts maintain contact at any time,

$$L_F - \delta_{Fc} - \delta_{Fe} = L_B + \delta_{Bc} + \delta_{Be}, \quad (51)$$

or

$$\delta' = \delta_{Bc} (1 + r_K) + \delta_{Be} (1 + r_F). \quad (52)$$

Since

$$\delta_{Be} = \frac{\delta_B L_B}{E_T},$$

$$\delta' = \delta_{Bc} (1 + r_K) + \frac{\delta_B L_B}{E_T} (1 + r_F),$$

or

$$\sigma_B = \frac{E_T}{L_B} \left[\frac{\delta' - \delta_{Bc} (1 + r_K)}{1 + r_F} \right]. \quad (53)$$

Differentiate (53) with respect to time:

$$\frac{d\sigma_B}{dt} = \frac{-E_T}{L_B} \left(\frac{1 + r_K}{1 + r_F} \right) \frac{d\delta_{Bc}}{dt}. \quad (54)$$

From the steady-state creep law,

$$\dot{\epsilon}_c = C_1 \sigma_B^n = \frac{d\epsilon_c}{dt} = \frac{d}{dt} \left(\frac{\delta_{Bc}}{L_B} \right),$$

or

$$\frac{d\delta_{Bc}}{dt} = L_B C_1 \sigma_B^n. \quad (55)$$

Substitute (55) in (54):

$$\frac{d\sigma_B}{\sigma_B^n} = \frac{-E_T C_1 dt}{R}. \quad (56)$$

Integrate (56), letting $\sigma_B = \sigma_t$:

$$\frac{\sigma_t^{-n+1}}{1-n} = \frac{-E_T C_1 t}{R} + C, \quad (57)$$

where C is a constant of integration. At $t = 0$, $\sigma_t = \sigma_0$. Therefore,

$$C = \frac{\sigma_o^{-n+1}}{1-n}.$$

From (57),

$$t = \frac{R}{C_1 E_T (n-1)} \left[\frac{1 - \left(\frac{\sigma_t}{\sigma_o} \right)^{n-1}}{\sigma_t^{n-1}} \right]. \quad (58)$$

Equation (58) also applies to the relaxation of the nut in a threaded connector design with R defined by Equation (18).

External Loads

Axial Load

The axial load P_A is assumed to be a tensile force which reduces the gasket pressure. The magnitude of the tube stress σ_A due to the axial load P_A is defined as a constant times the axial tube stress due to internal pressure:

$$P_A = \sigma_A A_T = \sigma_A \pi (d_T^2 - c_T^2), \quad (59)$$

where

$$\sigma_A = K_A \sigma_T = \frac{p K_A c_T^2}{(d_T^2 - c_T^2)}. \quad (60)$$

From (59) and (60),

$$P_A = \pi p K_A c_T^2 \quad (61)$$

Bending Moment

The required additional bolt load P_M accounts for the tendency of the tube bending moment M_T to reduce the gasket pressure. The magnitude of the tube stress σ_M due to the bending moment M_T is defined as a constant K_M times the axial tube stress due to internal pressure:

$$\sigma_M = K_M \sigma_T = \frac{p K_M c_T^2}{(d_T^2 - c_T^2)}. \quad (62)$$

From beam bending theory,

$$\sigma_M = \frac{4 M_T d_T}{\pi (d_T^4 - c_T^4)}. \quad (63)$$

Combining (62) and (63),

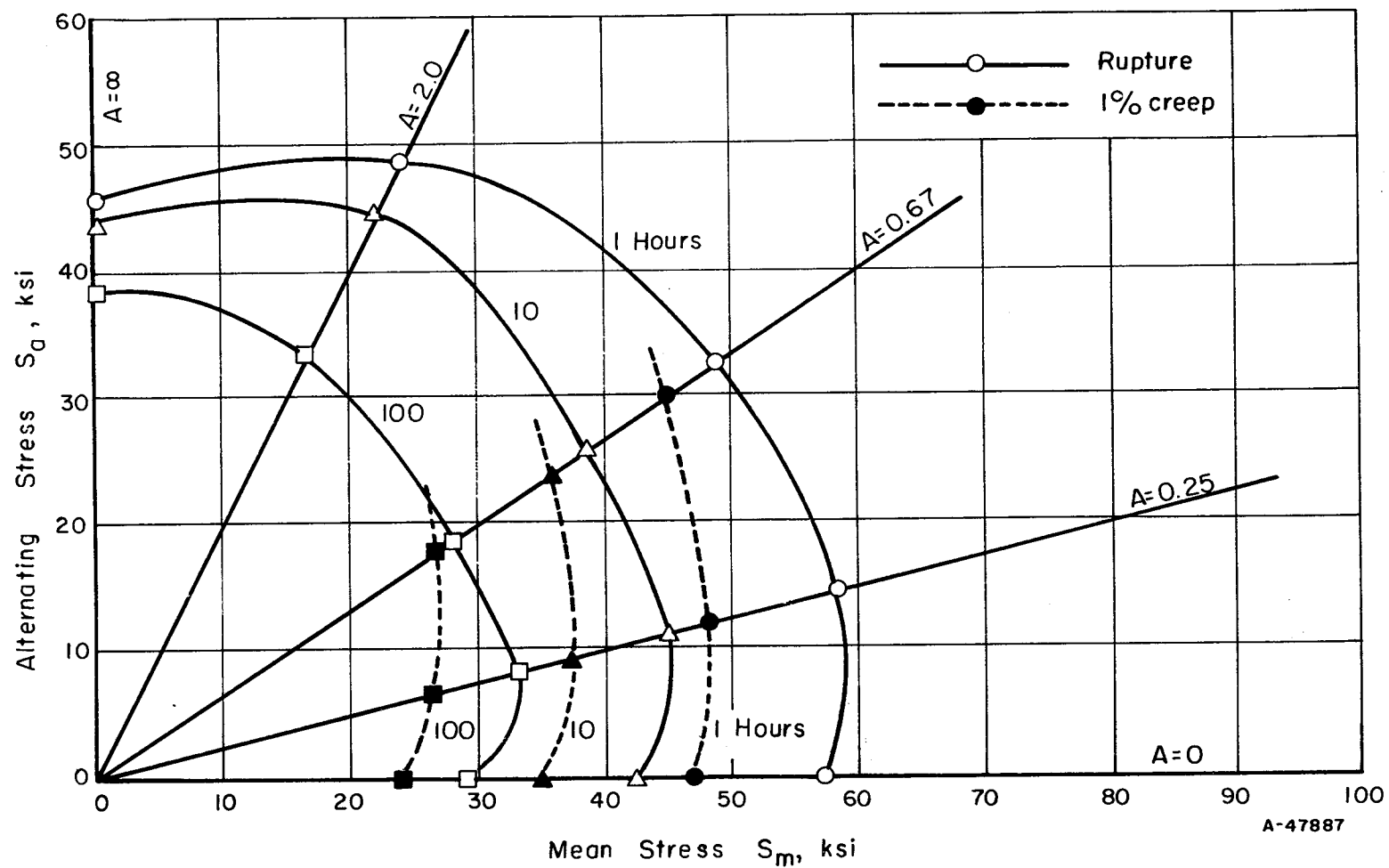


FIGURE 22. COMBINED CREEP AND FRACTURE STRESS RANGE DIAGRAM FOR 6.3% Mo-WASPALLOY AT 1500 F

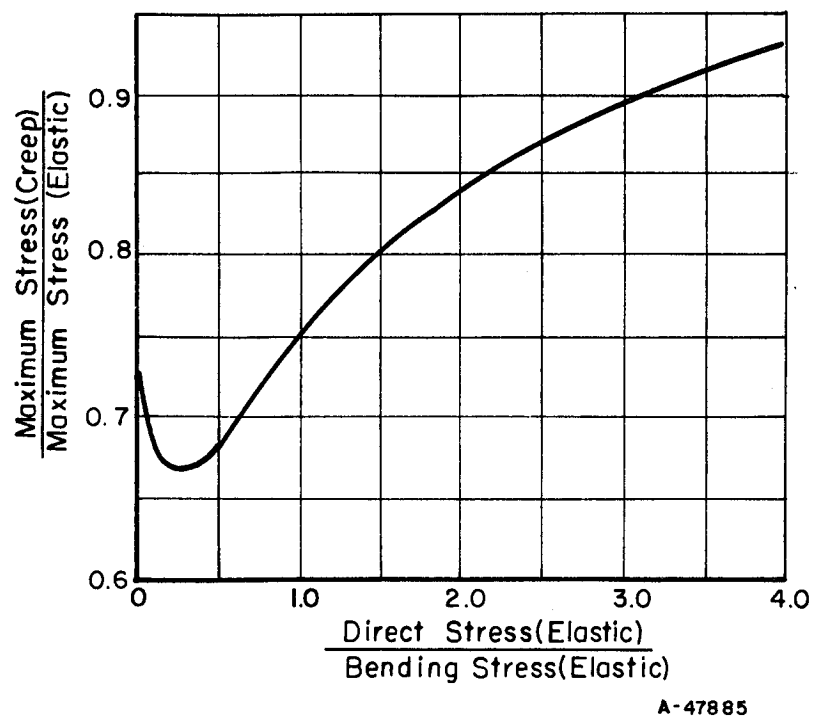


FIGURE 21. CREEP BENDING OF RECTANGULAR SECTION ($n = 6$)

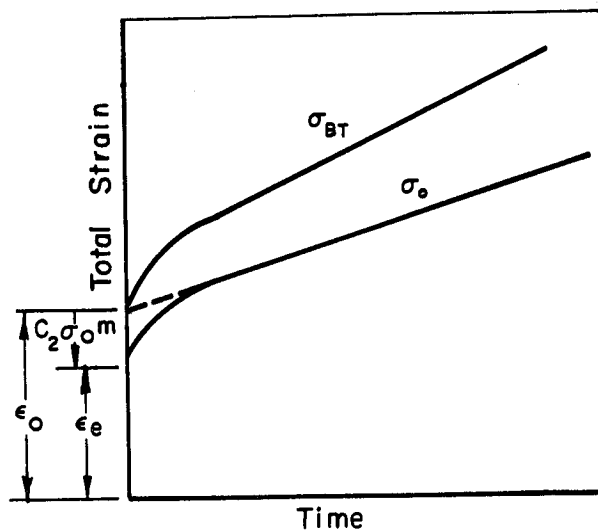
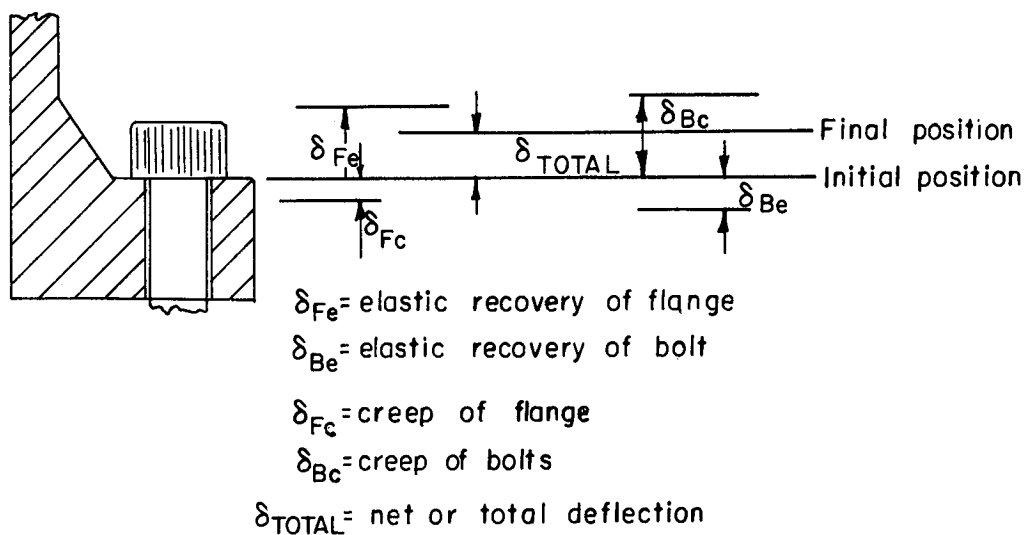


FIGURE 19. INTERCEPT STRESS REDUCTION



A-47884

FIGURE 20. CREEP OF FLANGE AND BOLT

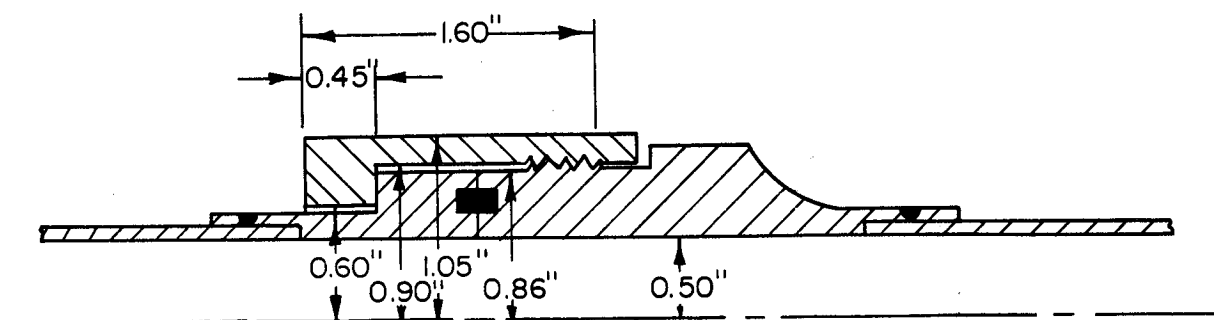


FIGURE 17. THREADED-CONNECTOR GEOMETRY

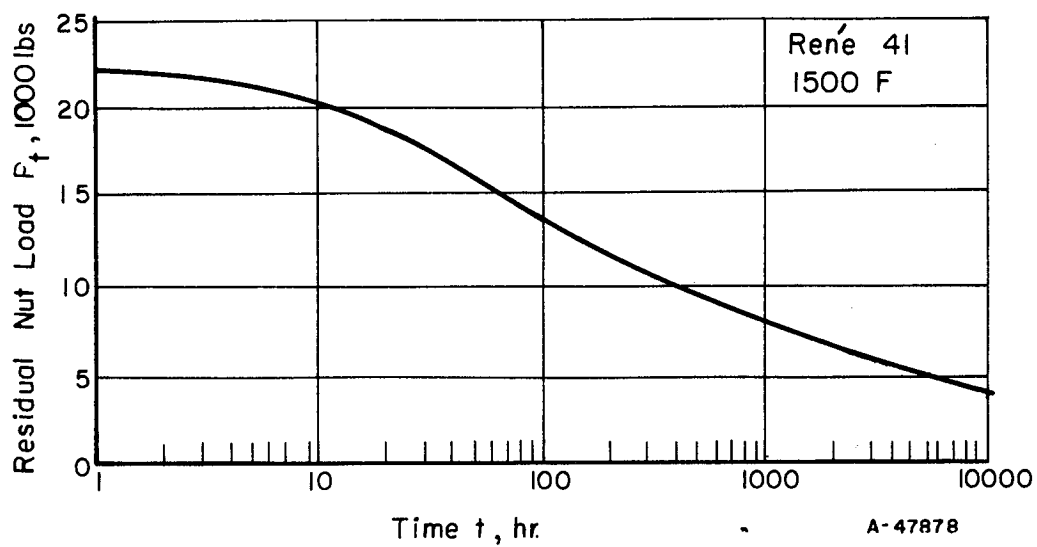


FIGURE 18. RESIDUAL NUT LOAD VERSUS TIME FOR THREADED CONNECTOR (SHOWN IN FIGURE 17)

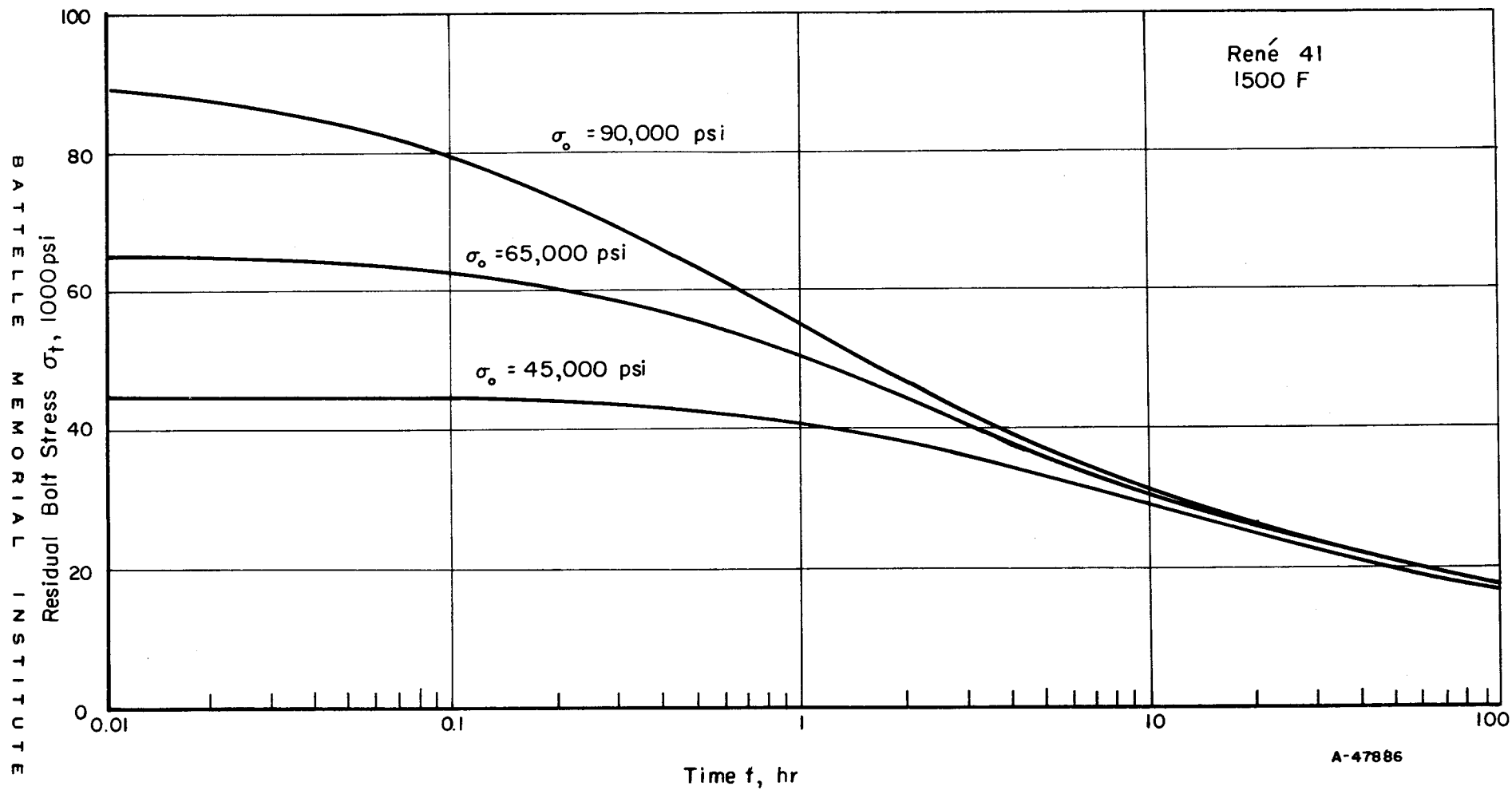


FIGURE 16. EFFECT OF INITIAL BOLT STRESS ON RELAXATION
(FLANGE GEOMETRY OF FIGURE 11)

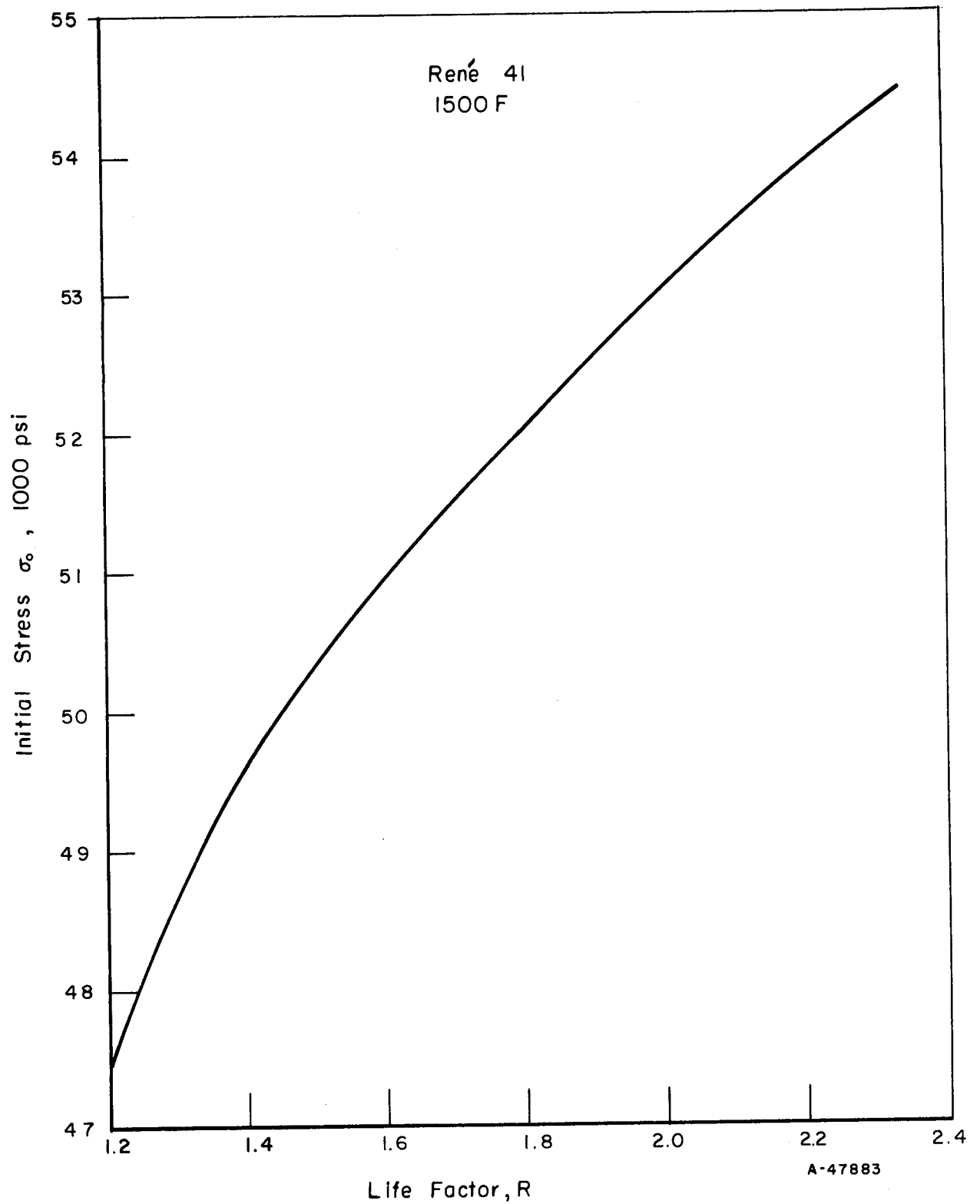


FIGURE 15. EFFECT OF LIFE FACTOR ON INITIAL STRESS ($\sigma_{BT} = 65,400$ PSI)

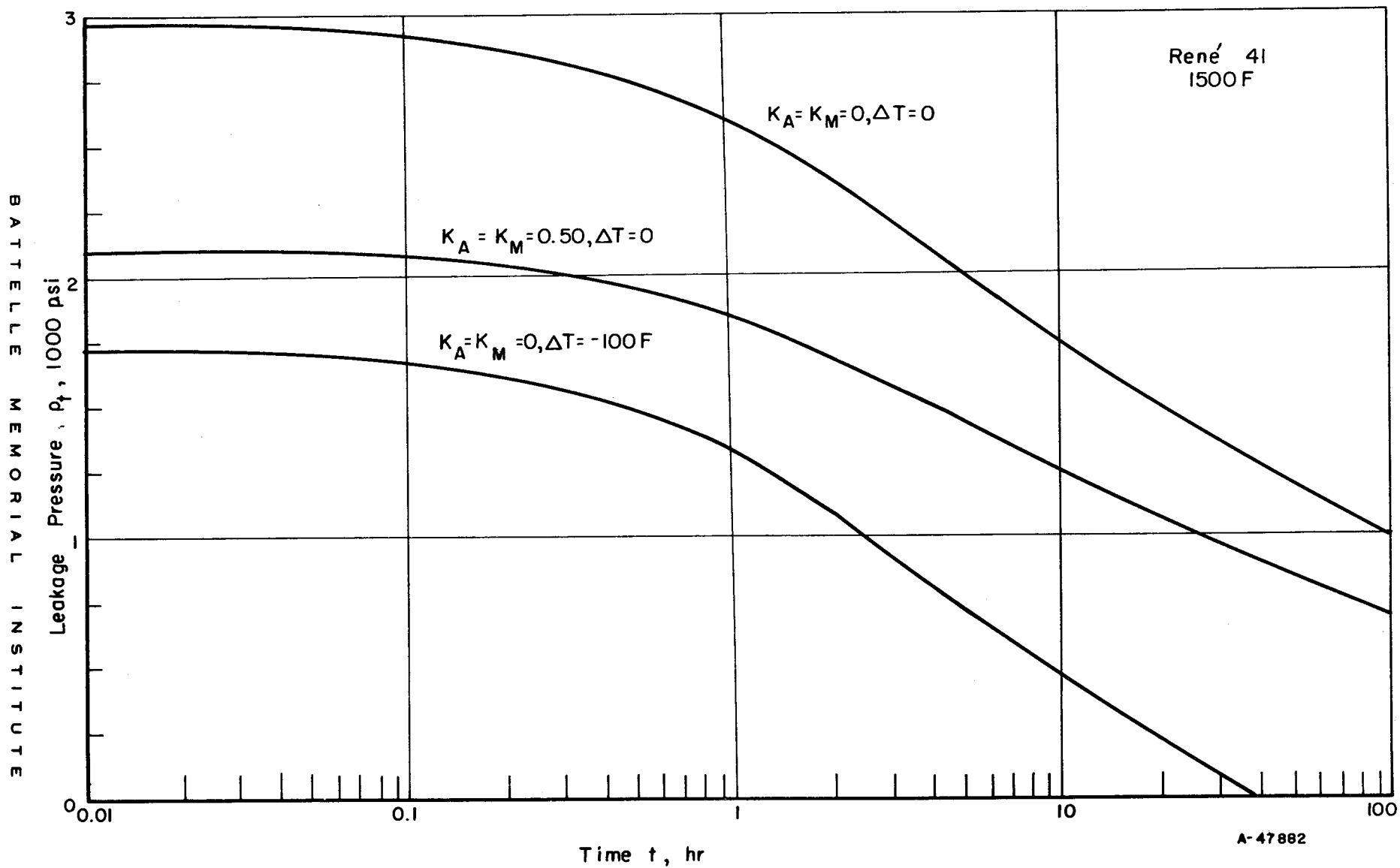


FIGURE 14. LEAKAGE PRESSURE VERSUS TIME FOR BOLTED-FLANGED CONNECTOR (SHOWN IN FIGURE 11)

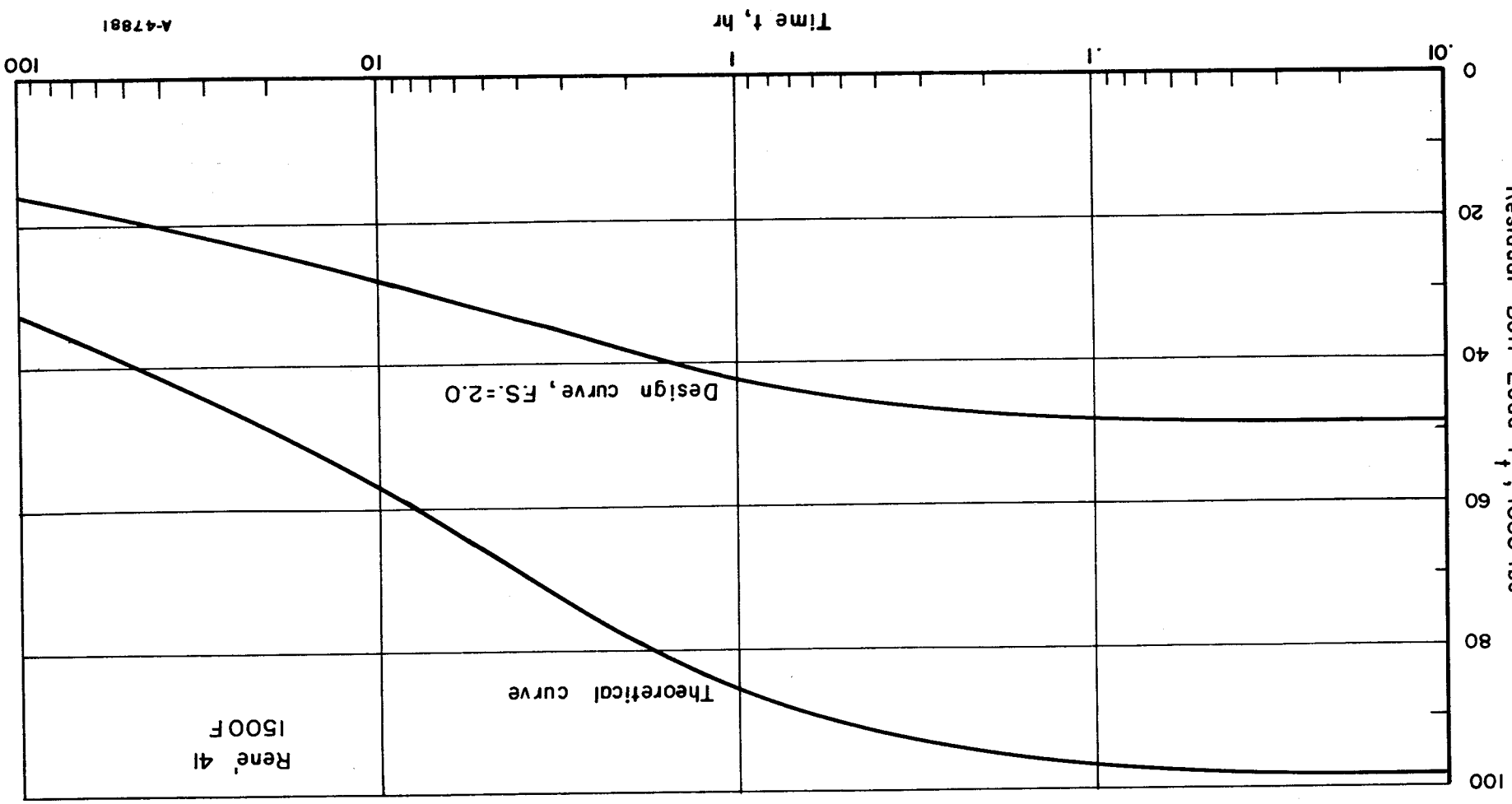


FIGURE 13. RESIDUAL BOLT LOAD VERSUS TIME FOR BOLTED-FLANGED CONNECTOR (SHOWN IN FIGURE 11)

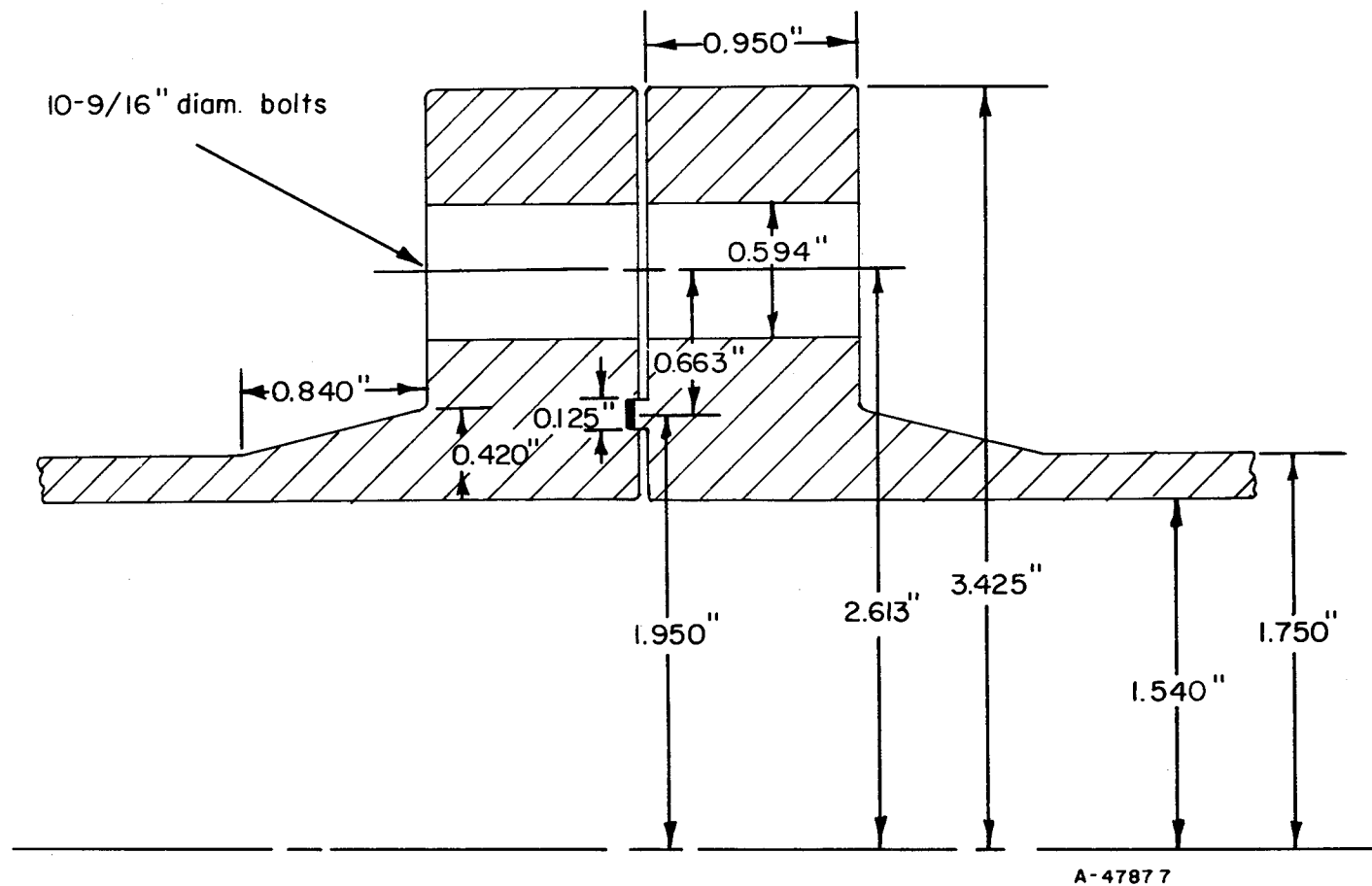


FIGURE 12. INTEGRAL-TYPE FLANGE GEOMETRY (RENÉ 41 - 1500 F)

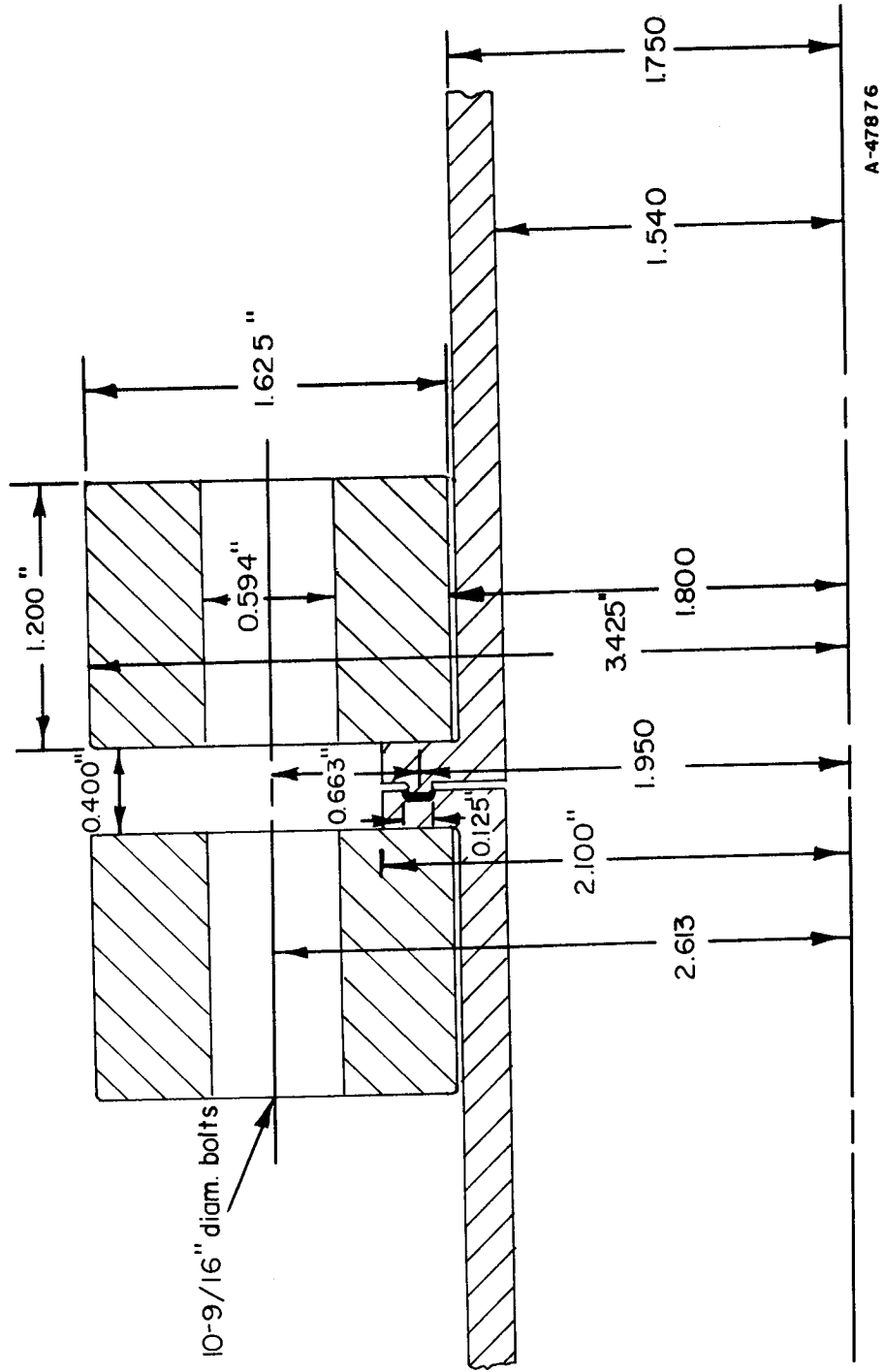
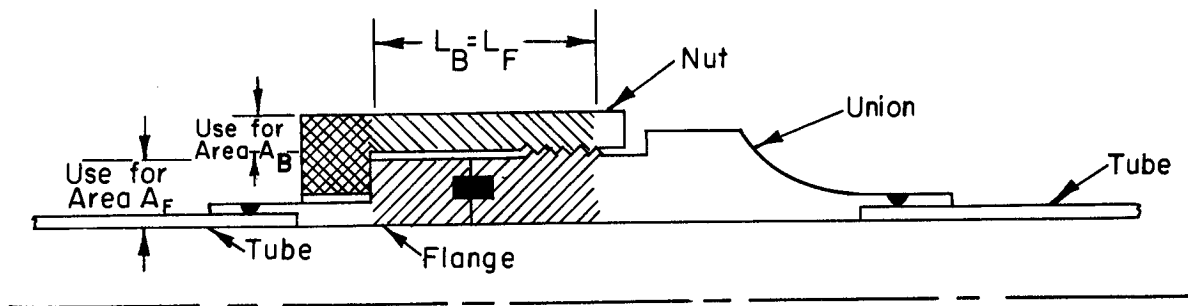


FIGURE 11. LOOSE-TYPE FLANGE GEOMETRY (RENÉ 41 - 1500 F)




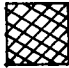
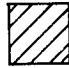
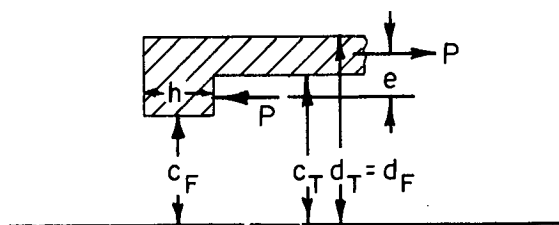
-  Considered as "bolt" axial deformations in analysis
-  Considered as "bolt" bending deformations in analysis
-  Considered as "flange" axial deformations in analysis

FIGURE 9. THREADED CONNECTOR MODEL



A-47879

FIGURE 10. INWARDLY PROJECTING FLANGE

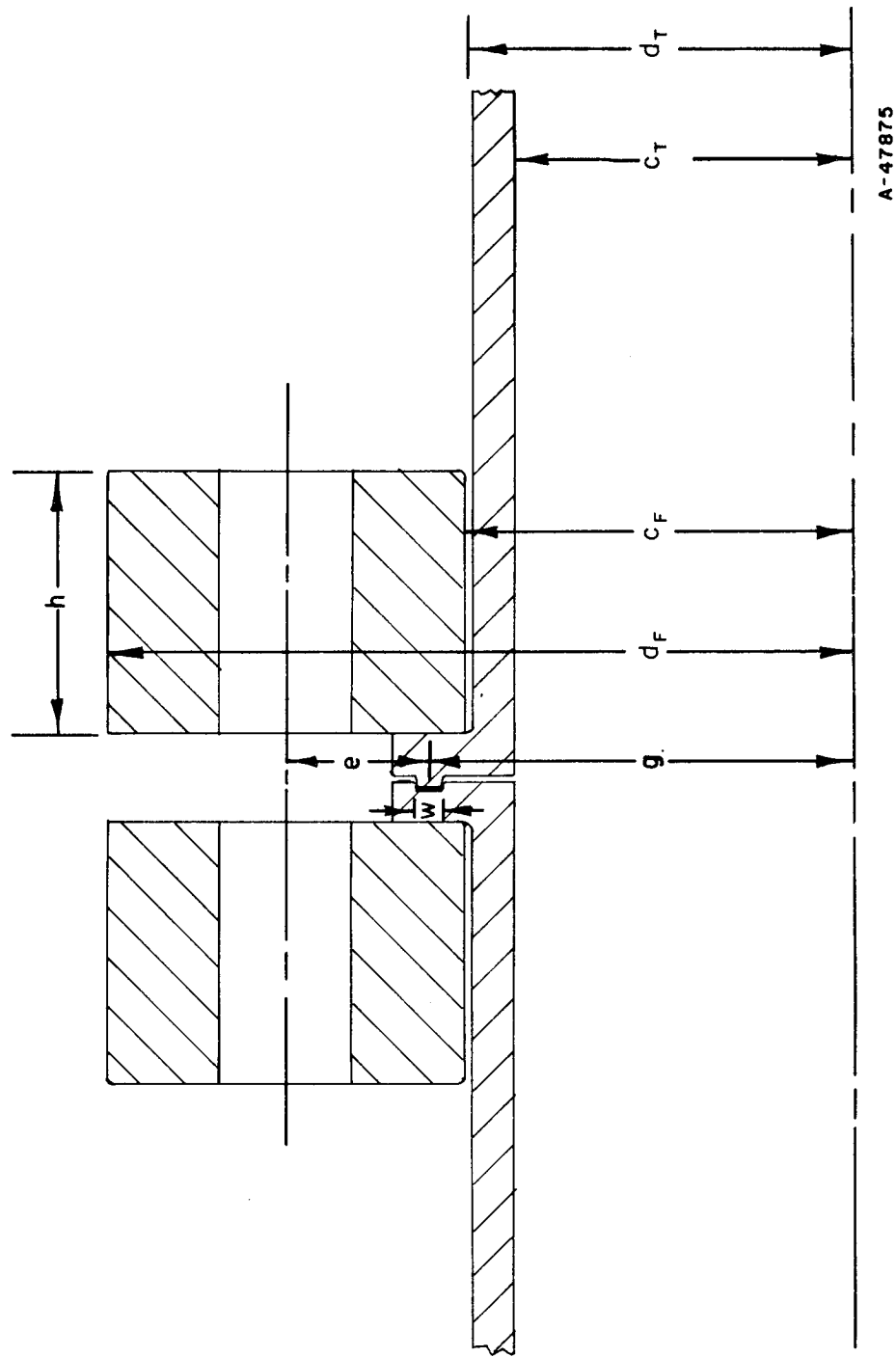


FIGURE 8. TYPICAL FLANGE GEOMETRY

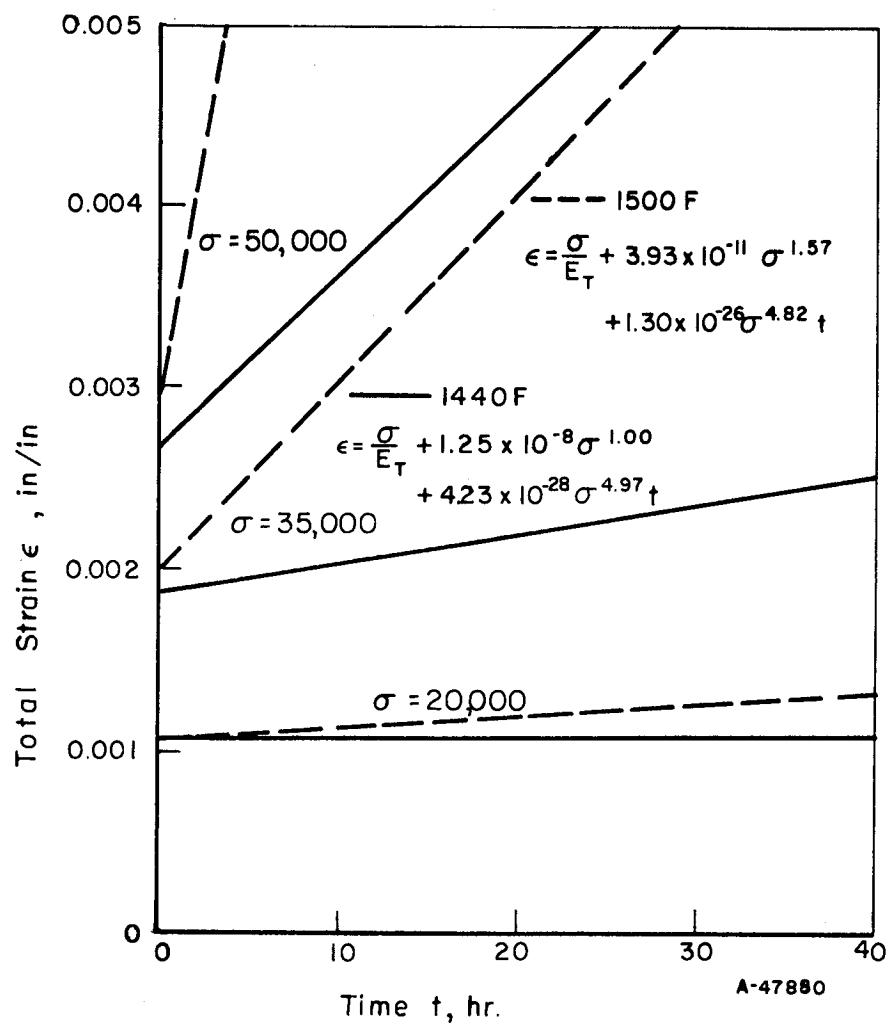


FIGURE 7. DESIGN CREEP PROPERTIES OF RENE 41

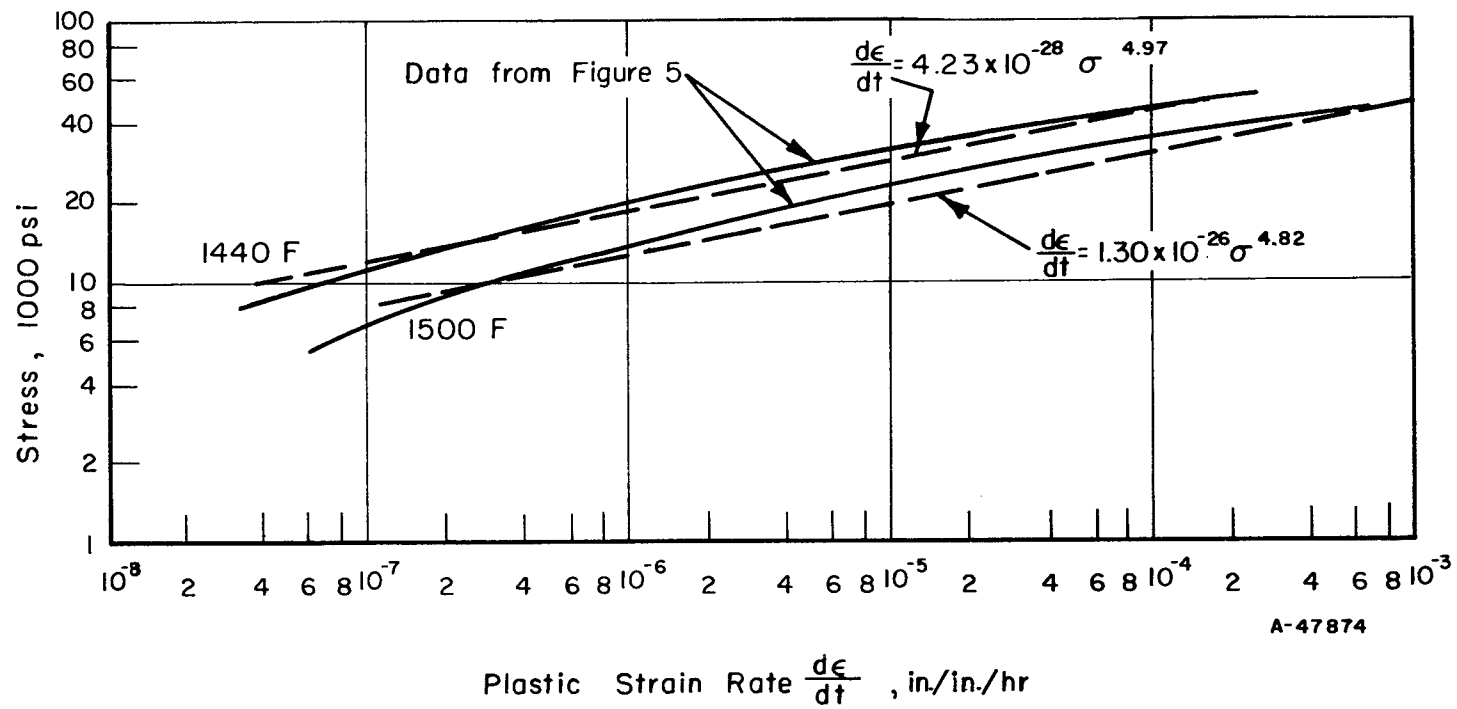


FIGURE 6. CREEP RATE OF RENÉ 41 AT 1440 F AND 1500 F

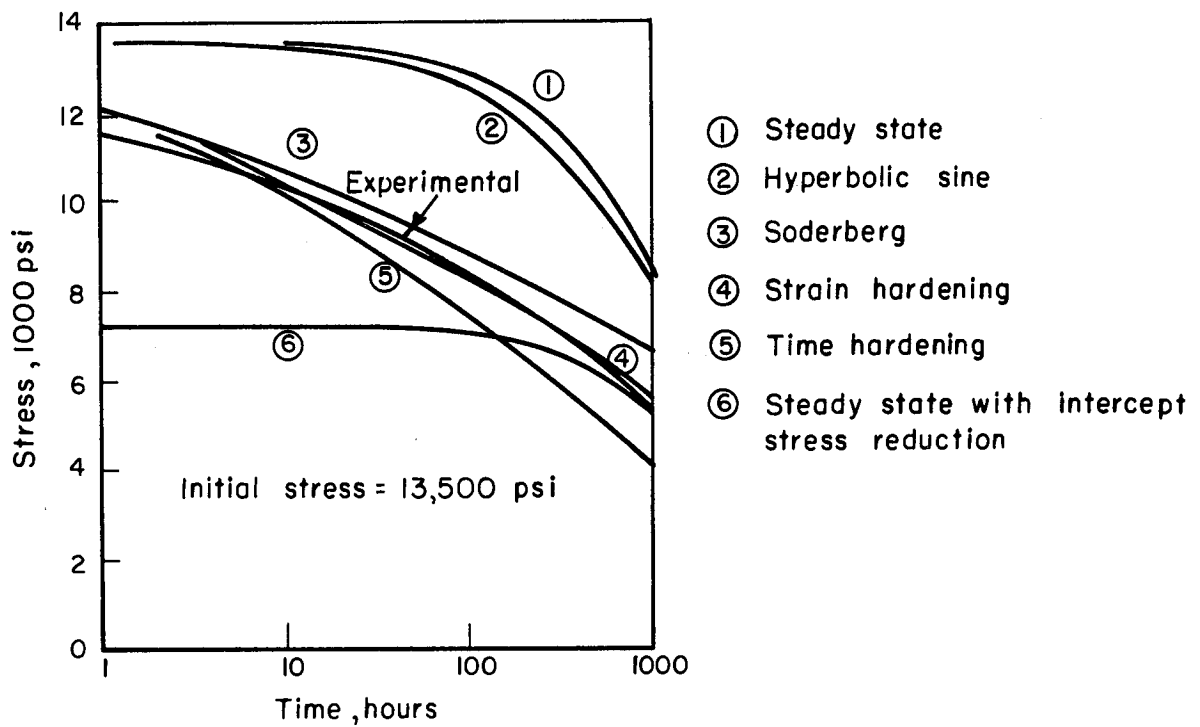


FIGURE 4. CREEP-RELAXATION COMPARISON
(COPPER AT 165 C)

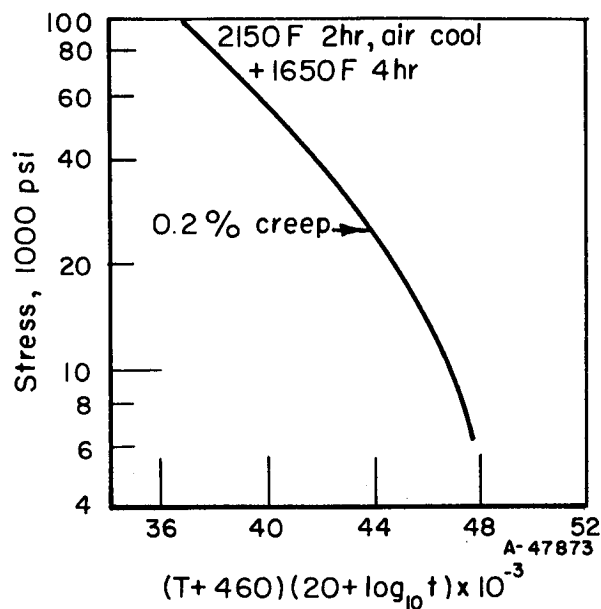


FIGURE 5. MASTER CREEP CURVE FOR RENÉ 41 BAR

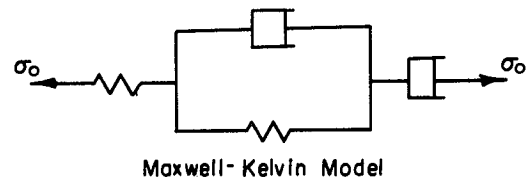
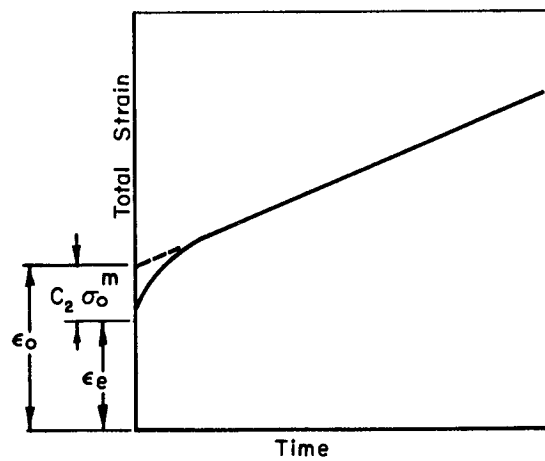


FIGURE 1. TYPICAL CREEP CURVE

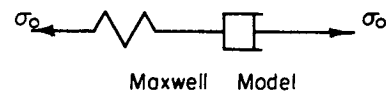
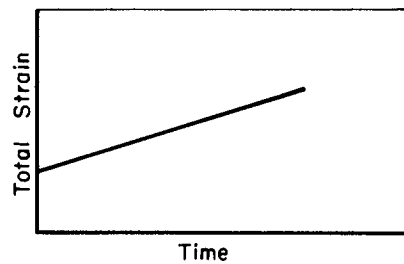
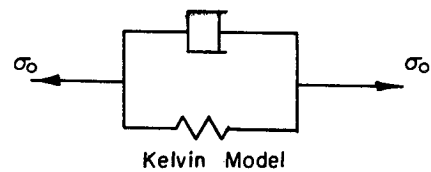
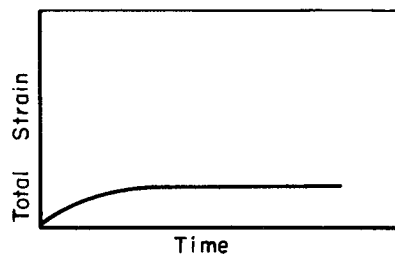


FIGURE 2. STEADY-STATE CREEP



A-47872

FIGURE 3. PRIMARY CREEP

Equations (72) reduce to the well-known Lamé formulas for $n = 1$. The tangential strain rate is

$$\dot{\epsilon}_{\phi} = C_1 \left(\frac{3}{4}\right)^{\frac{n+1}{2}} \left[\frac{p}{\left(\frac{d_T}{c_T}\right)^{2/n} - 1} \left(\frac{2}{n}\right) \right]^n \left(\frac{d_T}{r}\right)^2. \quad (73)$$

The steady-state creep stresses and strain rates in a thick-walled tube under combined internal pressure and axial load are presented by Finnie⁽²⁹⁾. Numerical solutions to the equations are tabulated for various values of the variables. In the case where the additional axial load is either small or large compared to the axial load due to internal pressure, simple approximate solutions are given. Finnie⁽³⁰⁾ also pointed out the lack of complete agreement between the theoretical and experimental studies on multiaxial creep in tubes, attributing the discrepancies to the effect of hydrostatic stress which is usually assumed negligible in creep strain predictions.

A method for predicting the creep failure time for either thin-walled or thick-walled circular cylinders can be found in Reference (31). True stress and true strain are used and the steady-state creep law is assumed valid until failure. The failure time is based on plastic instability, or the time at which the vessel wall is no longer sufficient to hold the load. Simplified formulas are obtained for both thin-walled and very-thick-walled cylinders.

Creep-rupture tests⁽³²⁾ were run on Type 316 stainless steel tubes at high temperatures and pressures. The results of the tests compare favorably with those of uniaxial tension tests if effective stress and effective strain rate are used. Rattinger and Padlog⁽³³⁾ also present a method of analysis for predicting creep rupture of cylindrical shells using conventional uniaxial creep data.

A method of analysis⁽³⁴⁾ for predicting the stresses and strains in thick-walled cylinders considers primary as well as secondary creep. The analysis is quite complicated and justifies a computer solution.

Equations (71) and (73) result in quite favorable strain rates for higher values of the exponent n . On this basis, the design procedure of the ASME Boiler Code⁽¹⁾, which compares the maximum design stress to the creep rate or rupture stress of a uniaxial tension test, provides for a safe design.

APPENDIX D

TUBE DESIGN

The tube design is considered on page 18 only to the extent that it affects the strength of the connector. The tube, however, is subjected to progressive creep deformations with each operating cycle. The tube thickness should satisfy the minimum requirements for a creep design. Some of the appropriate theories available for the tube creep design are reviewed below.

Finnie and Heller⁽⁷⁾ present the equation for the tangential strain rate in a thin-walled tube with closed ends under internal pressure:

$$\dot{\epsilon}_{\phi} = C_1 \left(\frac{pc_T}{d_T - c_T} \right)^n \left(\frac{3}{4} \right)^{\frac{n+1}{2}} = \dot{\epsilon} \left(\frac{3}{4} \right)^{\frac{n+1}{2}}, \quad (71)$$

where $\dot{\epsilon} = C_1 \sigma^n$ = the strain rate which would be produced by the tangential stress

$$\sigma = \frac{pc_T}{d_T - c_T}$$

acting alone in simple tension.

The creep of thin-walled tubes under internal pressure, axial loads, and moments is considered in Reference (7).

Finnie and Heller⁽⁷⁾ also analyzed the creep of thick-walled tubes subjected to internal pressure. Based on the Mises flow law and the steady-state creep law $\dot{\epsilon} = C_1 \sigma^n$, the radial, tangential, and axial stresses, respectively, are

$$\begin{aligned} \sigma_r &= -p \frac{\left(\frac{d_T}{r} \right)^{2/n} - 1}{\left(\frac{d_T}{c_T} \right)^{2/n} - 1}, \\ \sigma_{\phi} &= p \frac{\left(\frac{2-n}{n} \right) \left(\frac{d_T}{r} \right)^{2/n} + 1}{\left(\frac{d_T}{c_T} \right)^{2/n} - 1}, \\ \sigma_z &= p \frac{\left(\frac{1-n}{n} \right) \left(\frac{d_T}{r} \right)^{2/n} + 1}{\left(\frac{d_T}{c_T} \right)^{2/n} - 1}, \end{aligned} \quad (72)$$

where

r = variable radius, $c_T \leq r \leq d_T$.

APPENDIX D

TUBE DESIGN

Gasket Creep*

The gasket will contribute a certain amount of creep and flexibility to the connector assembly. This contribution is neglected in the design procedure in view of the relatively short length of the gasket in most designs. Also, for metallic gaskets, the stresses in the gasket are usually lower than those of the bolt assembly. In fact, the gasket area should be chosen, on the basis of the relative creep strengths of the gasket and bolt material, such that the creep rate of the gasket is negligible. The inclusion of the gasket creep and flexibility properties in the design procedure will unduly complicate the equations, with very little gain in design accuracy for most geometries.

Flange Rotations

Changes in the flange rotation and corresponding bolt-load changes due to the application of internal pressure are neglected in the design procedure. These effects are considered secondary from the standpoint of over-all bolt relaxation, but should be considered in the static design of the connector if found to be significant.

* The design procedure could be extended to include the effects of gasket creep in an approximate, but quite conservative manner.

APPENDIX C

SECONDARY EFFECTSStress Concentrations

Because of the accelerated rate of creep at higher stress levels, the presence of stress concentrations such as bolt threads might be expected to increase the over-all creep rates of the assembly. However, the results of the British Flange Tests⁽⁹⁾ indicate that the creep of the nut assembly was not exceedingly high if the nut material was equivalent to the bolt material. However, when carbon steel nuts were used with alloy steel bolts, the creep of the nut assembly was excessive.

A comprehensive review of stress concentrations under creep conditions was presented in Reference (25). The strength of a specimen with a notch under creep conditions is attributed partly to the ability of the material in the notch area to flow rapidly and redistribute stresses at high temperatures; also because the greater volume of lower stressed material away from the notch restrains the over-all deformations.

Creep Bending of Bolt

The tendency of the bolt in a flanged joint assembly to develop bending moments due to flange rotations and shifting of the nut reaction is well known. Under creep conditions, however, the stress distribution becomes more favorable because of the redistribution of the bending stresses. Bailey⁽³⁾ developed a solution, based on the steady-state creep law, for the creep stresses due to combined axial and bending loads on a rectangular cross section; the results are shown in Figure 21. The results for a solid circular section should be comparable because of the relative values of the plastic bending factor for the rectangular and solid circular sections.

Dynamic Creep

Superimposed alternating stresses are known to affect the creep rate of metals. However, Lazan⁽²⁶⁾ showed that the presence of alternating stresses did not appear to affect greatly the creep rate for most materials. Results for Waspaloy at 1500 F from Reference (27) are shown in Figure 22.

Langenecker⁽²⁸⁾ has recently discussed a problem of possible significance to connectors operating in a high acoustic radiation field. He found that intense ultrasound could have a marked effect on the physical properties of solids.

APPENDIX C

SECONDARY EFFECTS

$$M_T = \frac{\pi p K_M c_T^2 (d_T^2 + c_T^2)}{4d_T} . \quad (64)$$

The bending moment M_T is considered to reduce the gasket pressure by the amount σ_G on one side of the gasket. If the gasket width is assumed small compared to the gasket radius,

$$\sigma_G = \frac{M_T}{\pi g^2 w} = \frac{p K_M c_T^2 (d_T^2 + c_T^2)}{4d_T g^2 w} . \quad (65)$$

If the maximum gasket pressure is assumed to act on the complete gasket surface,

$$P_M = A_G \sigma_G = 2\pi g w \sigma_G = \frac{\pi p K_M c_T^2 (d_T^2 + c_T^2)}{2d_T g} . \quad (66)$$

Bolt-Flange Temperature Differential

The thermal bolt strain $\Delta \epsilon_B = \alpha(\Delta T)$ corresponds to a thermal bolt deflection $\Delta L_B = \alpha(\Delta T)L_B$ which is distributed according to the flexibility of the flange and bolt. From Figure 20,

$$\alpha(\Delta T)L_B = \delta_{Fe} + \delta_{Be} = \delta_{Be} (r_F + 1). \quad (67)$$

The change in bolt stress is

$$\Delta \sigma_B = \left(\frac{\delta_{Be}}{L_B} \right) E_T . \quad (68)$$

From (67) and (68),

$$\Delta \sigma_B = \frac{\alpha(\Delta T)E_T}{1 + r_F} . \quad (69)$$

Following a similar procedure for the threaded connector,

$$\Delta \sigma_B = \frac{\alpha(\Delta T)E_T}{1 + r_F + r'_F} . \quad (70)$$

